Copper Sulphide Precipitation in a Fluidised Bed Reactor

by

Karen Angeline Peterson

Thesis presented for the degree of
Master of Science
In the Department of Chemical Engineering
University of Cape Town

October 2002

Acknowledgements

I attempt to acknowledge all those persons who have contributed academically and socially to the completion of this thesis. I wish to thank:

My supervisor Professor Alison Lewis, for allowing me this valuable opportunity. It has been an enjoyable and learning experience. Thank you for all your guidance, time and motivation during these two years.

My co-supervisors Dr. Stella Lacour and Dr. Rob van Hille for all your patience and help during this project. I appreciate your time, dedication and most of all your enthusiasm. It has been great fun.

The members of the Green Group; Ashton, Fran, Jeeten, Shilpa and Ochieng for the friendship, fun and Ashton for your *sense of humor*. It's been a pleasure to work with you. A special thank you to Fran for all your help and for you constant motivation.

Caryn Vengadajellum and the members of the Bio's group for the welcome into your office. It has been fun getting to know you all. Morning tea just won't be the same.

Professor D. Chalton for his help in designing and analysing my statistical design.

The Water Research Commission and the National Research Foundation for the financial support to the work presented.

To Mandy Roberts: It has been 10 years of many fun times together. You have been an important part of my university career and I thank you for your friendship.

To Richard Bezuidenhout: A special thank you for your encouragement, support, understanding and motivation during these past years.

To Mom and Dad: I appreciate this valuable opportunity that you have provided for me. Thank you for all your understanding and encouragement.

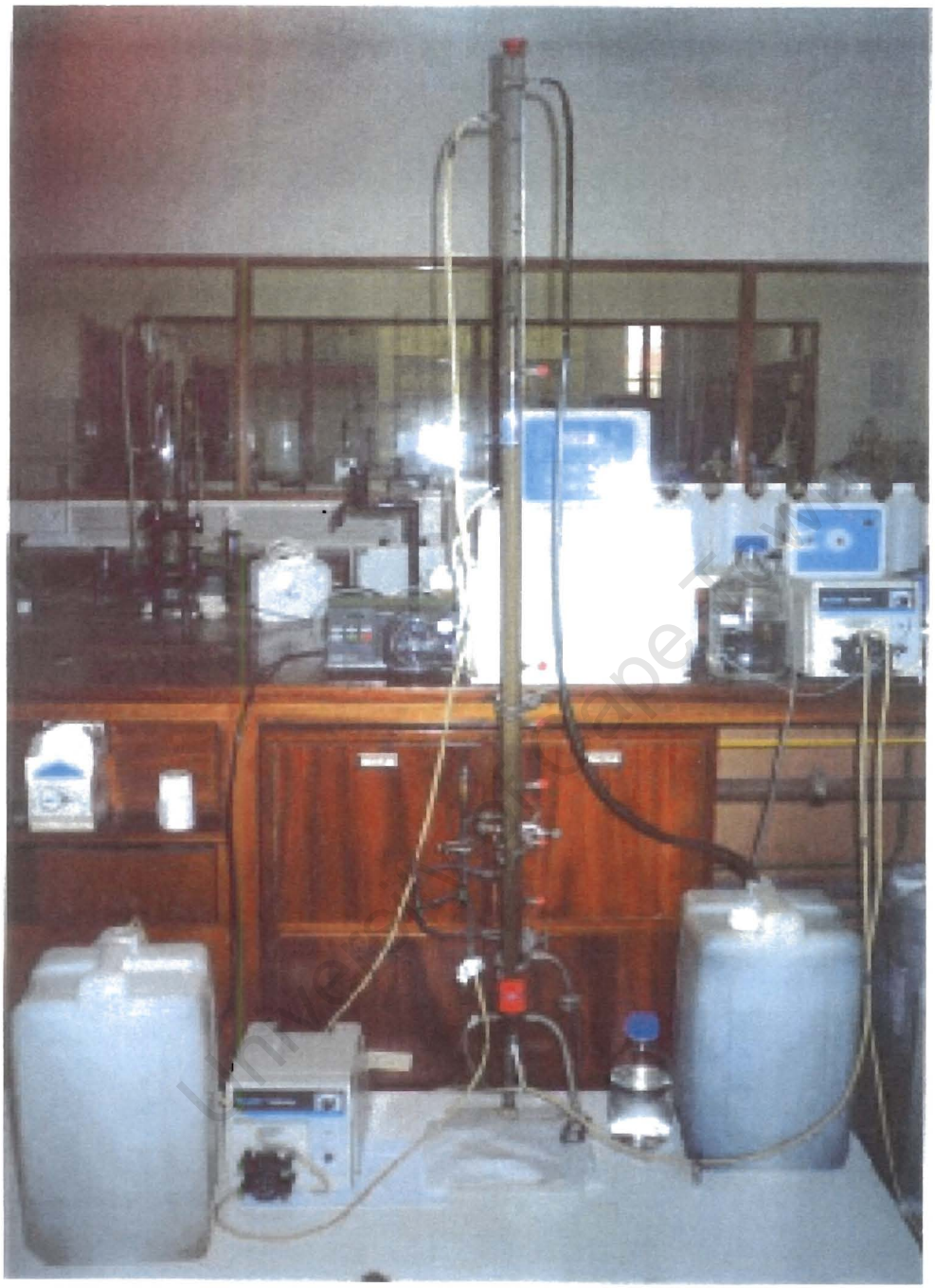

The 1.5m laboratory scale fluidised bed reactor used in this thesis.

Synopsis

Water resources are dwindling not only in South Africa but also in the world in general. The treatment of wastewater to acceptable standards is becoming an area of primary interest. Stringent environmental regulations relating to the levels of impurities including heavy metals and toxic organisms in effluent are being enforced by tougher government legislation.

Acid mine drainage (AMD), the result of oxidation of sulphide minerals, is a wastewater with the undesirable qualities of low pH and significant heavy metal content and typically originates from operating or abandoned mines.

The purpose of this thesis was an investigation into the feasibility of the removal of a single heavy metal (copper) by sulphide precipitation from a copper rich stream in a fluidised bed reactor, as well as developing an understanding of the behaviour of the copper sulphide system. The use of sulphide is motivated by the high sulphate levels in AMD and the integration of the metal removal process with a biological sulphate reducing process that produces an aqueous sulphide stream. Completed and current work includes the investigation of the removal of other metals (nickel, cobalt, zinc and magnesium) by carbonate and sulphide precipitation.

Fluidised bed technology was developed primarily for water softening in the Netherlands and was extended to the removal of heavy metals. The advantages of the fluidised bed included; excellent mixing in the reactor, a large surface area for chemical reaction (provided by seeds in the bed) and a low investment cost. These advantages together with the advantages of sulphide precipitation makes this an attractive method for the treatment of effluent streams.

A laboratory scale fluidised bed was used for this investigation. An extensive literature review identified S:Cu ratio, inlet copper concentration, re-circulation flow and inlet copper flow as the most important factors affecting precipitation in a fluidised bed reactor. All of these factors contributed to the supersaturation, which is the driving force behind the precipitation process. High local and global supersaturations led to the formation of fines within the reactor. These fines were

identified, with the use of concentration profiles in the reactor, by the difference between the total and dissolved copper. Reducing the supersaturation greatly reduced the formation of these fines. Concentration profiles as a function of time showed that once fines had been formed they persisted throughout the experiment.

Copper was found to have a weak affinity for sand particles in the absence of sulphide. However, after the addition of sulphide, copper reacted with the sulphide and rapidly formed a CuS precipitate. Acid was added to the system to reduce the pH to below 7, forming H_2S and increasing the reaction kinetics between the copper and the sulphide. A discharge pH value of 6-6.5 was maintained.

Steady state was consistently reached within 20 minutes of operation. Kinetics were found to be rapid with a significant decrease in copper concentration within the first 5 minutes. A maximum copper removal of 99.62% was achieved within the reactor and a total removal efficiency of 95.8%. A pH of 5 was found to promote faster kinetics and eliminated the need for post reactor pH adjustment.

A response surface methodology (RSM) statistical design systematically investigated the interactions between the factors mentioned in the previous paragraph and their effects on the efficiency of the process to remove copper from the system. The RSM identified the S:Cu ratio as the most important factor in the fluidised bed system and furthermore when sulphide was in excess the process produced better results. A first order one-half 2^4 design assumes that the surface mapped by the response is linear. The analysis of the first order design found the surface to be curved.

A second order analysis using four variables identified a stationary point. This point was situated outside the experimental constraints for the factors. The copper inlet flow rate was found to be optimised, using a ridge analysis, at a flow of 40ml/min and was almost constant for a range of different experimental conditions. A second second-order analysis identified a stationary point that was a global maximum. This is indicative of a region of maximum copper removal. However, this point also was situated outside experimental boundaries and a ridge analysis was used to locate a maximum point inside the experimental region.

The ridge analysis predicted that in order to achieve maximum copper removal, the fluidised bed needed to be operated under the following conditions: S:Cu ratio = 1.6:1, inlet copper concentration = 93ppm, re-circulation flow = 121ml/min and inlet copper flow = 40ml/min. The ridge analysis predicted a 100% removal efficiency under these conditions. However, the S:Cu ratio was slightly above the maximum value set at 1.5:1.

Analysis of the sulphide with a S:Cu ratio of 1.5:1 identified minimal residual sulphide. A recommendation would therefore be to investigate a S:Cu ratio in excess of 1.5:1. If residual sulphide was found, 1.5:1 would be an experimental constraint. An alternative seed could be investigated. Successful studies have been performed using magnetite. Possible future work could include an investigation into the size of the seed in a sulphide system. Although favourable results were achieved, the seed size was chosen as a result of research into the seed size for a carbonate system. Therefore, it might be advisable to experiment with this variable.

Table of Contents

Chapter Three
Solubility Theory

Chapter Four
Fluidised Bed Technology

Chapter Five
Equipment and Procedure

Chapter Six
Solubility Diagram

Chapter Seven
Response Surface Methodology

Chapter Eight
Results

Chapter Nine

Conclusions

List of Figures

List of Tables

Nomenclature

a_i	Activity of ion i	(mol/l)
$[A^+]$	Concentration of species A	(mol/dm^3)
a	Area of nucleus	(m$^{2)}$
A	Surface area of the crystal	(m^2)
A*	Activity of a saturated solution	(mol/l)
A_s	Total crystal surface area present in unit suspension volume.	
b	Adsorption energy co-efficient	
C	Concentration	(mol/l)
C*	Equilibrium saturation concentration	(mol/l)
C_e	Equilibrium concentration of metal	(mg/l)
c_l	Solute concentration in solution at crystal-solution interface	(mol/dm^3)
D	Diffusion coefficient	(m^2/s)
d	Diameter of particles	(m)
E	Potential gradient	(V)
e	Bed voidage	
e_{mf}	Bed voidage at the minimum fluidisation velocity	
f(x)	Probability of x	
G_{crit}	Activation energy barrier to the nucleation process	(J/m^3)
h	Height of nucleus	(m)
IAP	Ion activity product	(mol/l)
j	Molar deposition rate	(moles/s)
J	Molar flux	(moles/sm^2)
K	Boltzmann constant	(J/K)
K_1	Dissociation constant	(mol/l)
K_a	Activity solubility product of the salt	(mol/l)
k_d	A coefficient of mass transfer by diffusion	(m/s)
k_m	Coefficient of mass transfer	(m/s)
k_r	Rate constant for the surface reaction (integration) process	(m/s)
K_{sp}	Solubility product	(mol/l)
l	Bed Depth	(m)

m	Mass of solid deposited	(kg)
M	Molar mass of solid	(g/gmol)
N	Avogadro number =6.023e23	(mol^{-1})
q_e	Metal uptake	(metal/g biomass)
R	Gas constant	(J/mol.K)
r	Radius of nucleus	(m)
RR	Re-circulation ratio	
S	Supersaturation ratio	
SS_E	Error sum of squares	
T	Temperature	(K)
v_g	Linear face growth rate	(m/s)
V_m	Molar volume	(m^3/mol)
V_N	Volume of nucleus	(m^3)
$w_{M,in}$	Flow of the component metal in the recycle stream of the reactor	(ml/nin)
$w_{M,total}$	Flow of the component metal at the inlet of the reactor	(ml/min)
$w_{Mdissolved}$	Flow of the dissolved metal at the outlet	(ml/min)
w_{Sin}	Flow of the component sulphide at the inlet of the reactor	(ml/min)
x	Measurement of observation	
$\bar{x}$	Arithmetic mean	
x_i	Random independent values of a linear function	
X_m	Maximum adsorption capacity	
x_n	Dimensionless Coded variables	
y	Response variable yield	
yi	Response to the linear function for values of x_i	

ε	Error term	
η	True response function	
μ	Viscosity of the fluid	(cP)
μ	Mean of probability distribution	
ρ_l	Density of fluid	(kg/m^3)
ρ_s	Density of sand	(kg/m^3)
ξ	Independent natural variables	
ε	Error term	
η	True response function	
ρ_σ	Density of solid	(kg/m3)
σ^2	Variance of probability distribution	
γ	Activity coefficient	(J/m^2)
Δp	Pressure drop across the bed	(Pa)
ΔC	Concentration driving force	(mol/l)
$\Delta G°$	Standard free energy	(J/m^3)
ΔG_{hom}	Free energy change associated with homogenous nucleation	(J/m^3)
ΔG_n	Free energy change of the transformation per unit volume	(J)
$\Delta\mu$	Driving force	(J/mol)
δ	Length of the diffusion path	(m)

Chapter One

Introduction

"Sustainable development is development that meets the needs of the present without compromising the ability of future generations to meet their own needs."

In 1987 the World Commission on Environment and Development proposed the brief, widely used quote above to describe sustainable development. Three main dimensions of sustainable development can be identified: environmental, social and economic. Examples of socially relevant indicators are the rate of unemployment, industry's expenditure on worker health and safety, as well as gender-related indicators. When an economy is successful in generating capital, a contribution has been made to sustainable development.

Environmental indicators of sustainable development are numerous. Examples of these indicators are industrial components of energy and water consumption; emissions of greenhouse gases, sulphur dioxide and nitrogen oxides; the discharge of critical pollutants into water; and the generation of waste (including those of a hazardous nature). Many industries are under fire from 'green' parties who are demanding that they take greater measures to ensure that they reduce harmful emissions into the environment. The predicted high industrial growth rate in South Africa, coupled with the limited water resources, will necessitate the implementation of advanced effluent treatment systems (Bell, 2002).

Wastewaters from industrial, mining and metallurgical processes contain large amounts of soluble components which could be responsible for polluting river systems. Acid mine drainage (AMD) occurs at operating and abandoned mine sites as a result of oxidation of sulphide minerals and is characterized by low pH and heavy metal contamination (Petersen, 2002). The metal-refining industry has produced substantial amounts of sludge and solid waste. In several instances leaching of the solids by percolating rain and surface waters has caused substantial contamination of the underlying groundwater (Barnes *et. al*, 1991).

A variety of treatments for metal-containing effluents and acid mine drainage exist. These include lime treatment, evaporation, ion exchange, cementation, reverse osmosis and electrolysis. However, there are disadvantages associated with some of these treatments for example: lime treatment cannot meet new, more restrictive metal discharge standards nor reduce the sulphate concentration to below 1500 mg/l. It also produces a voluminous, mixed metal-hydroxide sludge that is difficult to dewater.

SRB Treatment

An alternative process for treatment of metal-containing wastes is an anaerobic sulphate-reducing microbial process (Knobel and Lewis, 2001). The process uses a range of carbon sources both for organism growth and as an energy source for sulphate reduction. In the course of the biological sulphate reduction process both sulphide and bicarbonate are simultaneously produced through microbial activity. Heavy metals can then be precipitated as insoluble sulphides. The removal of a wide range of heavy metals and sulphate to required levels has been demonstrated (Knobel and Lewis, 2001), but understanding of the process is limited.

A focus on metal precipitation

This thesis focuses on the metal precipitation aspect of a sulphate reduction process, using copper as a model metal and sulphide as the anion for precipitation. Previous work (Guillard and Lewis, 2001; 2002) has focussed on the simpler nickel carbonate precipitation system. In this study soluble copper and sulphides react to form a sparingly soluble copper sulphide precipitate.

Peters *et al* (1998) propose the use of sulphide precipitation as a viable method for the removal of heavy metals from water as it is a more effective process compared to hydroxide precipitation. Attractive features of sulphide precipitation are the attainment of a high degree of metal removal due to low solubilities over a broad pH range, effective precipitation of certain metals even at very low pH levels and fast reaction times. Sulphide precipitates exhibit less of an amphoteric nature than hydroxide precipitates and have less of a tendency to dissolve (McAnally *et al*, 1983).

Bhattacharyya (1981) indicated that studies show lower sludge volumes with sulphide than with hydroxide treatment.

Heavy Metals and Fluidised Bed Technology

DHV Consulting Engineers have developed a system of heavy metal recovery from wastewater using a fluidised bed reactor (Schöller *et al,* 1987). Previously, fluidised bed reactors have been used for the softening of drinking water (producing calcium carbonate crystals) (Wilms *et* al, 1988) and for the removal of phosphates from wastewater (producing calcium phosphate) (Seckler, 1994).

Seckler (1994) used carbonate precipitation in a fluidised bed for the removal of phosphates from wastewater. The main motivation for the work was to optimize the phosphorus removal efficiency and to minimize detrimental effects of impurities in wastewater.

Zhou *et al* (1999) described a heavy metal (Cu, Ni and Zn) removal process from wastewater in a fluidised bed reactor. The technology was based on inducing the nucleated (carbonate/hydroxide) precipitation of heavy metals on a sand surface. The study highlighted the influence of pH and inlet concentrations. At pH values higher than 8.7 a carbonate/hydroxy precipitate was formed. Maximum metal removal however was achieved at a pH of 9.0.

Guillard (2001) carried out a similar study where the precipitation of nickel-carbonate was investigated in a 1m laboratory scale fluidized bed reactor. The removal efficiency was found to depend on the pH, nickel feed and inlet ratio. Successful studies achieved high removal, however a post-filtration stage was found to be necessary in order to achieve removal greater than 99%.

Objectives

This thesis investigated the feasibility of combining fluidised bed technology with the attractive features of sulphide precipitation. The hypothesis stated that by controlling the factors affecting the local and global supersaturation in a fluidised bed reactor, it

would be possible to optimise removal of copper from a copper sulphate stream. Factors investigated included; metal/sulphide ratio, metal inlet flow rate, re-circulation flow rate and metal concentration. A systematic method, Response Surface Methodology (RSM) was employed in order to map an optimum experimental region.

Scope

Chapter 2 discusses the relevant theory pertaining to precipitation processes such as supersaturation, primary nucleation, growth and agglomeration. ***Chapter 3*** investigates solubility theory and makes a comparative study between different simulation packages (OLI, ASPEN^{TM}). In ***Chapter 4*** the principles of the fluidised bed are discussed and theoretical calculations tabulated for experimental use. Also investigated are existing seeding technology and polishing. ***Chapter 5*** lists equipment and describes the experimental procedure for precipitation in a fluidised bed. ASPEN PLUS^{TM} and OLI simulation packages are used to produce simulated results in ***Chapter 6***. Response Surface Methodology (RSM) is explained in ***Chapter 7*** with experimental results and discussion presented in ***Chapter 8.*** Conclusions are drawn in ***Chapter 9***.

Chapter Two

Literature Review

2. Introduction to precipitation theory

Precipitation has been defined as fast crystallisation (Söhnel and Garside, 1992). It has also been defined as the crystallisation of sparingly soluble substances (Kind, 1999). Crystallisation occurs by controlled cooling or evaporation when the solute exceeds its solubility and the solution is said to be supersaturated. In precipitation, however, the product formed by a chemical reaction and the precipitate is generally sparingly soluble in the solvent (Kind, 1999).

In order to obtain the desired product qualities, effective control of the precipitation process is required. This results in the need for a specifically designed reactor as well as optimisation of the operating parameters.

The following chapter discusses, in detail, the concepts of supersaturation, nucleation, crystal growth and agglomeration.

2.1 Supersaturation

High supersaturation and small crystals are characteristic of precipitation. Supersaturation is necessary in order for the solid to be formed (Gösele and Kind, 1991). A solution is supersaturated when the concentration of the solute exceeds its solubility.

Supersaturation is defined as a thermodynamic driving force, ΔC. Other terms derived from the supersaturation are the supersaturation ratio, S, or a quantity referred to as the relative supersaturation, σ.

$$\Delta C = C - C^* \tag{2-1}$$

$$S = C/C^* \tag{2-2}$$

$$\sigma = \Delta C/C = S-1 \quad (2\text{-}3)$$

where:

ΔC = Concentration driving force (mol/l)

C = Solution concentration (mol/l)

C^* = Equilibrium concentration (mol/l)

S = Supersaturation ratio

σ = Absolute or relative supersaturation

The following formulation is a method of relating the supersaturation ratio S to the chemical potential. The fundamental driving force for crystallisation in terms of the chemical potential may be written as follows:

$$\Delta\mu = \mu_2 - \mu_1 \quad (2\text{-}4)$$

$\Delta\mu$ = Driving force (J/mol)

μ_1 = Chemical potential in crystal state (J/mol)

μ_2 = Chemical potential in supersaturated state (J/mol)

$$\mu = \mu_0 + \mathbf{R}T\ln a \quad (2\text{-}5)$$

R = Gas constant (J/mol.K)

T = Temperature (K)

a = Activity (mol/l)

$$a = \gamma C \text{ (mol/l)} \quad (2\text{-}6)$$

γ =Activity coefficient

$$\Delta\mu/RT = \ln(a/a^*) = \ln S \quad (2\text{-}7)$$

a^* = activity of a saturated solution (mol/l)

Supersaturations in aqueous solutions of sparingly soluble electrolytes are best expressed in terms of the solubility product (Mullin, 2001).

$$S = (IAP/K_a)^{(1/\nu)} \quad (2\text{-}8)$$

IAP = Ion activity product (mol/l)

K_a = Activity solubility product of the salt (mol/l)

ν = Number of moles of ions in 1 mole of salt (mol)

$$K_a = (C_+\gamma_+)^x (C_-\gamma_-)^y \text{ (mol/l)} \quad (2\text{-}9)$$

2.2 Nucleation

The initial kinetic step that allows for transformation from a liquid into solid phase in a supersaturated solution is called nucleation (Hess and Kok, 1996). Nucleation or birth of crystals from solution is an important process in precipitation. It has a controlling effect over number, size, structure and morphology of the precipitated crystals (Elving and Kolthoff, 1979).

The theoretical description of nucleation depends on the mechanism responsible for nucleus formation. The various mechanisms can be schematically represented as (Mullin, 1992 in Söhnel and Garside, 1992):

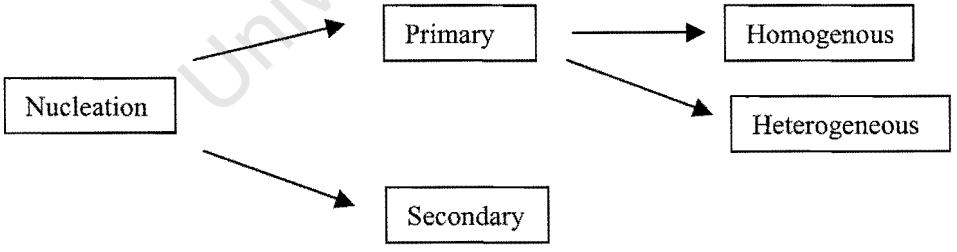

Figure 2.0 Nucleation mechanisms

Primary nucleation is the formation of a new solid phase, not influenced by the presence of an existing solid phase. Two types of primary nucleation may be identified:

Homogeneous: The formation of the solid phase is not initiated by the presence of any solid phase.

Heterogeneous: The formation of a new solid phase is catalysed by the presence of a foreign solid phase.

Secondary nucleation occurs when the solid phase is initiated by the presence of the crystallising material (Söhnel and Garside, 1992). Strickland-Constable (1968 in Mullin, 2001) describes several possible mechanisms of secondary nucleation, such as: 'initial' breeding (the detachment of weak outgrowths) and 'polycrystalline' breeding (the fragmentation of a weak polycrystalline mass). Of importance in a long thin vessel is 'collision' breeding (a complex process resulting from the interactions of crystals with one another or with parts of the crystallization vessel).

Franke and Mersmann (1995) demonstrated that at different points in a reactor different nucleation mechanisms dominate. At the feed point, very high local supersaturations can occur and homogeneous primary nucleation will be dominant, with extremely high nucleation rates. In regions where the homogeneous nucleation rate is negligible, but the system remains supersaturated, heterogeneous nucleation or secondary nucleation are the dominating mechanisms.

2.2.1 Primary Nucleation

(i.) Homogeneous nucleation

There are two theories that exist in formulating mathematical analysis for nucleation, classical and non-classical theory. Non-classical theories are analogous to classical theories in that they have very similar definitions. Classical theory, the more common definition, was found to compare well with experimental results (Söhnel and Garside, 1992) and will therefore be used to describe homogeneous nucleation theory.

Molecules or ions react to form a cluster formation that eventually results in the production of crystals. This process has been compared to a chemical reaction in that there is an activation energy, which presents a barrier, to be overcome. This barrier creates the need for a degree of supersaturation before spontaneous crystallisation may occur (Elving and Kolthoff, 1979).

Prior to nucleation there is a continuous formation and dissolution of ionic or molecular clusters in equilibrium with other clusters. If the concentration of ionic or molecular clusters is high enough they become sufficiently large and become fused into crystallites (Elving and Kolthoff, 1979). Crystal growth then follows.

Franke and Mersmann (1995) used classical theory to calculate the primary nucleation rate. This work confirmed the strong relationship between primary nucleation and supersaturation S.

Research performed by Gibbs (1948), Volmer (1939) and Becker and Döring (1935) led to the classical theory formulation. If the small, stationary spherical nucleus of radius r is created from stationary ions, the change of energy of the system is related to the ion "bonds" formed, leading to a heat of crystallisation (negative) and the energy required to create the surface. A model in figure 2.1 depicts the strong interaction between ions so that the internal lattice solvation is overcome and the configuration becomes that of a small piece of crystal in a solvent cavity.

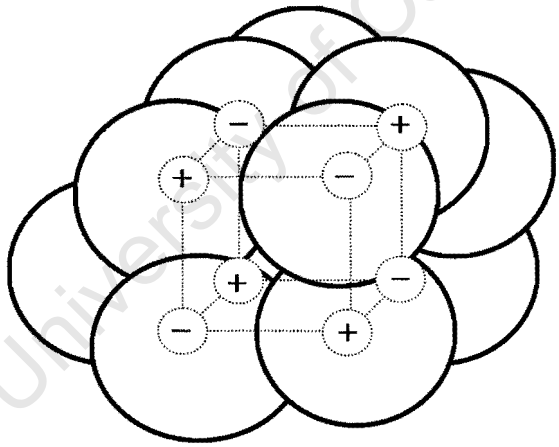

Figure 2.1 Model of ionic embryo involving strong interaction between ions modelled by the classical formulation (Elving and Kolthoff, 1979).

The standard free energy change is approximated by the following equation:

$$\Delta G^{\circ} = \frac{4\pi r^3}{3}\Delta G_v + 4\pi r^2\sigma \qquad (2\text{-}10)$$

ΔG° = Standard free energy (J/m^3)

ΔG_v = Free energy change of the transformation per unit volume (J)

r = Radius of solid particle simplified as a sphere (m)

σ = Interfacial tension i.e. between the developing crystalline surface and the supersaturated solution in which it is located.

The two terms of equation (2-10) have opposite signs and are dependent on r. Figure 2.2 shows how ΔG passes through a maximum value corresponding to a critical nucleus, r_c and is maximised when $d\Delta G/dr = 0$.

$$\frac{d\Delta G}{dr} = 8\pi r\sigma + 4\pi r^2\Delta G_v = 0 \qquad (2\text{-}11)$$

$$r_c = \frac{-2\gamma}{\Delta G_v} \qquad (2\text{-}12)$$

$$\Delta G_{crit} = \frac{\pi l^2\sigma}{3} = \frac{16\pi\sigma^3}{3\Delta G_v^2} \qquad (2\text{-}13)$$

G_{crit} = Activation energy barrier to the nucleation process (J/m^3)

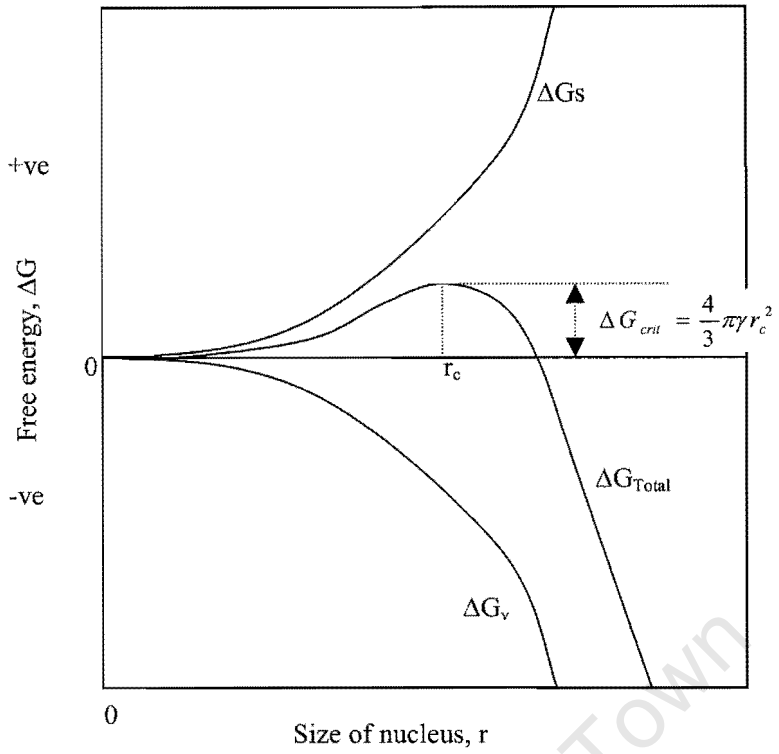

Figure 2.2 Free energy diagram for nucleation explaining the existence of a 'critical nucleus' (Mullin, 2001)

The rate of nucleation may be described by the Arrhenius reaction velocity equation:

$$\frac{dN}{dt} = J = A\exp(-G^{\circ}/kT) \qquad (2\text{-}14)$$

k = Boltzmann constant (J/K)

The Boltzmann constant is defined as the gas constant per molecule.

$$k = R/N = 1.3805\times10^{-23}JK^{-1} \qquad (2\text{-}15)$$

R = Universal gas constant = $8.314JK^{-1}mol^{-1}$

N = Avogadro number = $6.023\times10^{23}mol^{-1}$.

Figure 2.3 is a representation of the nucleation rate as a function of the degree of supersaturation. On increasing the supersaturation beyond a certain value S^*,

corresponding to the boundary of the 'metastable' zone under the given experimental conditions, rapid increase of the nucleation rate takes place (Nyvlt, 1992).

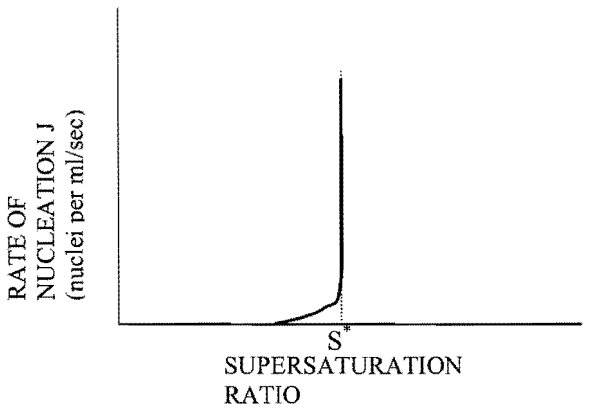

Figure 2.3 Graph of supersaturation ratio vs. rate of nucleation (Nývlt, 1992)

The critical supersaturation usually corresponds to the rate of one nucleus being formed per second per unit volume therefore:

$$\ln S = \frac{2\sigma v}{kTr} \tag{2-16}$$

T = Absolute temperature (K)

k = Boltzmann constant (J/K)

ν = Molecular volume (number of ions produced by one mole of electrolyte).

r = Radius of nucleus (m)

Theory allows the prediction of S therefore enabling the calculation of the interfacial tension σ to be the only unknown. Independent methods for calculating the σ result in a test for the accuracy of the model.

$$-\Delta G_v = \frac{kT}{v}\ln S = \frac{2\sigma}{r} \tag{2-17}$$

Hence from Equation (2-13):

$$\Delta G_{crit} = \frac{16\pi\sigma^3 v^2}{3(kT\ln S)^2} \tag{2-18}$$

and from equation (2-14):

$$J = A\exp\left[-\frac{16\pi\sigma^3 v^2}{3k^3T^3(\ln S)^2}\right] \quad (2\text{-}19)$$

This equation indicates that three main variables govern the rate of nucleation: temperature, T; degree of supersaturation, S and interfacial tension σ.

Primary nucleation increases strongly with supersaturation S (Frank and Mersmann, 1995). Due to the high supersaturation in precipitation processes, primary nucleation is very rapid and therefore a local process. Therefore in order to control the rate of primary nucleation it is important to control the local supersaturation rate (Franke and Mersmann, 1995).

(ii.) Heterogeneous nucleation

Particles of a foreign solid phase that can act as a 'catalyst' for nucleation are present in any liquid or gaseous system which has not thoroughly been cleaned (Söhnel and Garside, 1992). Many reported cases of spontaneous (homogeneous) nucleation are found on careful examination to have been induced in some way. It is generally accepted that homogeneous nucleation is not a common occurrence as it is virtually impossible to achieve a solution completely free of foreign particles (Mullin, 2001).

The catalytic effect of the foreign substance is explained by a decrease in the energy barrier to nucleation if a nucleus is formed on a foreign surface (Söhnel and Garside, 1992). The overall free energy change associated with the formation of a nucleus under heterogeneous conditions ΔG_{het}, is therefore less than the corresponding free energy change, ΔG_{hom}, associated with homogeneous nucleation (see equations (2-20) and (2-22)). Therefore for a cubic nucleus:

$$\Delta G_{\text{hom}} = -N\Delta G_v + 6\sigma_{13}V_N^{2/3} \quad (2\text{-}20)$$

$$\text{N} = \frac{V_N}{v} \quad (2\text{-}21)$$

ΔG_{hom} = Free energy change associated with homogeneous nucleation (J/m^{-3})

N = Number of separate molecules present in a unit volume of the system

V_N = Volume of nucleus (m^3)

ν = Molecular volume (m^3)

$$\Delta G_{het} = -N\Delta G_v + (6\sigma_o \sigma_{13}^2 V_N^2)^{1/3} \qquad (2\text{-}22)$$

$$\sigma_o = (\sigma_{13} + \sigma_{12} - \sigma_{23})/2 \qquad (2\text{-}23)$$

Interfacial tension, σ, had been identified as an important factor controlling the nucleation process. Figure 2.4 shows an interfacial energy diagram for two solid phases and one liquid phase in contact. These are denoted by σ_{13} for contact between solid crystalline phase, (1), and liquid, (3). σ_{23} for contact between solid surface, (2) and the liquid, (3) and σ_{12}, for contact between solid crystalline and the foreign solid surface.

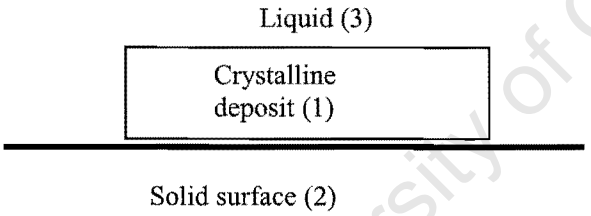

Figure 2.4 Interfacial tensions at the boundaries between three phases (two solid, one liquid) (Söhnel and Garside, 1992).

Equations (2-20) and (2-22) are not derived for definite values of N, therefore they apply to the critical nucleus. When $\sigma_o < \sigma_{13}$, then $\sigma_{13} < (\sigma_{12} - \sigma_{23})$, and therefore $\Delta G_{crit(het)} < \Delta G_{crit(hom)}$, the foreign phase reduces the energy barrier for critical nucleus formation, so acting as a nucleation catalyst.

2.2.2 Secondary Nucleation

A supersaturated solution nucleates much more readily when crystals of the solute are already present or deliberately added. This process is referred to as secondary

nucleation (Söhnel and Garside, 1992). Randolph and Larson (1988) have described secondary nucleation by six mechanisms.

Strickland-Constable (1968 in Randolph and Larson, 1988) described *initial breeding* as a crystalline "dust" adhering to larger seeds introduced into batch crystallisers. Initial breeding would occur only if seed were dry and directly introduced.

Nucleation by some sort of *fracture* process occurs in systems that produce crystals that break easily, where the suspension is very dense, and where the suspension is subjected to violent agitation or high-velocity pumping. Nucleation by *attrition* is merely fracture of a lesser degree and results from crystal-crystal interaction at high suspension densities as well as from crystal-apparatus contact. *Needle breeding* occurs because of dendritic growth on crystals, and can be reduced by lowering agitation and suspension density. Nucleation by *fluid shear* results when the fluid velocity relative to the crystal velocity is large and some of the "adsorbed layer" is removed (Randolph and Larson, 1988).

The most important source of nuclei in mixed suspension results from *contact nucleation*. It results when crystals contact the agitator, pump, flow lines or other crystals. Secondary nuclei produced by contact nucleation can be produced by energy levels far below that required for fraction or attrition. Secondary nucleation is different from heterogeneous primary nucleation in that secondary nucleation occurs on an existing crystal surface and heterogeneous nucleation occurs on a foreign substance.

(i.) Contact nucleation

Clontz and McCabe (1971 in Mullin, 2001) showed that at moderate levels of supersaturation, crystal contacts readily caused secondary nucleation of $MgSO_4 \cdot 7H_2O$, but crystal-crystal contacts gave up to five times as many nuclei as did crystal metal rod contacts. The faster growing faces were also found to produce fewer nuclei than did the slower growing faces thereby relating secondary nucleation to crystal growth (Mullin, 2001).

Strickland-Constable (1968 in Randolph and Larson, 1988) demonstrated that by sliding a growing crystal along the bottom of the beaker, nucleation was induced and in due course new crystals appeared on the bottom of the beaker. In this study we would have the same effect with crystals in contact with the wall of the reactor due to the upward and downward mixing movement of the crystals as well as crystal-crystal contact.

(ii.) Seeding

Crystal nuclei must be formed within a saturated solution as an initial step in precipitation. This however does not always occur spontaneously or it does not occur in a satisfactory manner in that fine particles are created (Weiss, 1985). Mullin (2001) suggests that the best method for inducing crystallization would be to seed the reactor. Particles that are used as seed particles include, atmospheric dust, inert amorphous materials, such as glass and silica or small crystals already present in solution (Weiss, 1985).

Seeding is used to control product size and size distribution. There are several reasons for the influential role of the size of seed crystals (Mullin, 2001). One may be that large seeds generate more secondary nuclei in agitated systems than do smaller ones because of the larger contact area. Another factor is that smaller crystals, less than 10μm, probably grow more slowly. The secondary nucleation rate was found to decrease with an increase in seed size or in the number of seeds of a given size (Mullin, 2001).

(iii.) The influence of mixing

In the case of the formation of substances with low solubility, $S = C/C^* >> 1$, very high levels of supersaturation can occur so that uncontrolled formation of solids proceeds in different regions and times, with different levels of supersaturation (Gösele and Kind, 1999). Besides varying crystal size distributions, different crystal modifications can occur, according to the level of supersaturation.

It is not possible for reagents to occur in stoichiometric ratios at all points in the crystalliser. Nielsen (1984 in Gösele and Kind, 1999) has shown that depending on the level and ratio of the ion concentrations, various crystallisation mechanisms and various precipitation products are formed. Work done by Seckler (1994) in a fluidised bed reactor also showed an inconsistent supersaturation profile throughout the bed. The supersaturation was found to decrease with bed height and high supersaturations were found near to inlet points in the reactor.

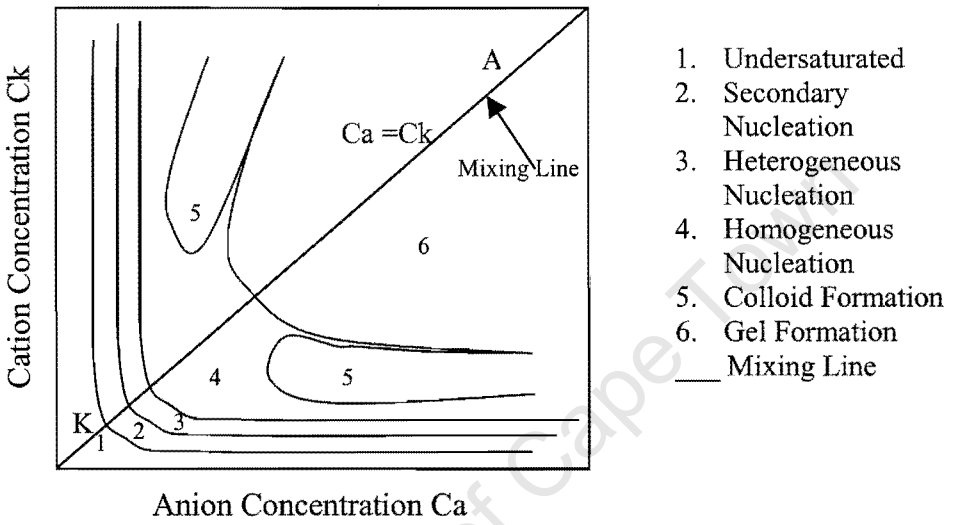

Figure 2.5 The effect of supersaturation on nucleation (Nielsen, 1984).

Figure 2.5 shows the position of various crystallisation regions. Zone 1 is an undersaturated region where no precipitation will occur. For ideal systems, the solubility curve will be a hyperbole, according to the solubility product. In real systems, this will not always be the case.

The line AK in figure 2.5 shows two possible reagent solutions. The rapid, ideal mixing of the anion containing solution A with the cation containing solution K would give a point on the line AK (mixing line). The concentrations Ca and Ck would be the same at the point of mixing for the reaction $A^+ + K^- \rightarrow AK\downarrow$ if the reagents are added stoichiometricaly. In a real reactor however we have inhomogeneity because of the high concentration of the various reactants at their feed points. It is therefore of utmost importance to facilitate good mixing in the reactor.

At very high supersaturations (regions 5 and 6) the formation of colloids and gels is observed. Colloids and gels have poor dewatering capabilities. In most instances they are not very useful products. Region 4 is the region of homogenous nucleation. They are generally small and have poor settling properties. Region 3 represents the region of heterogeneous nucleation. The starting-up conditions in the reactor are representative of region 3. At certain areas in the reactor, conditions favourable for secondary nucleation (region 2) may occur as a result of the fine particles present due to homogeneous nucleation in the fluid.

2.3 Precipitation and Growth Kinetics

The rate of crystal growth can be expressed as the rate of displacement of a given crystal face in the direction perpendicular to the face (Söhnel and Garside, 1992). The linear face growth rate, v_g having surface area A is determined by the mass flux of crystallising material to the surface according to the following relation

$$v_g = JV_m = j(V_m A) \tag{2-24}$$

v_g = Linear face growth rate (m/s)
J = Molar flux (moles/sm^2)
j = Molar deposition rate (moles/s)
V_m = Molar volume (m^3/mol)
A = Surface area (m^2)

$$j = \left({}^{dn_i}/_{dt} \right) \tag{2-25}$$

The above definition applies to sufficiently large crystals, but the growth of very small ones needs to be determined using an overall linear growth rate, r. r is defined as the time derivative of the radius of the sphere having a volume equal to the average

volume of one crystal, $\overline{V}$. Thus $r = \frac{dr}{dt}$. Crystallisation taking place in a closed system with no nucleation yields the following volume equation:

$$\overline{V} = n_i V_m / N \tag{2-26}$$

n_i = Number of moles of substance *i* deposited from unit volume of solution in the form of crystals

N = The number of crystals formed in one unit volume.

$$\overline{V}\frac{dV}{dt} = n_i \frac{V_m}{\frac{dV_o}{dr}N} \tag{2-27}$$

Söhnel and Garside (1992) describe the growth rate for crystals that are produced from new nuclei and then grow by an instantaneous overall growth rate:

$$r = \frac{-V_m}{A_s}c \tag{2-28}$$

$$c = \frac{dc}{dt} \tag{2-29}$$

c = The concentration in (moles/m^3)

A_s = Total crystal surface area present in unit suspension volume

The negative sign arises from the fact that concentration decreases with crystal growth.

2.3.1 Adsorption layer theories

Many researches have extended the concept of Volmer (1939) that atoms or molecules adsorb on a crystal face. This theory is based on thermodynamic reasoning. Söhnel and Garside (1992) describe this process as follows: Firstly a

growth unit adsorbs on the crystal surface. Part of the solvation shell is released, after which the growth unit diffuses in the adsorption layer until it either reaches a point where it is incorporated into the lattice or it leaves the adsorption layer and returns to the solution. If the growth unit reaches a point where it can be built into the lattice, it loses the remainder of the solvation shell before final lattice incorporation. Atoms, ions or molecules link to the lattice positions where the attractive forces are greatest, i.e. at the 'active centres', and under ideal conditions. This process continues till the whole plane is covered. There is also a suggestion that a monolayer island nucleus is necessary before the crystal face can continue to grow.

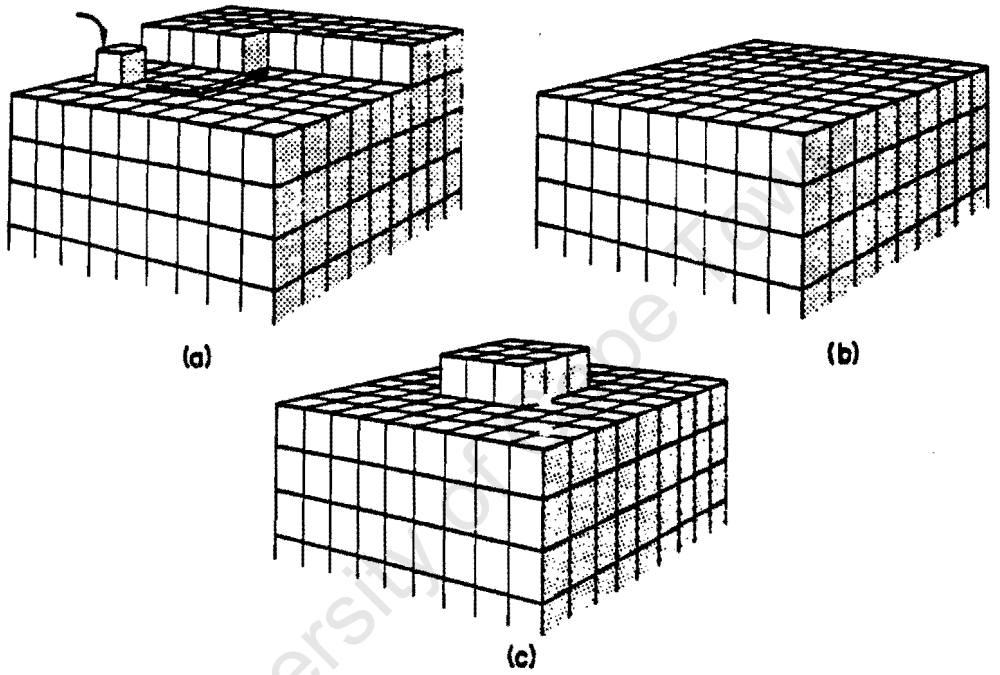

Figure 2.6 A model of crystal growth without dislocation: (a) migration towards desired location; (b) completed layer; (c) surface nucleation (Mullin, 2001)

The expressions for the energy requirement for a two-dimensional nucleation and critical size of a two-dimensional nucleus may be derived in a similar manner to that for three-dimensional nucleation (Mullin, 2001).

The overall excess free energy of nucleation may be written as:

$$\Delta G = a\gamma + \nu\Delta G_v \qquad (2\text{-}30)$$

a = Area of nucleus (m^2)

ν - Volume of nucleus (m^3)

For a circular disc the following equation is used:

$$\Delta G = 2\pi rh\gamma + \pi r^2 h\Delta G_v \quad (2\text{-}31)$$

r = Radius of nucleus (m)

h = Height of nucleus (m)

Maximising to find the critical size, r_c

$$\frac{d\Delta G}{dr} = 2\pi h\gamma + 2\pi rh\Delta G_\upsilon = 0 \quad (2\text{-}32)$$

therefore

$$r_c = -\frac{\gamma}{\Delta G_\upsilon} \quad (2\text{-}33)$$

This shows that the critical nucleus for a two-dimensional nucleus is half that of a three-dimensional one. (See equation 2-12.) Similarly,

$$\Delta G_{crit} = -\frac{\pi h\gamma^2}{\Delta G_\upsilon} \quad (2\text{-}34)$$

ΔG_v = A negative quantity

$$\Delta G_{crit} = -\frac{\pi h\gamma^2\upsilon}{kT\ln S} \quad (2\text{-}35)$$

The rate of two-dimensional nucleation, J', may be expressed in terms of the Arrhenius reaction velocity equation.

$$J' = B\cdot\exp(-\Delta G_{crit}/kT) \quad (2\text{-}36)$$

or

$$J = B \cdot \exp\left[-\frac{\pi h \gamma^2 \upsilon}{k^2 T^2 \ln S}\right] \quad (2\text{-}37)$$

The comparison of equation 2-13 and 2-35 show that with the input of some typical values, e.g.

$\gamma = 10^{-1} Jm^{-2}$

$\nu = 2 \times 10^{-29} m^3$

$h = 5 \times 10^{-10} m$

$kT = 4 \times 10^{-21} J$

the ratio between the two equations (equation 2-13 and 2-35) can be calculated and the ratio is about 50:1 for a supersaturation (S) = 1.1 and about 1.2:1 for S=10 (Mullin, 2001). It can be concluded that for two-dimensional nucleation to occur a relatively high degree of local supersaturation is necessary, but not as high as that required for three-dimensional nucleation under the same conditions.

Kossel (1934) depicted a growing crystal face to be made up of moving layers of monatomic height, which contain one or more kinks.

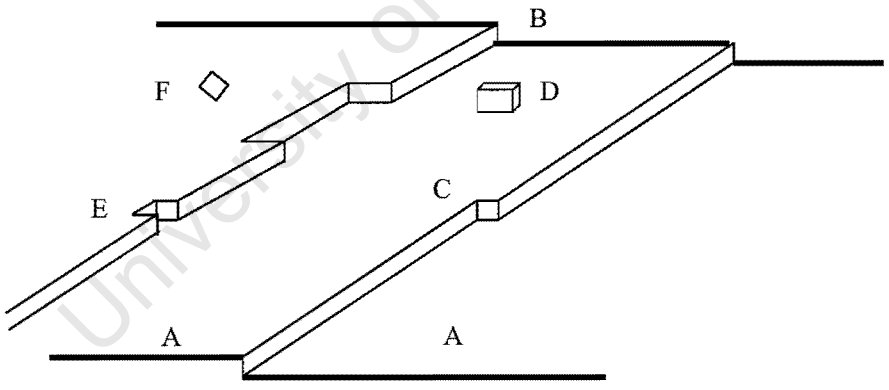

Figure 2.7 Kossel's model of a growing crystal surface showing flat surfaces (A), steps (B), kinks (C), surface-adsorbed growth units (D), edge vacancies (E) and surface vacancies (F) (Mullin 2001).

The crystal is also made up of loosely adsorbed growth units on the surface and in vacancies in the surfaces and steps. A fresh step could be created by surface

nucleation, and this often occurs at the corners. A crystal should grow fastest when its faces are entirely covered with kinks and the theoretical maximum growth rate can be estimated by

$$\frac{dr}{dt} = \frac{Dv(c-c^*)}{r} \tag{2-38}$$

r = Distance r from the centre of crystal (m)

D = Diffusion coefficient (m^2/s)

c = Solute concentration in the solution (supersaturated) (mol/dm^3)

c^* = Equilibrium saturation concentration (mol/dm^3)

v = Face growth rate (m^3/mol)

The growth rate of a crystal is not constant. Experience has led to the knowledge that a broken crystal surface repairs rapidly but grows at much slower rates (Mullin, 2001). Many crystal surfaces are seen to grow quite rapidly at low supersaturations contradicting Kossel's model and it is therefore concluded that this model does not relate to systems at low supersaturation.

2.3.2 Diffusion-reaction theories

Noyes and Whitney (1897) in Mullin (2001) considered the deposition of solid on the face of a growing crystal to be a diffusion process. It was assumed that crystallisation was the reverse of dissolution and that both rates were controlled by the difference between the concentration at the solid surface and that in the bulk of the solution.

$$\frac{dm}{dt} = k_m A(c-c^*) \tag{2-39}$$

m = Mass of solid deposited (kg)

A = Surface area of the crystal (m^2)

c = Solute concentration in the solution (supersaturated)(mol/dm^3)

c^* = Equilibrium saturation concentration (mol/dm^3)

k_m = Coefficient of mass transfer (m/s)

Taking into account a thin stagnant film surrounding the growing crystal the modified equation proposed by Nernst (1904) is as follows:

$$\frac{dm}{dt} = \frac{D}{\delta} A(c - c^*) \qquad (2\text{-}40)$$

D = coefficient of diffusion of the solute (m^2/s)

δ = length of the diffusion path (m)

Studies done by Miers (1904) led to the conclusion that the solution in contact with a growing crystal face is not saturated but supersaturated. This led Berthoud (1912) and Valeton (1924) to the following proposal. A diffusion process transports solute molecules to the solid surface from the bulk of the fluid phase, followed by a first-order 'reaction' when the solute molecules arrange themselves into the crystal lattice.

$$\frac{dm}{dt} = k_d A(c - c_i) \ (diffusion) \qquad (2\text{-}41)$$

$$\frac{dm}{dt} = k_r A(c_i - c^*) \ (reaction) \qquad (2\text{-}42)$$

k_d – a coefficient of mass transfer by diffusion (m/s)

k_r – a rate constant for the surface reaction (integration) process (m/s)

c_I – solute concentration in the solution at the crystal-solution interface (mol/dm^3)

The following diagram depicts these driving forces but it must be noted that the two forces are rarely equal, nor need the concentration drop across the stagnant film be linear (Mullin, 2001).

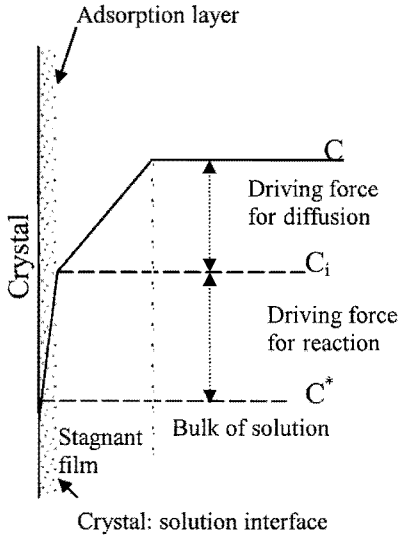

Figure 2.8 Concentration driving forces in crystallisation from solution according to the simple diffusion-reaction model

2.4 Agglomeration

Aggregation is the clustering of separate particles to form larger particles. This initial clustering may be as a result of a number of mechanisms and the particles may be held together by several different forces.

Agglomeration: clustering of particles formed initially to construct more or less strong secondary particles held together by crystalline bridges but also sometimes physical forces (Söhnel and Garside, 1992).

Coagulation: a specific case of agglomeration occurring only with very small particles when the clusters are bound by physical forces alone. In this study we will only examine agglomeration.

Agglomeration consists of three steps (Franke and Mersmann, 1995):

1. The collision of particles;
2. the staying together of particles and
3. the formation of crystalline bridges between these particles.

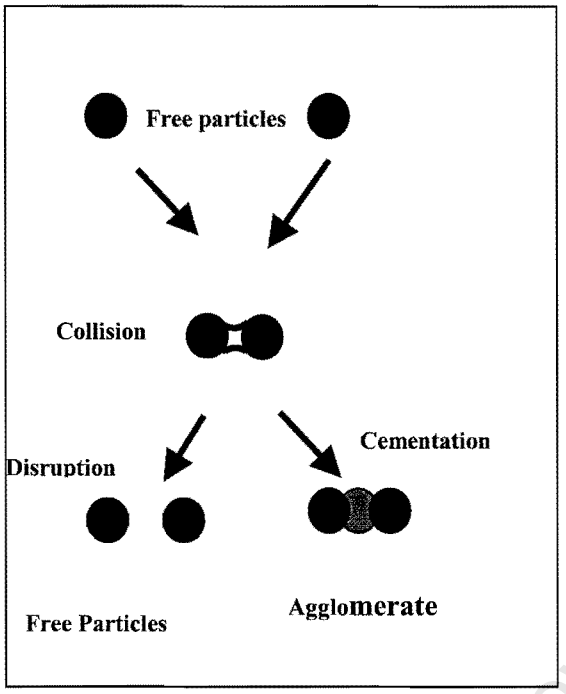

Figure 2.9 Schematic representation of agglomeration (Guillard, 2001)

During agglomeration, isolated particles in the initial dispersion form entities of larger size that can be bound by either weak or strong bonds. The total number of particles is thus decreased and the specific solid phase area is reduced. The rate of agglomeration, and thus the stability of the system, is determined by the forces prevailing in the dispersion, mainly between the solid particles. These forces may be attractive or repulsive (Söhnel and Garside, 1992). Repulsive electrical forces arise from the electromagnetic interactions of the charged layer surrounding the particles, the so-called electrical double layer. Because the system as a whole is electrically neutral, the charge on the solid surface must be balanced by an equal charge (but having an opposite sign) in the solution adjacent to the particle. The double layer thereby penetrates into the liquid and is distributed by random molecular motion. The liquid adjacent to the particle is termed the diffusion layer. The overall potential gradient E, between the solid surface and the liquid is termed the Nernst potential and is made up of the potential corresponding to the immobile layer at the surface as well at that of the diffusion layer (ζ) thus:

$$E = \phi + \zeta \tag{2-43}$$

E = Potential gradient (V)

ϕ = Potential corresponding to the immobile layer at the surface (V)

ζ = Potential corresponding to that of the diffusion layer (V)

Electrical repulsive forces arise due to electrostatic interactions within the double layer surrounding the particles and it is here that the zeta potential ζ, is of significance (Söhnel and Garside, 1992). The ϕ potential is defined as the gradient between the interface of the colloid and the body of solution. The ζ potential is the gradient between the slipping plane of the body of solution and is related to the particle charge and the thickness of the double layer. The thickness of the double layer X is inversely proportional to the concentration and valence of nonspecific electrolytes as shown in figure 2.10 (Eckenfelder, 1966).

The repulsive forces within the double layer surrounding the particles are due to electrostatic forces and are necessary to induce nucleation (Eckenfelder, 1966). A high zeta potential means that particles will repel one another and dispersion will be stable. However if the potential is small, then attractive forces will prevail. The particles then tend to form larger ones by agglomeration (Eckenfelder, 1966).

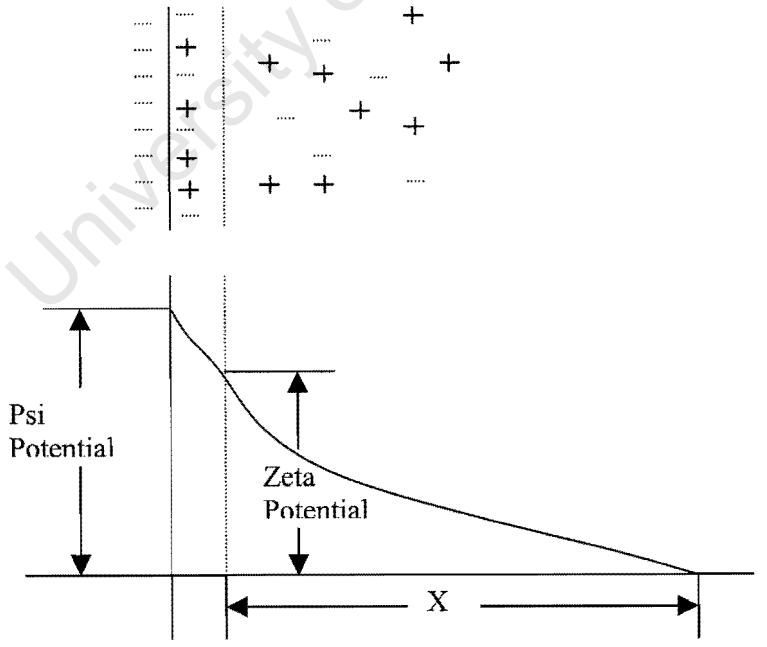

Figure 2.10 Electrochemical properties of a colloid particle

2.5 Precipitator Design

Many precipitation reactors are designed according to general chemical engineering techniques, rather than on the direct application of crystallisation kinetics. Theory however, is often used in trouble-shooting and predicting responses to changes of process conditions (Söhnel and Garside, 1992).

Often the size and shape of crystals are important and can be controlled by various mixing techniques in precipitation reactors. A narrow size distribution within a batch reactor is obtained with rapid nucleation that is abruptly stopped to allow crystal growth. Better mixing results in greater average supersaturations and higher nucleation rates and also smaller crystal sizes. Feed point locations were found to be of importance in inadequately stirred systems (Henning, 1990).

Semi-batch reactors were found to yield larger crystals by reducing the concentrations of reactant concentrations (Mullin *et al*, 1982 in Söhnel and Garside, 1992). In a mixed suspension mixed product removal (MSMPR) continuous precipitation reactor, a wider crystal size distribution (CSD) occurs. Reactant fed into this precipitator separately increases the mixing intensity and residence time increases the crystal size (Söhnel and Garside, 1992). Local supersaturation varies around the mixing points and an increase in the reactant concentration has little influence on the CSD. Premixing however, increases the mixing intensity and decreases the concentration, resulting in an increase in particle size (Pohoreki and Baldyga, 1988 in Söhnel and Garside, 1992).

In water treatment, the size distribution of the particles is often of secondary importance to the removal efficiency of the undesirable component. In the above reactors it is often necessary for the precipitator to be followed by a filtration process (Söhnel and Garside, 1992). An alternative water treatment technique uses a fluidised bed reactor (Scholler *et al*, 1987; Seckler, 1994; Guillard and Lewis, 2001; Zhou *et al*, 1999; Wilms *et al*, 1988; Nielsen *et al*, 1997) that if run effectively, would eliminate the need for post filtration.

Advantages of the fluidised bed:

- The fluidised bed is compact and has relatively low investment costs (Wilms, *et al.*, 1988).
- Operating efficiently it eliminates the need for solid/liquid separations.
- Provides a large surface area for precipitation to take place.
- The fluidised bed system is a continuous process.
- The fluidised bed provides excellent mixing within the reactor.

The technology was based on inducing the nucleated (carbonate/hydroxide/sulphide) precipitation of heavy metals on a sand surface. The relative importance of individual processes such as the precipitation upon the grains, primary nucleation, abrasion and aggregation depends on the supersaturation profile and thus on the hydrodynamic conditions in the bed as well as on the presence of impurities (Seckler 1994). The local supersaturation determines the nature of the crystalline phase, the kinetics of nucleation, growth and aggregation. Hydrodynamics is important in the sections of the reactor where mixing takes place, since localised high supersaturation can occur as a result of poor macromixing. The high local supersaturation induces high nucleation rates and therefore produces many fines (Seckler 1994).

The fluidised bed reactor has been applied to the softening of drinking water by DHV, a consultancy and engineering group in the Netherlands. $CaCO_3$ pellets are produced by precipitation in these reactors and sold to the livestock feed industry (Wilms *et al,* 1988). Seckler (1994) used a fluidised bed for the successful precipitation of calcium phosphate. An 80% removal of phosphate was achieved in the presence of carbonate or magnesium ions. Wilms *et al* (1988) also used a fluidised bed reactor for phosphate removal.

Guillard and Lewis (2001) investigated nickel carbonate removal in a fluidised bed. Nickel removal of 97.2% was achieved as nickel carbonate on sand pellets. Zhou *et al* (1999) describe a process by Nielsen *et al* (1997) for the removal of heavy metal in a fluidised bed by adsorption and coprecipitation using ferric oxyhydroxide or manganese dioxide as a coating on granule surfaces. The experiments were however carried out at low concentrations below 0.64mg/l. A 95% removal efficiency was

achieved by means of carbonate precipitation from 10 and 20mg/l influent streams in a fluidised bed reactor (Zhou *et al*, 1999).

Peters *et al* (1998) proposed the use of sulphide precipitation as a viable alternative for the removal of heavy metals from water as it is more effective than hydroxide precipitation. Robinson (1980 in McAnally *et al* 1984) proposed an optimum sulphide to heavy metal ratio in the range of 1.0 – 2.5 times the stoichiometric sulphide reagent demand. The rate of the precipitation reaction was found to increase with the use of H_2S (van Hille, 2001). Sulphides added in a soluble form will produce soluble H_2S at acidic pH values. The above technology will be applied in this thesis where copper sulphide is precipitated in a fluidised bed on a sand surface.

2.6 Factors

Four variables, determined to be important to the precipitation process, were identified from literature; A = S:Cu ratio, B = [Cu] (ppm), C = fresh feed flow rate (ml/min) and D = Recycle Flow rate (ml/min), to be used in a one-half replicate of a 2^4 factorial design in order to calculate the coefficients in a first order response. S:Cu ratios ranged between 1:1 and 1.5:1. Preliminary experiments showed that ratios with a significant excess of sulphide produces very fine, unfilterable particles. Insufficient sulphide would not remove the copper adequately therefore the minimum ratio of S:Cu was 1:1. The copper concentration range used in this work of between 50 and 150 was obtained from base metal refining and metal finishing plants (Moosa, 2000). The upper levels of the flow rates of the inlet streams (30 – 50ml/min) and re-circulation stream (101 – 181ml/min) were chosen so as to maximise the re-circulation rate without lifting sand particles out of the bed. The lower levels were chosen to investigate a tighter packed bed but at the same time treating as much effluent as possible.

pH was found to be very influential in the carbonate and hydroxide process. However due to the absence of the exchange of OH^- ions it was found that pH was not as important a factor. Low pH values were not used due to the formation of toxic H_2S gas (Kim, 1980; Bhattacharyya *et al*, 1981 and Peters *et al*, 1983). McNally *et al* (1984) obtained high nickel removal at a pH of 14. This would not be a viable

process as metal rich streams are usually very acidic and it would mean the addition of large quantities of base to increase the pH, then post-treatment to reduce the pH to within the discharge limit.

Chapter Three

Solubility Theory

3.1 Solubility

The calculation of solubility limits has become standard procedure (Thoenen, 1999) in the measure of efficiency of a system in precipitating metals from aqueous solutions. These calculations are based on the assumption that the process is controlled by thermodynamics rather than kinetics.

From a thermodynamic point of view, solubility considerations are of great concern in precipitation as the determination of the remaining metal concentrations in the solution, at equilibrium, allows the assessment of the precipitation process efficiency. The construction of these diagrams is a complex process and involves simultaneously solving a number of mass action expressions. Modern simulation packages provide a convenient method for performing such calculations. This chapter investigates solubility curves for the copper sulphide system and illustrates the diversion of the solubility curves from each other due to the use of different solubility constants.

A number of different authors (Baltpurvins *et al*, 1996, Dryssen, 1988, Smith and Martell, 1976, Bollinger, 1992 and Licht, 1988) have compiled lists of values of *solubility products* for a wide range of metal-hydroxides, carbonates and sulphides that differ markedly from each other. The reasons for these differences are as follows (Stumm and Morgan, 1996):

(i) The formation of a sparingly soluble phase (solubility less than 0.01mol per L (Ebbing, 1990)) and its equilibrium with the solution is a more complicated process than equilibrium reactions in a homogeneous solution phase (all species present in one phase).

(ii) The composition and properties, that is, reactivity, of the solids vary for different modifications of the same compound or for different active (disordered) forms of the same modification.

(iii) Species influencing the solubility equilibrium (e.g., species formed by hydrolysis, ion-pair, or complex formation) have been overlooked in defining K_{s0}.

Thermodynamically modelled solubility limited systems are often questionable if the following fundamental principles are not adhered to (Thoenen, 1999):

(i) The solubility-limiting solid must form under the relevant geochemical conditions (e.g. pressure, temperature and composition)
(ii) The required thermodynamic data for the solubility-limiting solid must be reliably known.
(iii) All relevant aqueous complexes involving the element under consideration must be accounted for, and their *complexation constants* must be reliably known.

3.1.1 Solubility Product

Metal sulphide precipitates form when a metal cation reacts with a sulphide ion in an aqueous solution. The solubility product (mass action product for sparingly soluble salts) of the metal sulphide, K_{sp}, for a divalent metal ion is given by:

$$M_xS_y \Leftrightarrow xM^{2y/x+} + yS^{2-} \tag{3-1}$$

$$\Rightarrow K_{sp} = \frac{(a_{M^{2y/x+}})^x (a_{s^{2-}})^y}{(a_{M_xS_y})} \tag{3-2}$$

where a_i is the activity of the i^{th} species (Licht, 1988).

3.1.2 Activity and activity coefficient

$$a_A = [A^+] \times \gamma_A \tag{3-3}$$

a_A - Activity (mol/dm^3)
$[A^+]$ - Concentration (mol/dm^3)

γ_A - Activity Coefficient

Ebbing (1990) showed that for very dilute solutions (less than 0.01 mol/dm^3), activities may be taken as practically equal to the concentration. In addition this relationship applies for the purposes of quantitative analysis, only to saturated solutions of slightly soluble electrolytes. Due to the need for a saturated solution during precipitation the electrolyte system presented in this thesis satisfies the requirements of the above assumption. Therefore when evaluating the relevant thermodynamic equations for solubility constants, concentrations will be used in equation 3-2 instead of activities.

3.1.3 Hydrogen Sulphide Chemistry

Many metal sulphides are insoluble in water, but dissolve in acidic solutions. The change in solubility with pH, or hydrogen-ion concentration, can be used to separate a mixture of metal ions. The equilibria between H_2S, HS^- and S^{2-} (Licht *et. al.,* 1988) is given by equations (3-4) and (3-5).

$$H_2S \Leftrightarrow 2H^+ + S^{2-} \qquad K_1 = 1.0 \times 10^{-24.3} \qquad (3\text{-}4)$$

$$HS^- \Leftrightarrow H^+ + S^{2-} \qquad K_2 = 1.0 \times 10^{-17.3} \qquad (3\text{-}5)$$

Studies by Rao and Hepler (1977) and others suggest that the value for K_2 has been underestimated. These values vary from 10^{-13} to as low as 10^{-19} (Licht, 1988), but these questions are beyond the scope of this thesis. The concentration of various sulphur species is a strong function of pH, as shown in Figure 3.1 using K_{sp} (equation (3-6) and (3-7) values from Peters *et al* (1983) as opposed to global constants as in equation (3-4) and (3-5) from Licht (1988).

$$H_2S \Leftrightarrow H^+ + HS^- \qquad K_{sp1} = 1.0 \times 10^{-7} \qquad (3\text{-}6)$$

$$HS^- \Leftrightarrow H^+ + S^{2-} \qquad K_{sp2} = 1.2 \times 10^{-13} \qquad (3\text{-}7)$$

For low pH conditions (ph < 4), the predominant species is $H_2S_{(aq)}$. The $H_2S_{(aq)} \Leftrightarrow H_2S_{(g)}$ equilibrium will result in a portion of the H_2S being lost into the air.

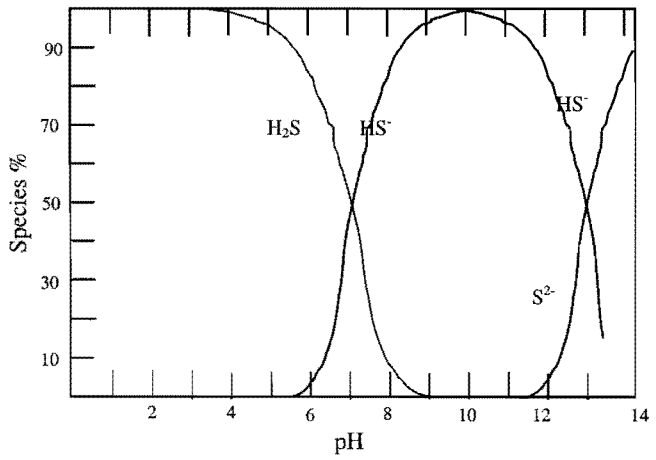

Figure 3.1 $H_2S - HS^- - S^{2-}$ equilibria

To be strictly correct, the solubility domain of a particular metal in an aqueous sulphide environment must be defined in terms of both sulphide and hydroxide precipitation as they will not occur alone but in competition with each other. The final solubility domain will be determined from a superimposition of the sulphide and hydroxide solubility diagrams (Tunay and Kabdasli, 1994).

The approach to drawing a metal hydroxy-sulphide solubility curve taken in this thesis is as follows:

1. Determination of the known and potential hydroxide and sulphide solids aqueous complexes and compounds that form.
2. Determination of the solubility products from literature. Calculations made at zero ionic strength and 25°C.
3. Determination of the solubility system (hydroxide or sulphide), under specific operating conditions (pH, sulphide concentration).
4. Definition of zone or lower solubility by the construction of phase diagrams.

Commercially available software, such as ASPEN PLUS™ and OLI Systems Inc. ESP, integrate large databases to construct thermodynamically and kinetically stable systems. These do not always reflect the real behavior of the system.

3.2 ASPEN PLUS™

In electrolyte systems, species dissociate partially or completely in solution and/or precipitate as salts. Aspen Plus™ provides extensive built in parameters for the Electrolyte Non-Random Two Liquid (NRTL) model and is able to generate the species and reactions using built-in knowledge of base reactions, equilibrium constant data and possible ionic species.

The Electrolyte NRTL model calculates activity coefficients, enthalpies and Gibbs energies. It accommodates very low and very high concentrations as well as handling aqueous and mixed solvent systems. The solubility of supercritical gases are modelled using Henry's law and the Redlich-Kwong equation of state is used for all vapour phase properties.

ASPEN PLUS™ is used to model metal removal from a waste stream by a precipitation process. A block flow diagram illustrates the equipment used as well as input streams for the simulation. In this thesis Aspen Plus™ is used to predict the thermodynamically stable species that precipitate at the specified conditions. The simulation will generate a graph of mass flow of precipitate as a function of pH in order to predict the optimum pH at which to operate the system in order to achieve maximum removal of metals from the system.

3.3 OLI Systems Inc.

OLI Systems uses a similar predictive thermodynamic framework for calculating the physical and chemical properties of multi-phase, aqueous-based systems. The aqueous simulation leads to the understanding of aqueous chemistry and simulates the effects of components, pH, temperature and other factors in chemical processes.

OLI Systems Inc. StreamAnalyzer™ and CorrosionAnalyzer™ use well-known thermodynamic equations in order to calculate activity coefficients (Extended form of Bromley equation is used to extrapolate when data is limited or unavailable), ion-molecule and molecule-molecule interactions (Pitzer model) and standard state properties (Helgeson-Kirkham-Flowers equations of state). Vapour phase fugacity

coefficients for non-ideal systems are calculated using the Soave Redlich-Kwong (SRK) equations of state.

OLI Systems StreamAnalyzer™ is also used to simulate metal removal from a waste stream by a precipitation process. Experimental input conditions are used to generate solubility curves that predict the metal precipitate as a function of pH.

Chapter Four

Fluidised Bed Reactor

4.1 Fundamentals of fluidised bed technology

When fluid is passed upwards through a bed of particles the pressure loss in the fluid due to frictional resistance increases with increasing fluid flow (Rhodes, 1998). A point is reached when the upward drag force exerted by the fluid on the particles is equal to the apparent weight of particles in the bed. At this point the fluid lifts the particles, the separation of the particles increases, and the bed becomes fluidised. The force balance across the bed is due to the fluid pressure loss across the bed of particles and is equal to the apparent weight of the particles per unit area of the bed (Coulson and Richardson, 1980).

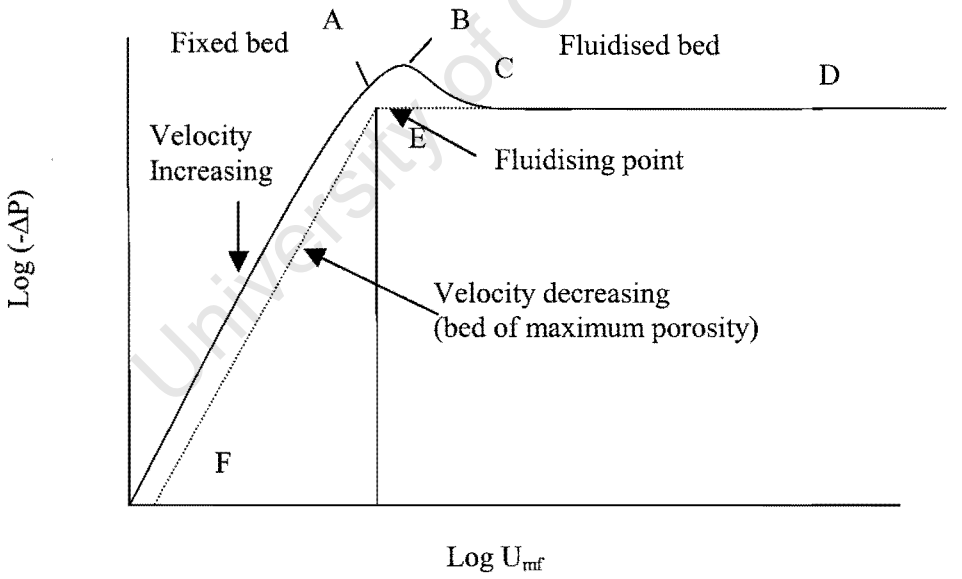

Fig. 4.1 Pressure drop over fixed bed and fluidised bed (Coulson and Richardson, 1980)

A graph of the pressure across the whole bed is plotted against velocity, on logarithmic coordinates in Figure 4.1. The figure shows that a linear relationship exists between the origin and point A. The slope moves towards a maximum as the bed begins to expand. As the velocity is increased, the pressure drop passes through a

maximum value (B) and stabilises to an approximately constant value, independent of fluid velocity (CD). If the velocity is reduced, the bed contracts until it reaches a condition where the particles are just resting on one another (E) (Coulson and Richardson, 1980). This is the maximum stable porosity of a fixed bed. Decreasing the velocity from E to F results in a decreased pressure drop across the bed, compared to the pressure drop on initially increasing the velocity from the origin to A.

The relationship for the total frictional force in a fluidised bed is given by equation (4-1).

$$\Delta p = (1-e)(\rho_s - \rho)\lg \tag{4-1}$$

Δp = Pressure drop across the bed (Pa)
e = Bed voidage
l = Bed Depth (m)
ρ_s = density of solid (kg/m^3)
ρ = Density of fluid (kg/m^3)
g = gravitational acceleration (m/s^2)

As the upward flow is increased, the point of incipient fluidisation is reached and the fluid freely supports the particles. The voidage of the bed in this condition (e_{mf}) is approximately 0.4 (Coulson and Richardson, 1980). The corresponding minimum fluidisation velocity (u_{mf}) is calculated as follows for streamline flow:

$$u_{mf} = 0.0055 \frac{e_{mf}^3}{1-e_{mf}} \frac{d^2(\rho_s - \rho)g}{\mu} \tag{4-2}$$

e_{mf} = bed voidage
d = diameter of particles (m)
ρ_s = density of solid (kg/m^3)
ρ = Density of fluid (kg/m^3)
μ = viscosity of the fluid (cP)

When particles are too large for streamline flow a more generalised equation such as the Ergun equation is needed for the pressure gradient (Rhodes, 1998).

$$\frac{-\Delta P}{l} = 150\frac{(1-e_{mf})^2}{e_{mf}^3}\frac{u_{mf}d\rho}{\mu} + \frac{1.75}{e_{mf}^3}\left(\frac{u_{mf}d\rho}{\mu}\right)^2 \quad (4\text{-}3)$$

Substituting for the voidage at the point of incipient fluidisation gives an expression in terms of the minimum fluidisation velocity u_{mf}.

$$\frac{\rho(\rho_s-\rho)gd^3}{\mu^2} = 150\frac{1-e_{mf}}{e_{mf}^3}\frac{u_{mf}d\rho}{\mu} + \frac{1.75}{e_{mf}^3}\left(\frac{u_{mf}d\rho}{\mu}\right)^2 \quad (4\text{-}4)$$

The Galileo number (Ga) and the Reynold's number at the minimum fluidisation velocity (Re'_{mf}) are shown by equations (4-5) and (4-6) respectively:

$$Ga = \frac{\rho(\rho_s-\rho)gd^3}{\mu} \quad (4\text{-}5)$$

$$Re'_{mf} = \frac{u_{mf}d\rho}{\mu} \quad (4\text{-}6)$$

Therefore following from equation (4-4) the Galileo number may be written as:

$$Ga = 150\frac{1-e_{mf}}{e_{mf}^3}Re'_{mf} + \frac{1.75}{e_{mf}^3}Re'^2_{mf} \quad (4\text{-}7)$$

In order to predict the minimum fluidisation velocity, the Galileo number is firstly calculated from equation (4-5). The Galileo number is then substituted into equation (4-7) and the quadratic equation is solved in order to calculate Re'_{mf}. Re'_{mf} is then substituted into equation (4-6) to calculate u_{mf}.

Liquid-fluidised systems are generally characterised by the regular expansion of the bed, which takes place as the velocity increases from the minimum fluidisation velocity to the terminal falling velocity of the particles. Therefore the terminal falling

velocity (in a laminar flow system) is considered to be the maximum fluidisation velocity specified by equation (4-8).

$$u_{oA} = \frac{d^2 g}{18\mu}(\rho_s - \rho) \qquad (4\text{-}8)$$

4.2 Use of the seeded fluidised bed reactor for metal removal

The fluidised bed works on the principle that the metal-bearing waste is pumped vertically upward through the fluidised bed and at the same time, the alkaline solution is injected into the side of the column. The process is based on the heterogeneous nucleation of the metal onto seed grains in the reactor. The sand bed provides a large surface area for precipitation. As the sand grains become coated with a precipitate, they become heavier and accumulated at the bottom of the reactor. These are then removed from the bottom of the reactor and replaced by fresh ones at the top. Un-reacted metal exits the column as soluble metal ions or as fine particles (Seckler, 1994). A block flow diagram (figure 4.2) shows the two inlet and two outlet streams for the system.

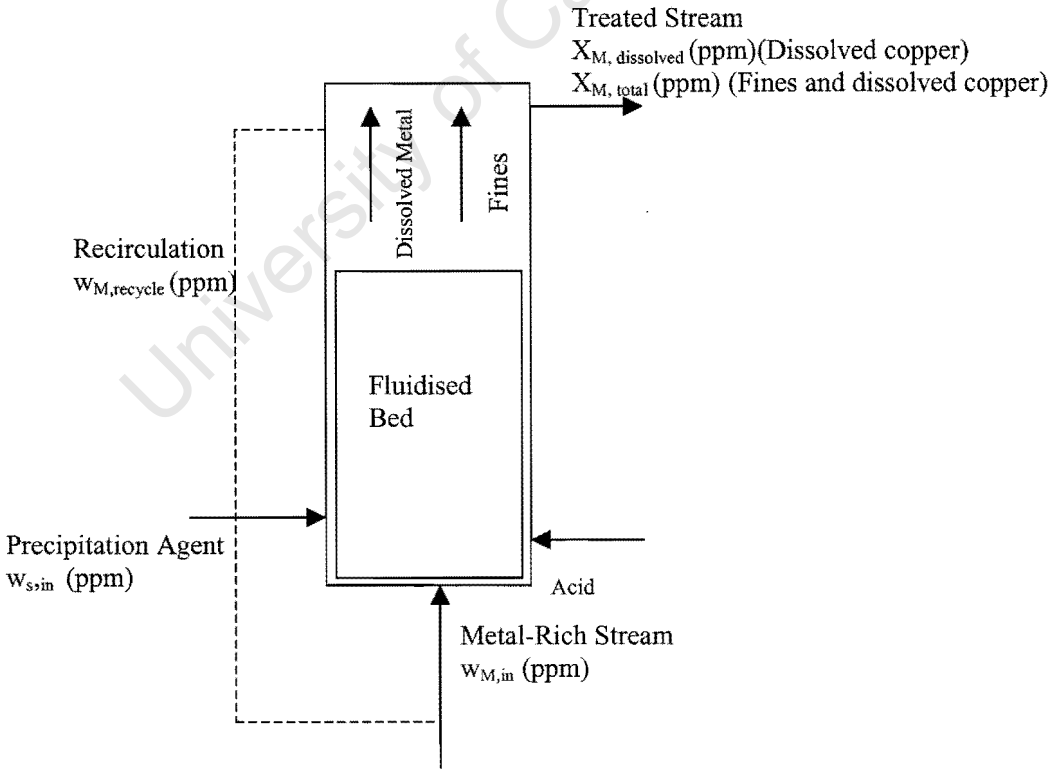

Figure 4.2 Schematic representation of the fluidised bed

4.2.1 Supersaturation comparison

Supersaturation ratio (S) is defined by the following equation from Söhnel and Garside (1992):

$$S = C/C^* \tag{4-9}$$

C = Aqueous concentration (mol/l)

C^* = Aqueous concentration at equilibrium (mol/l)

A comparison of the supersaturation for the experiments performed at steady state is calculated by taking into account the inlet concentrations of all the components as well as the concentration of ions in the recycle stream. The concentration of the ions in the recycle stream was taken to be equal to that of the effluent stream. Therefore, a measure of the outlet ions, from AA analysis, was used as a measure of ions in the recycle. c_{eq} is a constant value for the copper sulphide system experiments. The limiting solubility is very difficult to measure for sparingly soluble systems. The K_{sp} value for copper sulphide is $10^{-35.1}$ (Peters *et al*, 1983). As a result of this low value it would be impossible to accurately measure equilibrium concentrations at this value using AA analysis.

Homogeneous, heterogeneous nucleation and aggregation are dependent mainly on the supersaturation profile within the bed and thus on the hydrodynamic conditions (Seckler, 1994). Hydrodynamics is particularly important near the inlet points, where the mixing of reagents takes place and homogeneous nucleation resulted in the formation of fines. Fluidisation increases the amount of fines due to abrasion of particles not firmly cemented to the sand.

The streams defined in figure 4.2 are used to determine the metal removal efficiency (η) (dissolved + fines) and the metal conversion (X) and are defined as follows:

$$\eta = 100 \times \frac{(w_{M,in} - w_{M,total})}{w_{M,in}} \tag{4-10}$$

$$X = 100 \times \frac{(w_{M,in} - w_{M,dissolved})}{w_{M,in}} \quad (4\text{-}11)$$

$w_{M,in}$ = Flow of the component metal at the inlet of the reactor (ppm).

$w_{M,,total}$ = Flow of the dissolved and fines metal at the outlet (ppm).

$w_{M,dissolved}$ = Flow of the dissolved metal (obtained by filtering off the fines) at the outlet (ppm).

Figure 4.3 is a graphical representation of equations (4-10) and (4-11).

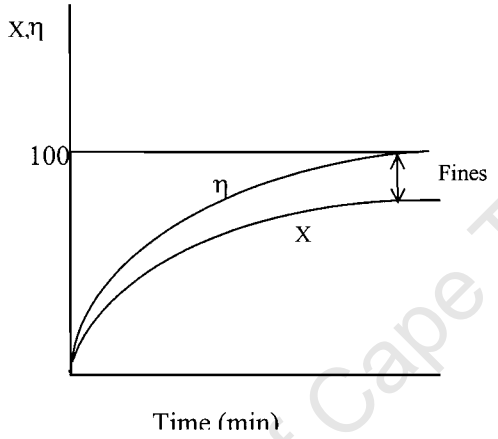

Figure 4.3 Efficiency (η) and Conversion (X) expressed graphically as a function of time.

4.2.2 Seeding of the Reactor

Nucleation has been extensively reviewed in Chapter 2. One of the best methods for inducing precipitations is to seed a supersaturated solution (Weiss, 1985). Sand has been identified as a viable seed for the precipitation process in the fluidized bed (Seckler, 1994; Zhou *et al*, 1999; Guillard and Lewis, 2001). A diameter of 0.2-0.5mm has been identified as good sand size (Söhnel and Garside, 1992). Seckler (1994) used sand grains within the range of 0.2 – 0.6mm.

4.2.3 Factors affecting supersaturation

Supersaturation is of critical importance to the precipitation process. Therefore by investigating the factors that influence the supersaturation in the reactor, the efficency of the process can be maximized by operating at these conditions.

pH was found to be a critical parameter for carbonate precipitation (Guillard and Lewis, 2001; Seckler 1994; Zhou *et al,* 1999; Wilms *et al,* 1988; Mcanally *et al,* 1984). The advantage of sulphide precipitation is that due to the low solubility limits, compared with that of hydroxide or carbonates, metals precipitated readily over a wider range of pH values (Kim, 1981; Bhattacharyya *et al,* 1981; Feng *et al,* 2000; Peters and Ku, 1998; Mcanally *et al*, 1984).

Guillard and Lewis (2001) identified the metal/carbonate ratio, pH and inlet metal feed as being the most important factors affecting supersaturation in the fluidized bed reactor. This is consistent with the findings of other researchers (Zhou *et al,* 1999; Wilms *et al,* 1988; Mcanally *et al,* 1984). The recirculation rate could not conclusively be included as an important factor by Guillard and Lewis (2001) as it was constrained by a very narrow operating range due to the height of the column. However, Seckler (1994) identified the recirculation as an important factor in phosphate precipitation because of the low efficiencies obtained by a single pass. Homogeneous nucleation produced fine particles in the fluidized bed and these exited the reactor with the liquid effluent (Seckler, 1994). Wilms *et al* (1988) identified that if the metal inlet concentration was too high, a higher recirculation ratio (Equation 4-12) was in order to decrease the supersaturation levels in the column and inhibit spontaneous nucleation and the formation of fines.

$$RR = \frac{w_{M,Recycle}}{w_{M,in} + w_{S,in}} \qquad (4\text{-}12)$$

RR = recirculation ratio

$w_{M,Recycle}$ = Flow of the component metal in the recycle stream of the reactor (ml/min).

$w_{S,in}$ = Flow of the component sulphide at the inlet of the reactor (ml/min).

$w_{M,in}$ = Flow of the component metal at the inlet of the reactor (ml/min).

Nickel loading studies performed by Wilms *et al* (1988) showed that an increase in loading increased the total nickel in the effluent but that the soluble nickel was unaffected. This is due to the increased supersaturation promoting spontaneous nucleation of fine particles.

4.2.3 Start-up and shut down

At the start of each new experiment fresh sand was placed in the column to a constant height of 90cm and the reactor was flushed with 3*l* of CuSO4.5H2O to ensure homogeneity for each new experiment. The inlet concentration in the tank as well as at the top of the column was measured prior to the start of each experiment. It was thus possible to monitor the start-up and the gradual shift towards steady state of the system. Guillard (2000) reached steady state within the first hour of operation.

Following the example of Guillard (2000) a test was performed to investigate the behaviour of the sulphide precipitate on the sand pellets by introducing water into the system at reactor inlets and maintaining the experimental flow rates. These results would confirm attrition if there was an increase in the amount of fines detected after a period of time, subsequent to the cessation of reactant flow into the column. No precipitation would be expected to occur if there were no reactants entering the system to ensure supersaturation.

The shut down of the system was achieved by initially reducing the flow rate to a reasonable flow. This was done to ensure that the pressure within the pipes did not cause any rupture when the clamps on the pipes were tightened to prevent back flow into the reactant feed tanks. The clamp was closed swiftly and the feed pump switched off. The feed pumps were always switched off first, followed by the acid pump and the recycle pump last. Switching off the recycle pump first would cause unnecessary pressure at the base of the column when switching off the inlet flow.

Selected preliminary experiments investigated the growth of the precipitate on the seed particle and the sand was therefore not removed from the column but left for a number of days. The particles were then investigated at the SEM unit.

4.2.4 Polishing

Precipitation does not work effectively at removing very low concentrations of metal ions in solution (Zhao and Duncan, 1997). Experiments performed in the fluidised bed reactor reduced metal concentration in synthetic effluent streams to as low as

2ppm but this is not low enough to meet most legislative requirements. Discharge limits for drinking water are 0.5 to 1ppm of copper SABS (2001). An even lower limit is required for discharge streams into rivers. The acceptable limit for copper is 0.1ppm (The South African Department of Water Affairs and Forestry, 1988). This was determined to be 1/10 of the LC_{50} (i.e. the concentration to kill 50% off specific warm and cold water fish or aquatic invertebrate species).

Heavy metals can be removed from aqueous solutions by sorption onto a variety of biological material, including *Azolla filiculoides*. In some areas in South Africa this Azolla rapidly takes over water surfaces to form a dense mat. As a result it is sometimes necessary to control the reproduction of this aquatic fern. Azolla is capable of removing heavy metals to low residual concentrations. Zhao and Duncan (1997) performed nickel removal studies, by sorption onto Azolla, using a waste stream from an electroplating plant in Port Elizabeth. They used equation (4-12) to plot Langmuir isotherms in order to model the metal loading capacity of the Azolla.

$$\frac{C_e}{q_e} = \frac{1}{(X_m b)} + \frac{C_e}{X_m} \qquad (4\text{-}12)$$

X_m = Maximum adsorption capacity
b = Adsorption energy
q_e = Metal uptake (metal/g of biomass)
C_e = Equilibrium concentration of metal (mg/l)

The nickel uptake was found to be consistent with the Langmuir isotherms well. The loading was found to be pH dependent. Metal binds to the Azolla within the first 10 minutes. Figure 4.5 shows the nickel removal as a function of time at different nickel loading concentrations (Kratochvil, 1997). As expected higher loading results in lower removal efficiencies. Similar experiments assessing the adsorption of copper by Azolla, were performed by van Hille (in press).

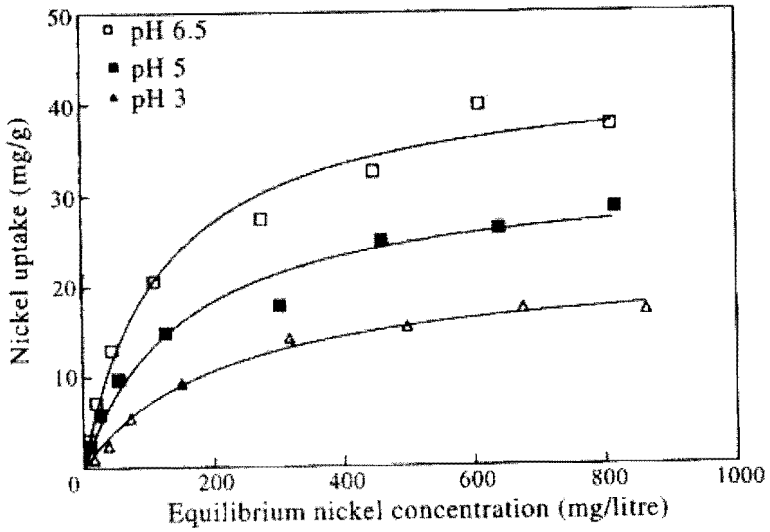

Figure 4.4 Adsorption isotherms for Azolla-Ni system. Temperature 18 ℃; incubation time, 5 hours; biomass 4g/l.

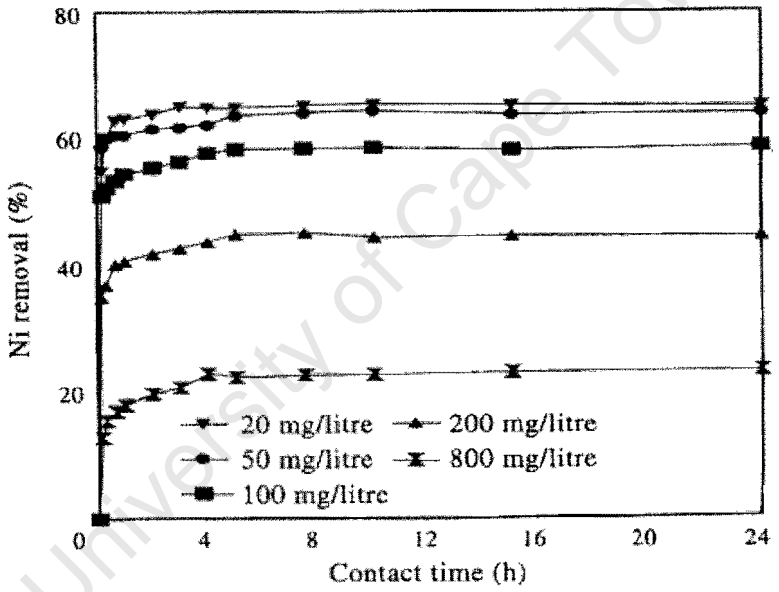

Figure 4.5 Effect of contact time on the sorption of Ni by Azolla biomass at pH 6.5. biomass 4g/l.

According to Kratochvil (1997) the most effective apparatus for the sorption process is a fixed-bed column. A fixed bed makes best use of the concentration difference used as the driving force. The fixed bed is similar to the fluidised bed except that there is no fluidisation. The same equations (4-1) may be used to calculate the pressure drop. For higher flow rates the Ergun equation (4-3) may be used as a semi empirical correlation for the pressure drop (Coulson and Richardson, 1980).

Chapter Five

Equipment and Procedure

5.1 Experimental Equipment and Procedure

5.1.1 Experimental set-up

The pellet reactor system is shown in figure 5.1. The reactor consists of a 1.5m high and 0.025m ID cylindrical vessel filled to a height of 90cm with beach sand (SiO_2) (250-500μm) as a seed material.

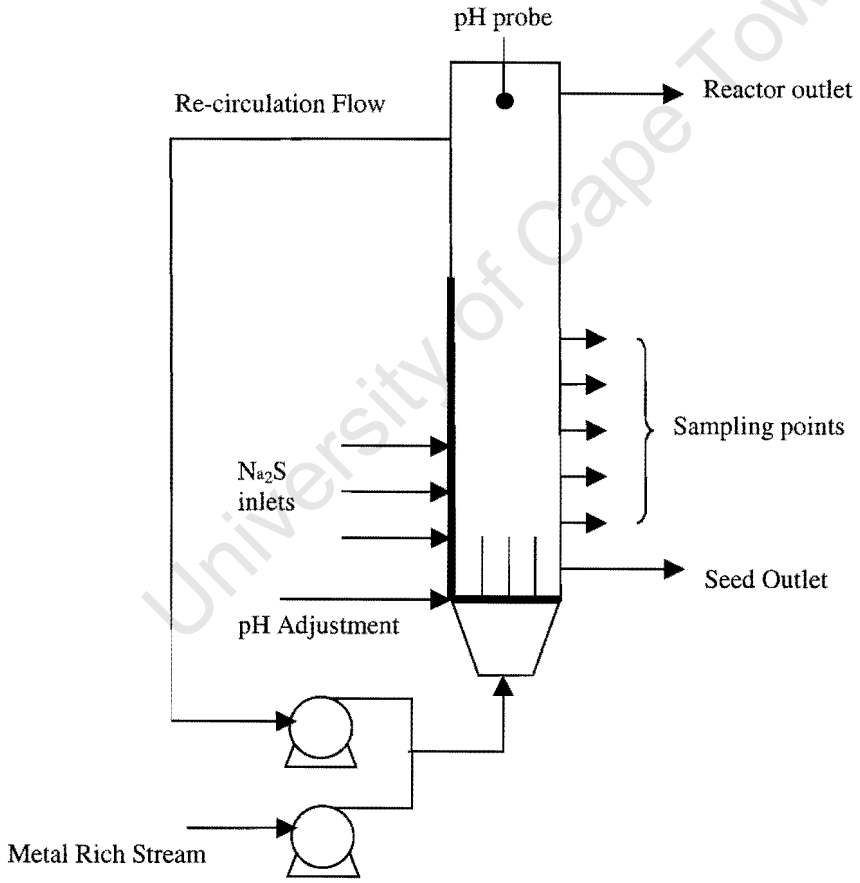

Figure 5.1 Schematic representation of the pellet reactor

Table 5.1: Experimental equipment

Re-circulation	Watson Marlow 505S
Metal rich stream	Masterflex, Console drive, 6-600RPM Marprene tubing 16"
Na_2S stream	Masterflex, Console drive, 6-600RPM Marprene tubing 16"
pH adjustment	UCT custom-made pump
pH controller	UCT custom controller
ph probe	Metrohm 6.0219.100 (pH 0-14) (temp. 0-70°C)
Reactor	1.5 m high custom-made fluidised bed
Tank	$2 \times 25l$ storage tanks

The bottom of the reactor was fitted with a 25mm diameter plastic disk containing 2mm holes for flow distribution. A circular, 25mm diameter, wire gauze (180μm) was positioned above the disk to prevent sand clogging the inlet flow pipe. A 2cm bed of 5mm glass beads provided extra support for the sand (see figure 5.2). This sand support system decreased the potential for channelling in the column.

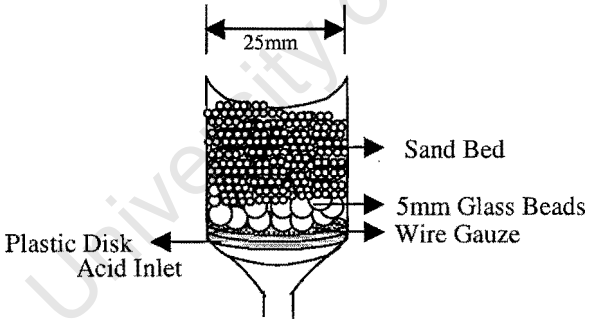

Figure 5.2 Inlet of the pellet reactor

Aqueous copper sulphate (metal rich stream) together with the re-circulation stream entered via the bottom of the column. The re-circulation stream helped to fluidise the bed. Air was excluded from the system, as air bubbles ascending through the column could result in the loss of seed material to the re-circulation or effluent streams.

The mixture of re-circulation and influent streams at the bottom of the reactor was supersaturated with respect to copper sulphate and this acted as a driving force for the crystallisation of metal sulphide onto the pellets (heterogeneous nucleation). The distance between the re-circulation inlet, influent inlet and inlet to the reactor was kept to a minimum to prevent homogeneous nucleation within that region.

Sodium sulphide was introduced via three inlet points on the side of the reactor. They were equally spaced 10cm from each other with the first point being 10cm from the bottom of the reactor. The splitting of the sulphide inflow into three reduced the local supersaturation at the point where the sulphide ions and copper ions mixed. Initially problems were encountered with backflow of sand flowing into the sulphide inlet tubes due to the peristaltic motion of the pumps. This was eliminated by inserting a small circular piece of wire gauze (180μm) into the tube to allow for liquid flow but not of sand particles.

The acid inflow was monitored using the UCT controller and pumped at 8ml/min with the UCT peristaltic pump. The acid (0.1M H_2SO_4) inlet flow was situated 2cm from the bottom of the reactor. The acid maintained the pH at a value below 7 to promote the formation of aqueous H_2S. NaOH was only used for batch experiments to investigate the effect of higher pH values on the precipitation process.

Five equally spaced sampling points on the side of the reactor were used to create column profiles. The first point was situated 15cm from the bottom of the reactor with additional points at 10cm intervals. These points were closed off using rubber seals. These are rubber seals that allow for a syringe needle, used to take a liquid sample, to penetrate the seal a number of times before it needed to be replaced. Depending on the quality of the rubber, these seals could be used approximately for approximately 16 to 20 injections. The needle passes far enough into the column to allow for a sample to be taken in the flow region and not in the dead zone (see figure 5.3).

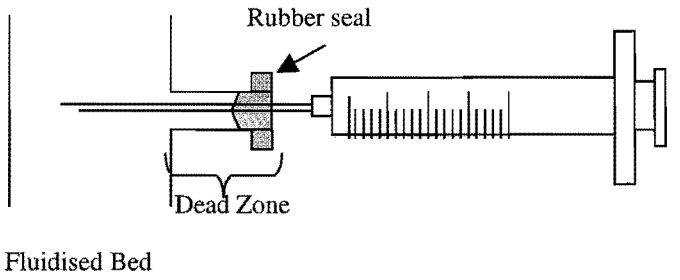

Figure 5.3 Illustration of sample points

A seed outlet was situated 5cm from the bottom of the reactor. This allowed for the removal of coated sand particles.

5.1.2 System operation and Reagents

The flow of the copper inlet stream and the sulphide flow were controlled using Masterflex pumps (see Appendix A3.1 Table A5-1. for calibration curves). The inflow of the copper and the sulphide were always equal. A Watson Marlow 505S peristaltic pump was used for the re-circulation flow.

The inlet copper flow together with the re-circulation flow (see Appendix A5.2 Table A5-2 for experimental velocity values) always exceeded the minimum fluidisation velocity, 78ml/min (Equation 4-2), but did not exceed the maximum fluidisation velocity of 760ml/min (Equation 4-8). The fluidisation of the bed was primarily due to the re-circulation flow.

Table 5.2 Calculation for the minimum and maximum fluidisation velocities

Diameter of sand, d_s	0.0005m
Viscosity of liquid, μ	1 cP
Density of liquid, ρ_l	998 kg/m^3
Density of sand $Si0_2$, ρ_s	2550 kg /m^3
Galileo Number	1897
Reynolds Number	1.314
Minimum Fluidisation Velocity	**77.63 ml/min**
Maximum Fluidisation Velocity	**760.5 ml/min**

Unlike in the case of nickel carbonate (Guillard, 2001) no scaling was observed on the walls of the reactor. The bed height varied between 1.0 and 1.4m. During the course of the experiment, the sand became coated with the copper sulphide precipitate and the bed height decreased slightly (between 1-3cm). The Reynolds number was <2 (see Appendix A5.3 for calculations) therefore flow within the reactor was laminar (Coulson and Richardson, 1980). Due to constraints on the column height, it was not possible to test velocities close to the maximum fluidisation velocity without having the sand bed passing into the recycle. Channelling was observed at the bottom of the reactor but did not hamper the mixing within the column. The sand in the reactor discoloured gradually due to the deposition of copper sulphide. Good mixing was observed by visually tracing fresh sand added to the top of the reactor, which soon moved from the top, through the bed of sand and mixed completely with the coated sand in the bed.

Fresh reagents were prepared for each experiment. A synthetic solution (5l) of copper sulphate penta-hydrate ($CuSO_4.5H_2O$), varying between 50 and 150ppm, was prepared in a 25l container. The sodium sulphide nona-hydrate ($Na_2S.9H_2O$) was prepared using S:Cu ratios between 1 and 1.5. This resulted in a sulphide mass concentration between 25.23 and 113.53ppm. All compounds were weighed out on the laboratory *Precisa 205A* balance before dissolving them in distilled water.

5.2 Preliminary Experiments

A series of batch experiments were performed in order to characterise the copper sulphide system. These consisted of mixing different concentrations of copper sulphate and sodium sulphide and visually investigating the precipitate that formed. Changes in pH, S/Cu ration and concentration were investigated.

(i.) Batch Experiments

Batch experiments were conducted using a 250ml conical flask. Equal volumes of known concentration of $CuSO_4.5H_2O$ and $Na_2S.9H_2O$ were combined to give a desired molar ratio of Cu:S. The flasks were stirred using a MSH 300 magnetic stirrer at a speed of 500 rpm. Samples were filtered though 0.45μm nitrocellulose Millipore filters. Samples were analysed using AAS. The pH was recorded using a Hanna pH 211 microprocessor and a HI 1332 pH probe.

(ii.) Fluidised Bed

Initial experiments performed in the fluidised bed resulted in the formation of a large amount of fine particles due to homogeneous nucleation. Samples from these experiments could not be analysed using an AA spectrometer as a result of the fines. These fines were also too small to be removed by filtration using 0.22μm Millipore nitrocellulose filters. The reason for the formation of these fines was the high supersaturation in the reactor.

The inlet copper stream (see figure 5.1) was used to fluidise the bed and had an inlet flow of 110ml/min. A 1:1 S/Cu ratio was maintained in the reactor. The inlet copper concentration was 150ppm. The sulphide inlet flow was set according to that of Guillard (2001) at 20ml/min. In order to maintain the 1:1 S/Cu ratio a high sulphide concentration of 416ppm was required. This resulted in a high supersaturation value for preliminary experiments, 0.3 compared with 0.04 for subsequent experiments. The latter value is a result of reducing the inlet flow and fluidising the bed using the recycle stream. The copper and sulphide streams were always at an equal flow rate. This resulted in a

reduced local supersaturation at the inlet points and a considerable reduction in the amount of fine particles that formed.

A Response Surface Methodology (RSM) statistical design (Myers and Montgomery, 1995) investigated various combinations of factors (S/Cu ratio, inlet [Cu], recycle rate and inlet flow rate) that influence precipitation. The RSM was used to find suitable conditions to achieve an optimum supersaturation, minimising spontaneous nucleation in the fluid and maximising the copper removal efficiency.

5.3 Modelling

For the simulation model a simplified electrolyte system was generated using copper (Cu^{2+}) as a representative metal ion in $CuSO_4$ form and Na_2S. This system was then extended to include a representative selection of metals found in acid mine draingage (AMD) namely, calcium, magnesium, zinc, copper and nickel. The AMD and Na_2S stream were fed into a mixer, representative of the fluidised column. The acid (H_2SO_4) and base (NaOH) were used in a sensitivity analysis to investigate the influence of a pH change in the system. Figure 5.4 is the flowsheet generated by ASPEN PLUS™.

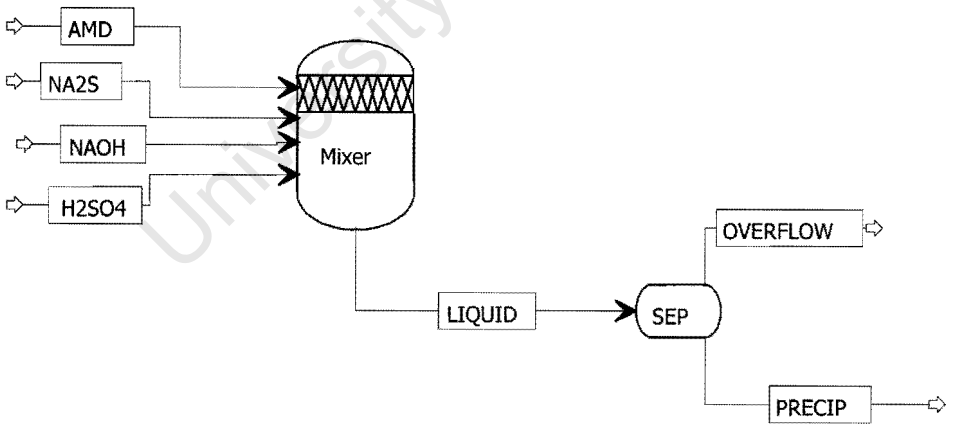

Fig.5.4 A Schematic representation of the Process Configuration

Chapter Six

Solubility Diagrams

6.1 The *Four Step* Approach to drawing Solubility Diagrams

The results from the approach set out in chapter 3 for constructing solubility diagrams for the copper/sulphide system are presented in this chapter:

Steps 1 and 2: Hydroxide/Sulphide solids and complexes are determined and the solubility products obtained from literature are presented in equations (6-1) to (6-13). The constants have been obtained from various literature sources (Licht, 1988; Dyrssen, 1988; Smith and Martell, 1976) and are not global constants. The constants are all calculated relative to log K_a of $H_2S/HS/S$ given in equation (6-12) and (6-13). All constants have been selected at (ionic strength) I = 0 mol/l and 25°C, or recalculated at I = 0 with the Davies equation.

The *primary* reactions involved with copper sulphide precipitation are:

$CuS(s) \Leftrightarrow Cu^{2+} + S^{2-}$	$\log K_{so} = -35.1$	Bollinger (1992)	(6-1)
$Cu(OH)_2(s) \Leftrightarrow Cu^{2+} + 2OH^-$	$\log K_{s1} = -18.3$	Dyrssen (1988)	(6-2)
$Cu^{2+} + S^{2-} \Leftrightarrow CuS^o$	$\log K_{s2} = 19.5$	Bollinger (1992)	(6-3)
$Cu^{2+} + H^{2+} + S^{2-} \Leftrightarrow CuHS^+$	$\log K_{s3} = 31.4$	Dyrssen (1988)	(6-4)
$Cu^{2+} + 2H^{2+} + 2S^{2-} \Leftrightarrow Cu(HS)_2$	$\log K_{s4} = 56.2$	Dyrssen (1988)	(6-5)
$Cu^{2+} + OH^- \Leftrightarrow Cu(OH)^+$	$\log K_{s5} = 6.5$	Smith and Martell (1976)	(6-6)
$Cu^{2+} + 2OH^- \Leftrightarrow Cu(OH)_2^o$	$\log K_{s6} = 15.2$	Smith and Martell (1976)	(6-7)
$Cu^{2+} + 3OH^- \Leftrightarrow Cu(OH)_3^-$	$\log K_{s7} = 15.1$	Smith and Martell (1976)	(6-8)
$Cu^{2+} + 4OH^- \Leftrightarrow Cu(OH)_4^{2-}$	$\log K_{s8} = 16$	Smith and Martell (1976)	(6-9)
$2Cu^{2+} + 2OH^- \Leftrightarrow Cu_2(OH)_2^{2+}$	$\log K_{s9} = 17.4$	Smith and Martell (1976)	(6-10)
$3Cu^{2+} + 4OH^- \Leftrightarrow Cu_3(OH)_4^{2-}$	$\log K_{s10} = 34.8$	Smith and Martell (1976)	(6-11)
$S^{2-} + H^+ \Leftrightarrow HS^-$	$\log K_{a1} = 17.3$	Licht (1988)	(6-12)
$S^{2-} + 2H^+ \Leftrightarrow H_2S$	$\log K_{a2} = 24.3$	Licht (1988)	(6-13)

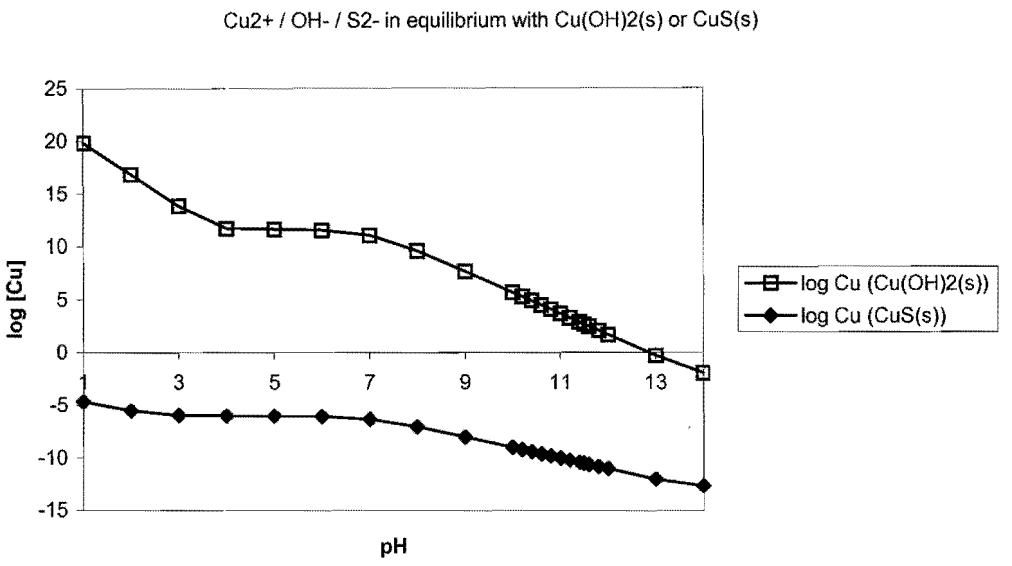

Figure 6.1. Illustration of the dominance of the CuS system

Figure 6.1 illustrates the dominance of the CuS(s) precipitate. The graphs are drawn using constants from Licht (1988) for the sulphide ligand, Dyrssen (1988) for copper bisulphides (CuHS, $Cu(HS)_2$), Bollinger (1992), for CuS and soluble CuS and Smith and Martell (1982) for the hydroxide species ($Cu(OH)_2^0$, $Cu(OH)_3^-$, $Cu(OH)_4^{2-}$, $Cu_2(OH)_2$, $Cu_3(OH)_4$. The CuS(s) is therefore the only solid precipitate that needs to be considered when drawing the theoretical solubility diagram. Log [Cu] total from $Cu(OH)_2$(s) takes into account all the soluble hydroxide, sulphide and bisulphide complexes that form. Similarly for the Log [Cu] total from CuS(s).

The solubility product constants from the above reactions are as follows (the $[Cu^{2+}]$ is as a result of the CuS(s) species only):

$$K_{S0} = [Cu^{2+}]\,[S^{2-}] \quad (6\text{-}14)$$

$$K_{S2} = [CuS^{o}]/[Cu^{2+}]\,[S^{2-}] \quad (6\text{-}15)$$

$$K_{s3} = [CuHS^{+}]/[Cu^{2+}]\,[S^{2-}][H^{+}] \quad (6\text{-}16)$$

$$K_{s4} = [Cu(HS)_2]/[Cu^{2+}]\,[S^{2-}]^2[H^{+}]^2 \quad (6\text{-}17)$$

$$K_{S5} = [Cu(OH)^{+}]/[\,Cu^{2+}]\,[OH^{-}] \quad (6\text{-}18)$$

$$K_{S6} = [Cu(OH)_2^{o}]/[\,Cu^{2+}]\,[OH^{-}]^2 \quad (6\text{-}19)$$

$$K_{S7} = [Cu(OH)_3^{-}]/[\,Cu^{2+}]\,[OH^{-}]^3 \quad (6\text{-}20)$$

$K_{S8} = [Cu(OH)_4^{2-}]/[Cu^{2+}][OH^-]^4$ (6-21)

$K_{S9} = [Cu_2(OH)_2^{2+}]/[Cu^{2+}]^2[OH^-]^2$ (6-22)

$K_{S10} = [Cu_3(OH)_4^{2-}]/[Cu^{2+}]^3[OH^-]^4$ (6-23)

K_w is the ionic product of water (Ebbing, 1990):

$K_w = [OH^-][H^+] = 10^{-14}$ (6-24)

pH is related to the hydrogen ion as shown in equation (6-25) (Stumm and Morgan, 1996):

$pH = -\log [H^+]$ (6-25)

and $\log [OH^-] = pH - 14$ (6-26a)

In order to calculate the total sulphide ion concentration, both H_2S equilibrium reactions need to be considered (Licht, 1988) (assuming excess sulphide and neglecting the formation of CuS, CuHS and $Cu(HS)_2$):

$$T_s = [H_2S] + [HS^-] + [S^{2-}] \quad (6\text{-}26)$$

$$= 1\times10^{24.3}[H^+]^2[S^{2-}] + 1\times10^{17.3}[H^+][S^-] + [S^{2-}] \quad (6\text{-}26a)$$

Therefore taking out the common sulphide concentration ion and making it the subject of the formula:

$$[S^{2-}] = \frac{T_s}{1\times10^{24.3}[H^+]^2 + 1\times10^{17.3}[H^+] + 1} \quad (6\text{-}26b)$$

Step 3: Determining the solubility system.

Linearizing equations (6-12 – 6-21) we obtain the following logarithmic equations:

$\log [Cu^{2+}] = \log K_{S0} - \log [S^{2-}]$ (6-27)

$\log [CuS^o] = \log K_{S1} + \log[Cu^{2+}] + \log [S^{2-}]$ (6-28)

$\log [CuHS^+] = \log K_{S3} + \log[Cu^{2+}] - pH + \log [S^{2-}]$ (6-29)

$\log [Cu(HS)_2] = \log K_{S4} + \log[Cu^{2+}] - 2\times pH + 2\log [S^{2-}]$ (6-30)

$\log [Cu(OH)^+] = \log K_{S5} + \log [Cu^{2+}] - 14 + pH$ (6-31)

$$\log [Cu(OH)_2^o] = \log K_{S6} + \log [Cu^+] - 28 + 2\times pH \quad (6\text{-}32)$$

$$\log [M(OH)_3^-] = \log K_{S7} + \log[Cu^{2+}] - 42 + 3\times pH \quad (6\text{-}33)$$

$$\log [M(OH)_4^{2-}] = \log K_{S8} + \log[Cu^{2+}] - 56 + 4\times pH \quad (6\text{-}34)$$

$$\log [Cu_2(OH)_2^{2+}] = \log K_{S8} + 2\times\log[Cu^{2+}] - 28 + 2\times pH \quad (6\text{-}35)$$

$$\log [Cu_3(OH)_4^{2-}] = \log K_{S8} + 3\times\log[Cu^{2+}] - 56 + 4\times pH \quad (6\text{-}36)$$

Step 4: Copper Sulphide Solubility Diagram

The solubility diagram (shown in figure 6.2) takes into account a number of possible curves using different constants from a number of literature sources (see above equations). These curves illustrate the above statements by Stumm and Morgan (1996), and Baltpurvins (1996), that different constant values and the number and the nature of the species taken into account give a range of minimum solubilities and will only be used as a guideline to the concentrations of copper that may be removed in the copper sulphide system.

In figure 6.2, curves 1, 6 and 7 take into account all the species that may be formed but the selected constant values come from different literature sources. Curves 2 and 3 omit CuHS and $Cu(HS)_2$, while 4 and 5 do not consider CuHS, $Cu(HS)_2$ and CuS^o. The small value of the second hydrogen sulphide dissociation constant of $1\times10^{-17.3}$ from Licht (1988) indicates that, free S^{2-} never exists in solutions containing metal sulphide salts. As shown in figure 6.2, soluble sulphide complexes not taken into account in the model (curves 2, 3, 4, 5) lead to a dramatic underestimation of the minumum solubility reached by the system. Graphs containing these species (Figure 6.2 - 1, 6 and 7) should be considered a more realistic representation of the system. See Appendix A6.1 for a detailed description of the graphs.

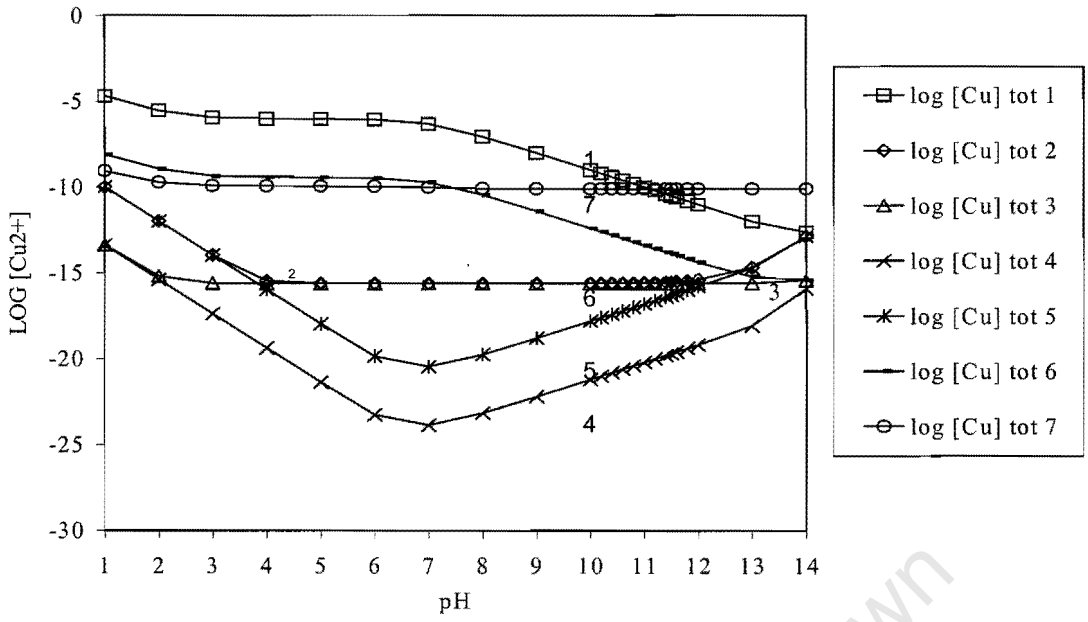

Figure 6.2 Comparison of Copper Sulphide solubility curves

6.2 OLI solubility diagrams

Figure 6.3 shows a large discrepancy between graphs constructed with OLI (curve 3, species include: Cu^{2+}, CuS(s), $Cu(OH)^{+}$, $Cu(OH)^{0}_{2}$, $Cu(OH)_2(s)$, $Cu(OH)_3$ and $Cu(OH)_4$) and that which takes into account all the soluble sulphide species (curve 1).

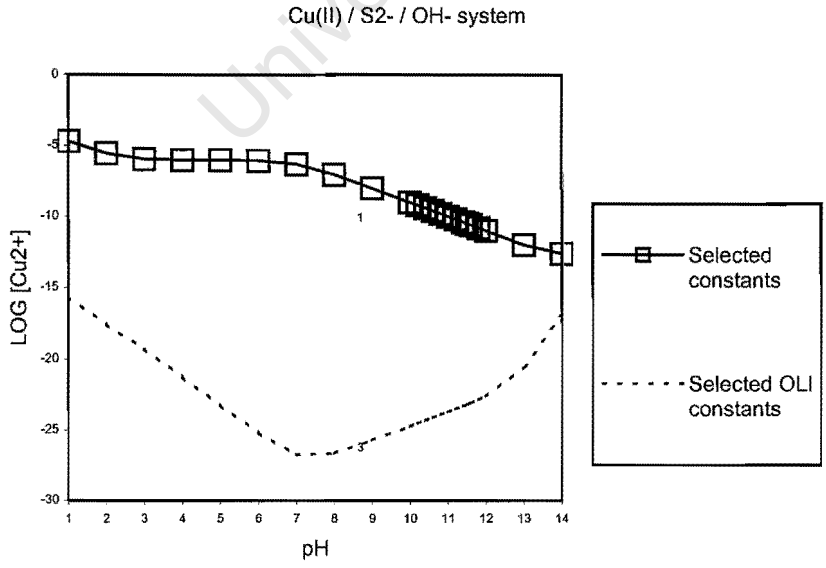

Figure 6.3 Comparison between Theoretical and Simulation (OLI) Copper Sulphide

As mentioned before, it would be more accurate to represent the system by accounting for all possible species that may form. Moreover, as shown in figure 6.2, the difference in thermodynamic constants changes the shape of the solubility curve. It is not in the scope of this thesis to try and predict which thermodynamic constants are correct, but merely to highlight the importance of the role that the soluble complexes play in the solubility of a given system. In addition, the importance of critically evaluating any theoretical or simulated results is highlighted. Blindly relying on simulation results to predict removal efficiency might result in a gross over-estimation of the success of the system.

6.3 ASPEN PLUS™

The composition of the simulated acid mine drainage may be seen in table 6.1 and is used as an input stream in an ASPEN PLUS™ simulation (Hansford *et al,* 2000).

Table 6.1. Composition of simulated acid mine drainage.

Mineral	Metal	Species	Concentration (mg mineral/l)
$ZnSO_4$	Zn	Sulphate	38
$MgSO_4$	Mg	Sulphate	50
$CuSO_4$	Cu	Sulphate	50
$NiSO_4$	Ni	Sulphate	50

Figure 6.4 shows the effect of changing pH on all precipitating salts using ASPEN PLUS™ simulation. This simulation was used to determine the dominant precipitating metal species over a range of pH values. ASPEN PLUS™ predicts that copper sulphide will precipitate completely at all pH values between 1 and 12. This was seen from bench-scale experimentation in beakers. Zinc sulphide precipitates after a pH of 2 with nickel sulphide precipitating out soon after at approximately pH 3. Magnesium precipitates as hydroxide and not a sulphide at a pH above 11.

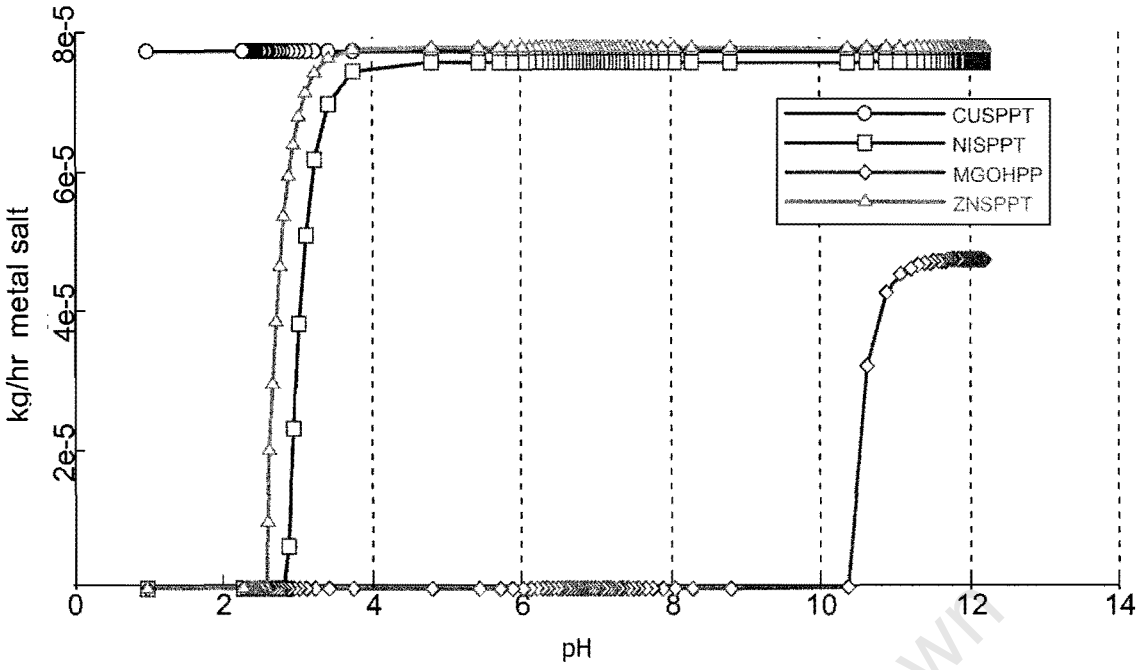

Figure 6.4 Effect of change in pH on metal precipitation – ASPEN PLUS™

Chapter 7

Response Surface Methodology (RSM)

RSM is often applied in the industrial world in order to investigate the effect of several input variables on the performance of a process (Myers and Montgomery, 1995). The measure of the performance is called a response (y). The input variables (ξ_1, ξ_2, ξ_3, ..., ξ_k) are often referred to as independent variables and are controlled by the process operator. RSM was used to find a relationship between the response and the independent variables.

$$y = f(\xi_1, \xi_2, \xi_3, ..., \xi_k) + \varepsilon \qquad (7\text{-}1)$$

y = Response variable yield

ξ = Independent natural variables

ε = Error term

Equation (7-1) is an empirical model and is called a response surface model. ε is an error term and represents variability that was not accounted for e.g. analytical errors, background noise, etc and is often treated as a statistical error. It is assumed to have a normal distribution with mean equal to zero and variance σ^2 (Calculation of σ^2 may be found in Appendix A7.1). If the mean is zero then the response is reduced to equation (7-3);

$$E(y) = \eta = E[f(\xi_1, \xi_2, \xi_3, ..., \xi_k)] + E(\varepsilon) \qquad (7\text{-}2)$$

$$\eta = f(x_1, x_2, x_3, ...,x_k) \qquad (7\text{-}3)$$

η = True responce function

x_n = Dimensionless coded variables

ξ_1, ξ_2, ξ_3, ..., ξ_k are called natural variables and are measured in °C (temperature), kPa (pressure), g/l (concentration) etc. In RSM the natural variables are transformed to

coded, non-dimensional variables x_1, x_2, x_3, ….,x_k. These coded variables are calculated as follows:

$$x_1 = \frac{\xi_1 - [\max(\xi_1) + \min(\xi_1)]/2}{[\max(\xi_1) - \min(\xi_1)]/2} \tag{7-4}$$

The unknown function f is often approximated using a first or second order model. Equation (7-5) is the first-order model for two independent variables:

$$\eta = \beta_0 + \beta_1 x_1 + \beta_2 x_2 \tag{7-5}$$

The response surface for a two variable (x_1 and x_2) system results in the generation of a plane surface (Myers and Montgomery, 1995). The first order model illustrates the main effects between the variables. Curvature may be investigated by adding an interaction parameter x_1x_2 to the first order equation (7-5).

$$\eta = \beta_0 + \beta_1 x_1 + \beta_2 x_2 + \beta_{12} x_1 x_2 \tag{7-6}$$

Adding the interaction term was often not adequate to represent a system and a second order model is required to accurately describe the system.

$$\eta = \beta_0 + \beta_1 x_1 + \beta_2 x_2 + \beta_{11} x_1^2 + \beta_{22} x_2^2 + \beta_{12} x_1 x_2 \tag{7-7}$$

Equation (7-7) is representative of a 3-dimensional surface. Construction of the response surface occurred in three phases:

Phase zero:

- Important factors needed to be identified.
- Preliminary tests eliminated factors of lesser importance.

Phase one:

- Levels or settings of variables were identified such that levels existed within viable operating conditions.

- A first-order model identified significant variables as well as the importance of interaction parameters.

Phase two:

- A second-order model is used to accurately describe the system if interaction terms are found to be of importance.

7.1 Two-level Factorial Design

Two-level factorial designs are used for screening variables used for RSM. They are first-order factorial designs and are used to investigate the significance of factors as well as the possible existence of interaction between factors. A special case of factorial design is one in which there are k factors and 2 levels (2^k design). The simplest design is of the form 2^2. Levels of the factors are usually arbitrarily called high (+) or low (-). As an example consider 2 factors: concentration (A) and reactant feed rate (B). Table 7.1 is an illustration of a 2^2 factorial design consisting of four experiments.

Table 7.1 2^2 Factorial Design

	A	B
Experiment 1	-	-
Experiment 2	-	+
Experiment 3	+	+
Experiment 4	+	-

Figure 7.1 is a pictorial representation of a 2^3 design with three factors: A, B and C. The more complicated 2^3 design may be used to illustrate the interaction between factors.

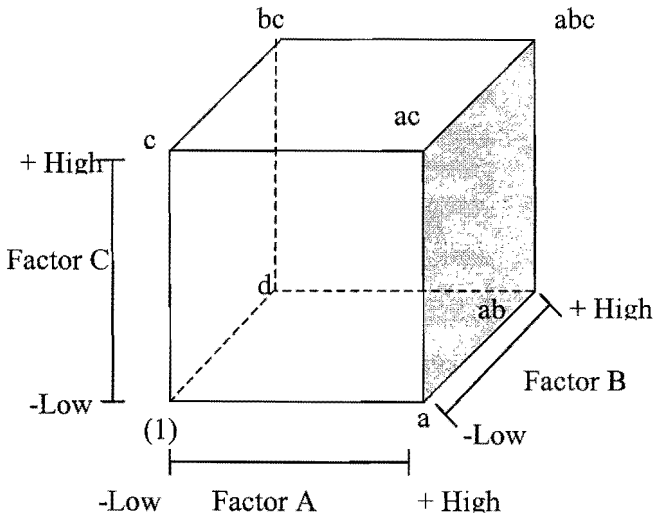

Figure 7.1 Pictorial representation of a 2^3 factorial design (Myers and Montgomery, 1995)

2^k designs are said to be single replicate designs. This means that there is no repetition of experiments to calculate the experimental error. The addition of center points allows for this calculation as well as for the investigation of curvature.

A 2^k system assumes linearity between factors, but still works well if there is slight curvature. The calculation for the curvature of a 2^2 system is as follows:

- n_c is the number of replicates at the center point (0,0)
- $\overline{y_f}$ is the average response of four runs of the factorial design
- $\overline{y_c}$ is the average response of four runs of the center points

If the difference between $\overline{y_f}$ and $\overline{y_c}$ is large then curvature is present.

7.1.1 One-half factorial design

As the number of factors increases, the number of experiments increases exponentially. Due to time restraints or expensive reagents, a complete factorial design often cannot be completed. It is then possible to carry out a one-half fraction of the 2^k design and the number of experiments is reduced. An example of this would be the one-half replicate of the 2^3 design, in which case eight experiments would be reduced to four. The factorial design for the 2^3 design is shown in table 7.2.

Table 7.2 2^3 Factorial Design

Treatment	Factorial Effect							
Combination	I	A	B	C	AB	AC	BC	ABC
a	+	+	−	−	−	−	+	+
b	+	−	+	−	−	+	−	+
c	+	−	−	+	+	−	−	+
abc	+	+	+	+	+	+	+	+
ab	+	+	+	−	+	−	−	−
ac	+	+	−	+	−	+	−	−
bc	+	−	+	+	−	−	+	−
(1)	+	−	−	−	+	+	+	−

The one-half fractional design is the top half of table 7.2 and does not consider the interaction between the variables. However, it may be shown, but is beyond the scope of this thesis, that the main effects (variables a, b and d) and interaction factors (variables ab, ac and bc) are linked. So, by investigating the main effects, the interaction factors are indirectly taken into account.

7.2 Second-order factorial design

As previously mentioned, if the first order response is inadequate, a second-order surface model is required. The detection of the stationary points is one of the main aims of the second order analysis. The following curves show the geometric nature of the 2^2 second-order responses i.e. k=2. Figure 7.2 exhibits a maximum response at the stationary point ($x_{1.0}$, $x_{2.0}$). A stationary point showing a minimum response is shown in figure 7.3 at ($x_{1.0}$, $x_{2.0}$). The hyperbolic contours in Figure 7.4 represent a saddle point.

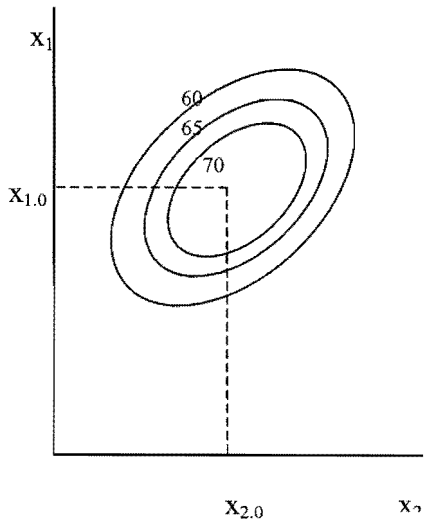

Figure 7.2 Second-order system with point of maximum response.

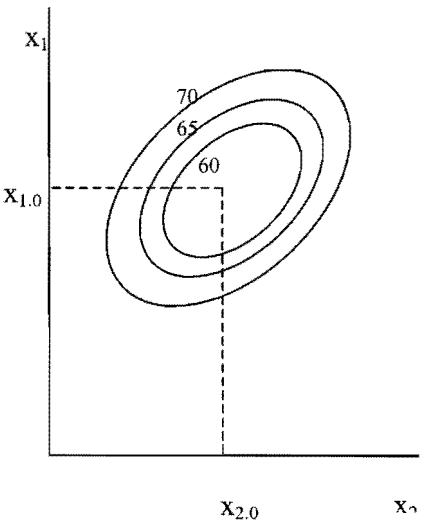

Figure 7.3 Second-order system with point of minimum response.

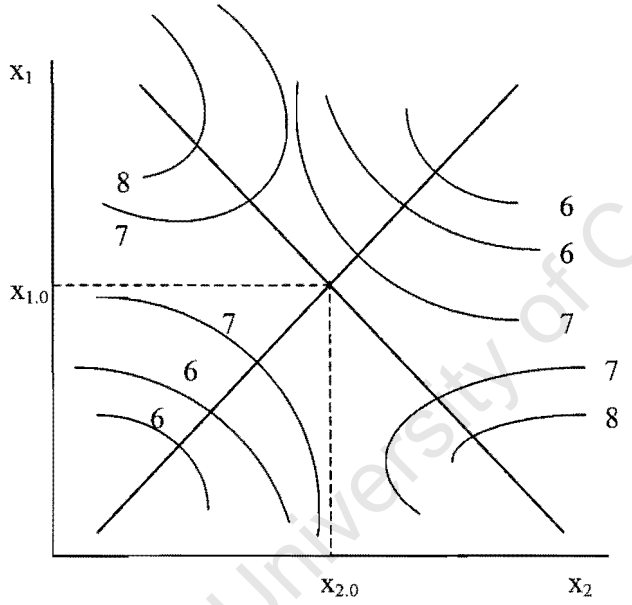

Figure 7.4 Second-order system with saddle point (Myers and Montgomery, 1995)

For k=3 the resultant response is a surface. A maximum is shown in figure 7.5 and a saddle point in figure 7.6.

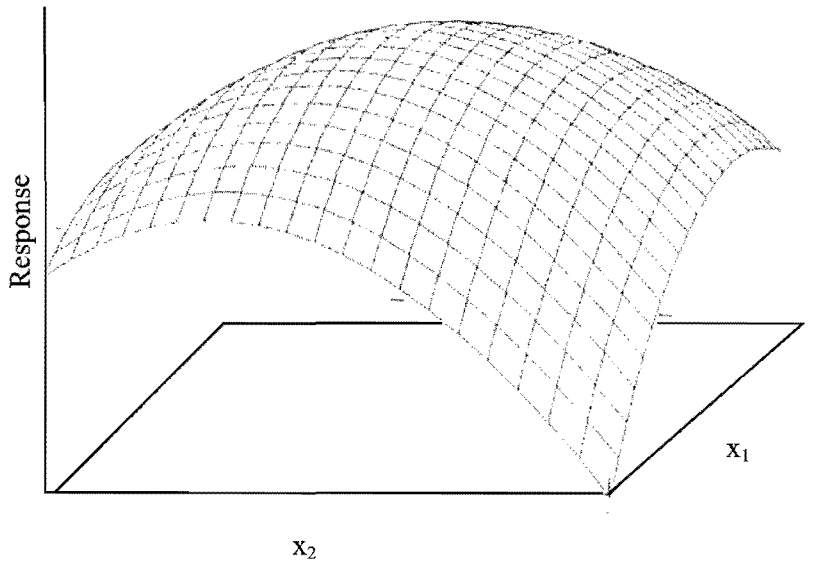

Figure 7.5 Three-dimensional response surface with maximum point (Myers and Montgomery, 1995)

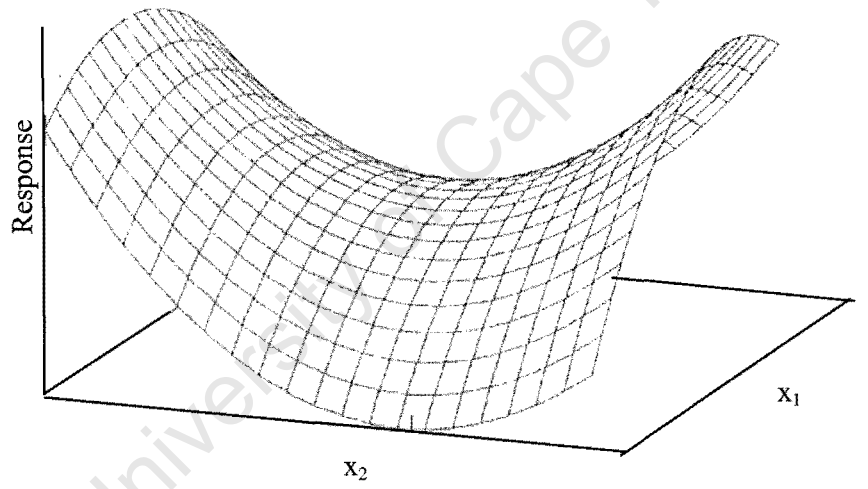

Figure 7.6 Three-dimensional plot for a saddle point (Myers and Montgomery, 1995)

7.2.1 Design of a second-order experiment

The second-order experiments for a 2^2 design comprise:

(i) 4 experiments representing the 2^2 factorial experiments at upper and lower levels

(ii) 4 experiments at an upper or lower level in combination with a center point.

(iii) 3 center point experiments.

These are graphically represented in figure 7.7. The points are equally spaced on a circle of radius $\sqrt{2}$. The points outside the square at radius $\sqrt{2}$ are called the axial points and estimate the quadratic terms of the second order equation.

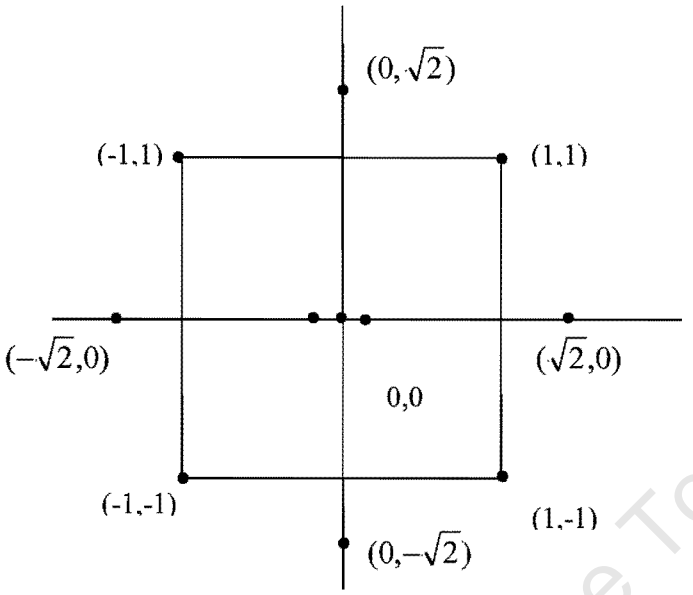

Figure 7.7 Graphical depiction of 2^2second order design (Myers and Montgomery, 1995)

The nature of a stationary point such as those shown in figures 7.2, 7.3 and 7.4 is determined from the signs of the eigenvalues of the matrix $\hat{\mathbf{B}}$ in equation (7-8).

$$\hat{y} = b_o + \mathbf{x}'\mathbf{b} + \mathbf{x}'\hat{\mathbf{B}}\mathbf{x} \qquad (7\text{-}8)$$

$\mathbf{x}' = [x_1, x_2, \ldots, x_k]$

$\mathbf{b}' = [b_1, b_2, \ldots, b_k]$

$\underline{\mathbf{B}}$ is a k×k symmetrical matrix. $\hat{y}$ in equation (7-8) is a fitted second order response surface, $\mathbf{b_o}$, $\mathbf{b}$ and $\hat{\mathbf{B}}$ represent the intercept, linear and second-order coefficients respectively. Negative eigenvalues signify that the stationary points show a maximum response. Positive eigenvalues signify that the stationary points show a minimum response. Mixed eigenvalues signify that the stationary points are saddle points.

7.3 Analysis of experiments using SAS

7.3.1 First-order model analysis

Two of the most important terms in statistics are the mean and variance (Miller and Freund, 1985). These values are vital to any evaluation in statistics and will be defined in order to better understand the results obtained from the SAS package. The mean probability distribution is simply the mathematical expectation of a corresponding random variable (Miller and Freund, 1985). If the random variable takes values (x_1, x_2, …, x_k) with the probabilities ($f(x_1)$, $f(x_2)$, …, $f(x_k)$) the mathematical expectation is defined in equation (7-9):

$$\mu = \sum_{all\,x} x \cdot f(x) \qquad (7\text{-}9)$$

μ = Mean of probability distribution

x = Random variable (in figure 7.8 distance from the origin in the x direction)

f(x) = Probability of x

The variation of a probability distribution with values f(x) is measured using the following equation:

$$\sigma^2 = \sum_{all\,x} (x-\mu)^2 \cdot f(x) \qquad (7\text{-}10)$$

σ^2 = Variance of probability distribution

μ = Mean of probability distribution

x = Random variable (in figure 7.8 distance from the origin in the x direction)

f(x) = Probability of x

Equation (7-10) is referred to as the variance of probability distribution. This mean and variance of probability distribution is a measure of the center and their spread respectively (Miller and Freund, 1985). Analogous measurements are available to describe numerical data or their distribution.

The arithmetic mean, defined by a more familiar equation (7-11) is the mean of n measurements of $x_1, x_2, \ldots, x_n$ observations (Miller and Freund, 1985):

$$\bar{x} = \frac{\sum_{i=1}^{n} x_i}{n} \tag{7-11}$$

$\bar{x}$ = Arithmetic mean

x = measurement of observation

n = number of measurements

Like the variance of a probability distribution the variance of n measurements of $x_1, x_2, \ldots, x_n$ observations measures the average of the squared deviations from the mean $\bar{x}$ and is defined by equation (7-12).

$$s^2 = \frac{\sum_{i=1}^{n} (x_i - \bar{x})^2}{n-1} \tag{7-12}$$

It is possible to estimate σ^2 by the sum of squares, illustrated in Equation (7-13). (see Appendix A7.1 for comprehensive calculations). In linear regression σ^2 is defined by the vertical deviations of the sample points from the least squares line. (The method of fitting least squares finds a relationship between x and the mean of the corresponding distribution of y shown in figure 7.8.)

$$SS_E = \frac{1}{n-2} \sum_{i=1}^{n} [y_i - (a + bx_i)]^2 \tag{7-13}$$

SS_E = Standard error of estimate or Error sum of squares

x_i = Random independent values of a linear function

y_i = Response to the linear function for values of x_i

n = number of independent random values

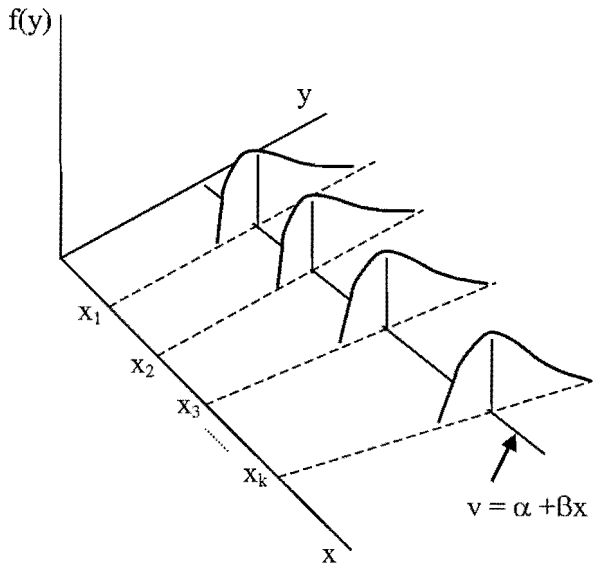

Figure 7.8 Method of least squares illustrating σ^2.

(i.) Analysis of variance

The test for significance of a regression is to determine if there is a linear relationship between the response variable y and a subset of regression variables (Myers and Montgomery, 1985). This test is called an analysis of variance (ANOVA). The total sum of squares is divided into the sum of squares due to the model and the sum of squares due to error (Equation (7-14)). Table 7.3 is a general layout of an ANOVA.

$$S_{yy} = SS_R + SS_E \qquad (7\text{-}14)$$

Table 7.3 Analysis of variance general table layout

Source of Variation	Sum of Squares	Degrees Of Freedom	Mean Square	F_0
Regression	SS_R	k	MS_R	MS_R/MS_E
Error	SS_E	n-k-1	MS_E	
Total	S_{yy}	n-1		

If the F_0 value is greater than those in the appropriate statistical tables (Miller and Freund, 1985) the response is significant and there is a linear relationship (see

Appendix A7.2). It is also possible to test for the significance of individual variables or interaction parameters.

(ii.) Confidence intervals

A t-test is used to construct confidence intervals. A confidence interval is an interval in which it can be asserted with a reasonable degree of certainty that the parameter under consideration will be found (Miller and Freund, 1985). These tests are used to determine the quality of the variables in the regression model. The model might be more effective with the addition of new variables or deletion of existing ones.

The addition of a variable increases the sum of squares of the regression model and decreases the sum of squares of the error. However, careful consideration must be taken when adding a variable as an unimportant variable could increase the mean square due to error and decrease the reliability of the model. If the value of the t-test is smaller than 0.05 then the variable is said to be significant at the 95% confidence interval.

7.3.2 Second-order and ridge analysis

The second order model is also analysed by SAS, using a canonical analysis. Generated eigenvalues evaluate the stationary point and the error in the response is evaluated using the standard error for each variable.

If a stationary point is outside the experimental area it is often not possible to operate the system at this point and the fitted model is not reliable outside the region of the experiment. The aim of the analysis is to determine the nature of the system inside or on the perimeter of the experimental region (Myers and Montgomery, 1985). This is called ridge analysis and produces a locus of points, each of which is a point of maximum response with a constraint that the point lies on a sphere of a certain radius (figure 7.9).

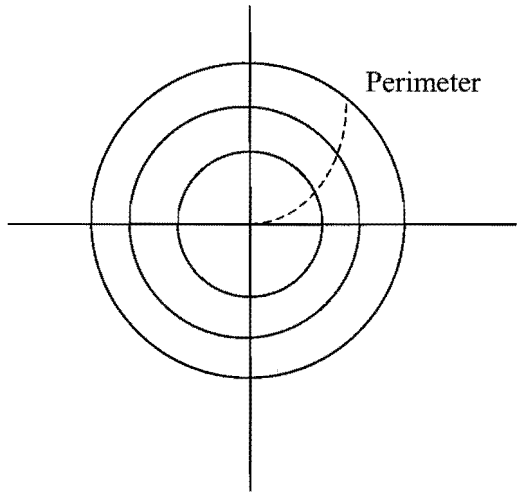

Figure 7.9 Ridge analysis

The purpose of the ridge analysis is to anchor the stationary points inside the experimental region. The output is a set of coordinates of the maximum (or minimum) response $\hat{y}$, at each computed point on concentric radii. The results provide useful information regarding the roles of the variables and suggest a set of improved operating conditions.

Chapter Eight

Results

8.1 Batch experiment results

The series of batch experiments to characterise copper sulphide precipitate are shown in Table 8.1. A dark Cu_xS_y complex formed instantaneously in every experiment after the addition of aqueous $Na_2S.9H_2O$ to $CuSO_4.5H_2O$. However, depending on the ratio of Cu:S, the colour was slightly different, ranging from a chocolate brown to a black colour. The complex produced from a 1:2 Cu:S ratio or a 1:1 Cu:S ratio was a fine precipitate that passed through a 0.45μm filter. The precipitate settled after three days. The dark brown homogeneous mixture matured into a fine black/green precipitate. These results are consistent with van Hille (2001). Silvester *et al* (1991 in Pattrick, 1997) also reported a brown precipitate and identified it as poorly crystalline covellite (CuS). On aging a green sol formed and was identified as crystalline covellite but with a significant amount of Cu(II). Mosselmans *et al* (1995) also describes the formation of a large, complex copper system ranging between Cu_2S and CuS. He also reports the formation of covellite on aging.

Table 8.1 Batch Experiments

Experiment No.	$CuSO_4.5H_2O$ g/l	$Na_2S.9H_2O$ g/l	Measured pH	Cu/S ratio
1	1.080	2.097	10.45	1:2
2	1.080	2.097	5.25	1:2
3	1.080	1.0395	6.21	1:1
4	2.160	2.097	6.06	1:1
5	4.322	4.158	6.1	1:1
6	4.322	2.079	5.17	2:1

A Cu:S ratio of 2:1 produced larger and more readily settleable particles. However, the stoichiometry of CuS dictates that one copper molecule requires one sulphide molecule. An excess of copper would therefore result in 50% removal efficiency.

This theory was tested and proved using AA analysis and was therefore not investigated any further.

8.2 Fluidised bed characterisation

Copper was measured in the outlet stream as both dissolved copper and as fines. The fines were removed in the outlet stream and represent inefficiency in the system. Initial experiments performed in the fluidised bed under the conditions shown in Table 8.2 resulted in the formation of a large number of fine particles due to homogeneous nucleation.

Table 8.2 Experimental conditions in the fluidised bed reactor

Variable	
S:Cu (mole:mole)	1:1
$[Cu^{2+}]$ (ppm)	100
Copper Inlet flow (ml/min)	110
Sulphide Inlet flow (ml/min)	40
Recycle Ratio	3.05

The reason for the formation of these fine particles was the high supersaturation within the reactor. The supersaturation of the inlet copper and sulphide stream was calculated to be 3.03×10^{32} (See Appendix A8.1 Table A8.1) compared with 8.36×10^{31}, the highest inlet supersaturation value calculated for all of the factorial experiments that followed. Samples from these experiments could not be analysed using an AA spectrometer, due to the presence of solid particles. Fines could not be separated from the liquid by filtration using a 0.22μm Millipore nitrocellulose filter paper. Equation 8.1 shows the calculation for a comparison of supersaturation values between experiments. As the outlet stream of the preliminary experiments could not be analysed, zero concentration was assumed in the recycle [$Cu_{recycle}$]. Equation 8-1 shows that any value greater than zero would only increase the value of the supersaturation. Even with this unrealistic value the supersaturation is still 4 times greater than the supersaturation used in the factorial experiments. C_{eq} is constant for the copper sulphide system and as the supersaturation value was used for comparative purposes a value of 1×10^{-37}.

$$SS_{comparison} = \frac{[Cu_{inlet\ stream} + Cu_{recycle}] \times [S_{inlet\ stream} + S_{recycle} = 0]}{C_{eq}} \quad (8\text{-}1)$$

$C_{eq} = 1 \times 10^{-37}$ solubility product of CuS (mol/l)

$Cu_{inlet/recycle}$ = Copper inlet concentration (mol/l)

$Su_{inlet/recycle}$ = Sulphide inlet concentration (mol/l)

The high supersaturation levels led to the re-examination of the experimental set-up and an attempt was made to reduce the local supersaturation at the inlet points of the reactor. A successful experiment with significantly reduced fines was performed at the conditions set out in table 8.3. A one-half factorial design experiment was generated to systematically identify the important variables for the precipitation process in the fluidised bed.

Table 8.3 Experimental conditions in the fluidised bed reactor

Variable	
S:Cu (mole:mole)	1
$[Cu^{2+}]$ (ppm)	100
Inlet flow (ml/min)	30
Recycle Ratio	3.05

8.3 General results from selected factorial design experiments

The conditions for the first-order (FO01 – FO13) and second-order (SO01 – SO08) experiments may be found in Appendix A8.2, Tables A8.2 and A8.3.

8.3.1 Start-up characterisation

An unexpected decrease in the concentration of copper was observed in the reactor outlet in the flushing process during start-up. This suggests that the copper becomes adsorbed onto the sand without any chemical reaction. Table 8.4 shows the initial copper concentration ($[Cu]_i$) in the feed tank compared to the decreased copper concentration in the ractor outlet ($[Cu]_f$).

Table 8.4 Start-up results after flushing the column.

	(ppm)	
Experiment	$[Cu]_i$	$[Cu]_f$
FO9	150	60.3
FO10	45.0	20.0
FO11	95.0	33.6
FO12	93.1	35.6
FO13	143	42.9
SO3	108	23.4
SO4	103	32.5
SO5	103	29.1
SO6	107	31.8
SO7	180	64.7
SO8	97.1	43.6

Sulphide tests were carried out on the reactor outlet stream during a second order statistical design experiment (SO8). Initial conditions had a Cu:S ratio of 1.25:1. Despite the fact that the copper adsorbed onto the sand, insignificant amounts of sulphide were found in the treated stream (Table 8.5). Controlled experiments have led to the reasoning that there is a weak association between the copper and the sand. However, as soon as sulphide is introduced into the system, it reacts immediately with the copper, due to the strong affinity for each other, to form a copper sulphide precipitate. The low sulphide concentrations suggest that there is an amorphous copper/sulphide complex forming. The aim of the thesis was a feasibility study into the use of the fluidised bed for copper removal. Classification of the type of complexes that form in the reactor was deemed to be beyond the scope of this work.

Table 8.5 Sulphide concentrations as a function of time.

Time	[S] (ppm)
2	0
5	0.11
12	0.13
32	0.24
62	0.88

8.3.2 Supersaturation

Figures 8.1 and 8.2 illustrate the effect of supersaturation on the formation of fines in the reactor. The difference between the total and the dissolved copper indicates the formation of fines due to homogeneous nucleation. The result of high supersaturation (SS = 5.6×10^{34} is depicted in figure 8.1. At lower supersaturation values (SS = 9.55×10^{33}), there is an insignificant difference between dissolved and total copper (Figure 8.2). Table 8.6 presents the conditions for the experiments in Figure 8.1 and 8.2.

Table 8.6 Experimental conditions

	Experiment Number	
Variable	***FO 1***	***FO10***
S:Cu (mole:mole)	1	1.5
$[Cu^{2+}]$ (ppm)	150	50
Inlet flow (ml/min)	50	30
Recycle Ratio	2.24	1.68
$SS_{comparison}$	5.6×10^{34}	9.55×10^{33}

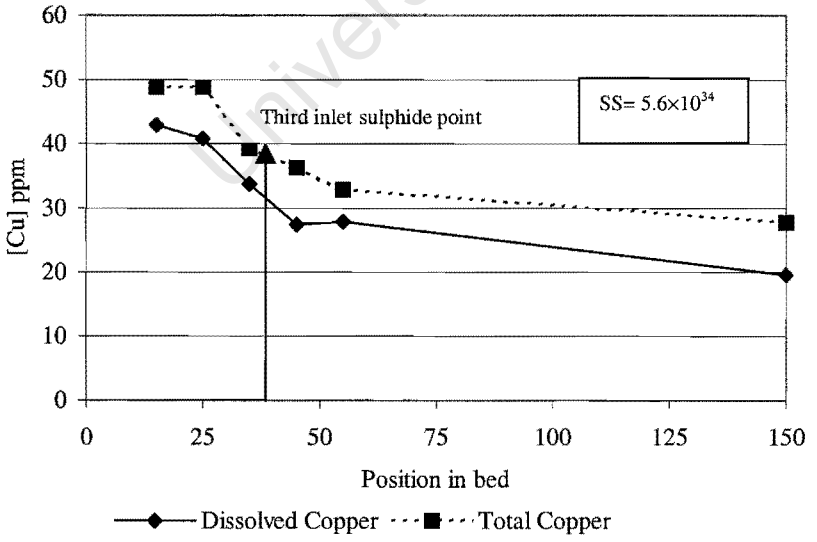

Figure 8.1 Copper concentration in the reactor as a function of position in the bed (FO 1)

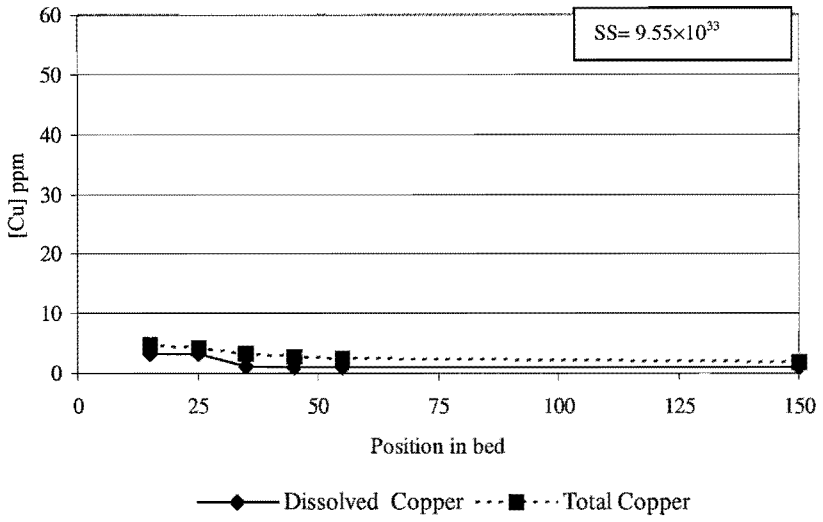

Figure 8.2. Copper concentration in the reactor as a function of position in the bed (FO 10)

Figure 8.1 and figure 8.2 also show that the fines that form do not agglomerate onto the sand particles in the reactor. This is suggested by the almost constant difference between the total copper and dissolved copper in both cases. It is therefore vital that fines formation be kept to a minimum, as it is almost impossible to eliminate these once they have formed. Figure 8.1 also shows that the reaction is instantaneous by the fact that the copper remaining in solution decreases till the third sulphide inlet point and then stabilises.

Figure 2.2 in chapter 2 is a good illustration of the types of nucleation that occur in different regions of supersaturation. It shows the spontaneous formation of fines at high supersaturation by homogeneous nucleation. However, since the solubility of Cu-S species is extremely low ($K_{sp} = 10^{-35.1}$) the graph for the sulphide system would probably consist of a much larger homogeneous nucleation region with an almost non-existent undersaturated region.

8.3.3 Concentration vs. time graphs

Figures 8.3 and 8.4 represent the copper concentration profile in the reactor as a function of time. Reproducibility of results (AA analysis readings performed in triplicate and samples taken in duplicate) is shown by the error bars in figure 8.3. The

small error bars indicate good reproducibility. Figure 8.3 and 8.4 show a difference in total efficiency for different S:Cu ratios as well as different supersaturation values.

The rapid decrease in copper concentration within the first five minutes is evidence of the rapid kinetics of the precipitation reaction. Fast kinetics are favourable when there is a need to treat large volumes of effluent as it decreases the required residence time in the reactor.

The experiments demonstrate a consistent trend (See Appendix A8.3). Instabilities were observed during start-up as shown in Figure 8.4 but steady state was reached after about 20mins. As with the column profiles, the concentration vs. time measurements indicate that the formation of fines persists throughout the experiment and no agglomeration of fines takes place on the pellets once they have formed.

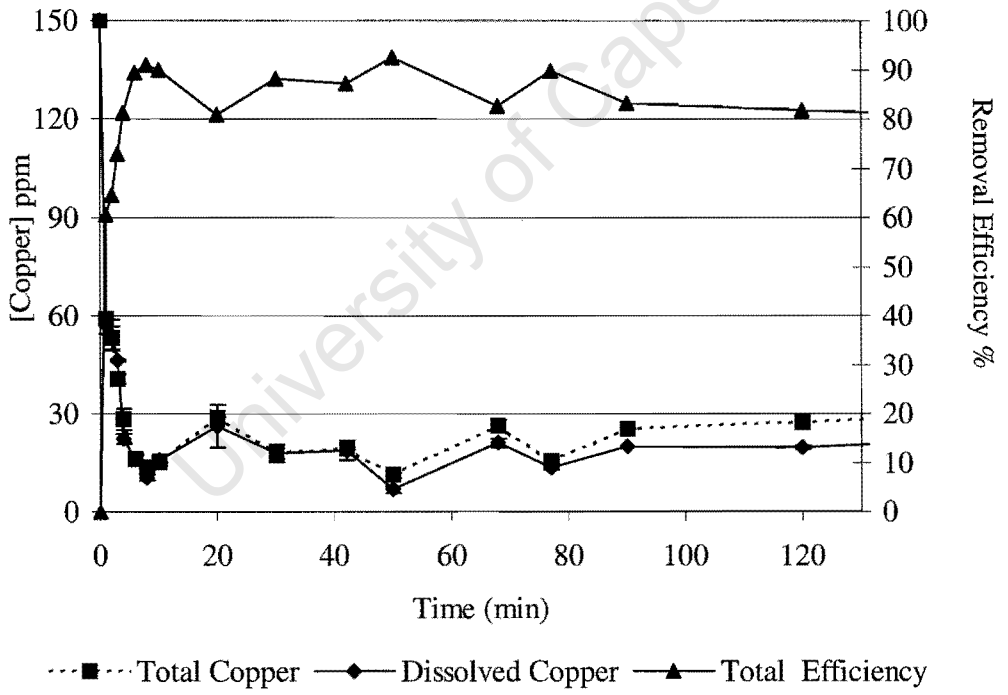

Figure 8.3. Copper concentration in the reactor as a function of time (FO 1)

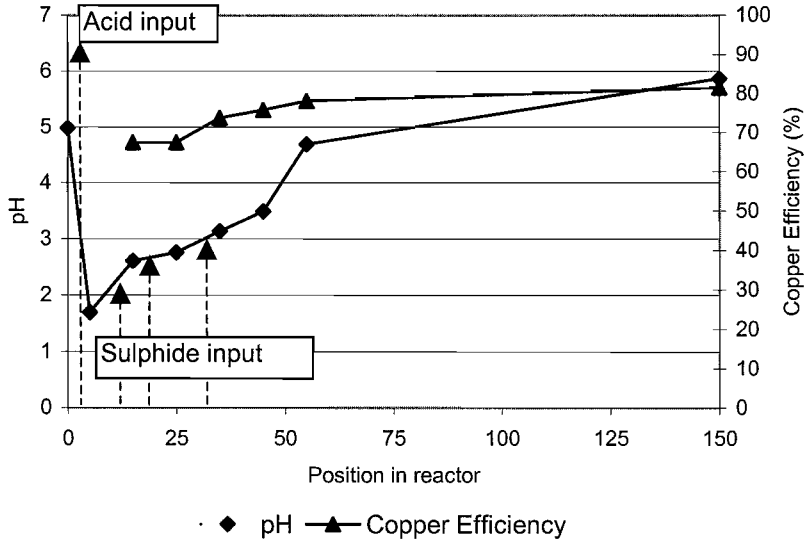

Figure 8.5 pH profile as a function of position in the reactor (FO 1)

The pH remains reasonably constant for the entire period of the experiment (figure 8.6). After the third sulphide inlet point, the pH increases more dramatically, as the system reaches near-equilibrium. Approximately 80% of the copper is removed and the excess sulphide consumes protons to form HS^- and H_2S (depending on the pH see figure 3.1) or is complexed to the copper, suggested by the lack of excess sulphide in the system (see Table 8.4). These phenomena, underlying the pattern of pH increase up the column also correspond to the increase in copper removal efficiency, with no significant increase in efficiency observed after the third sulphide addition point.

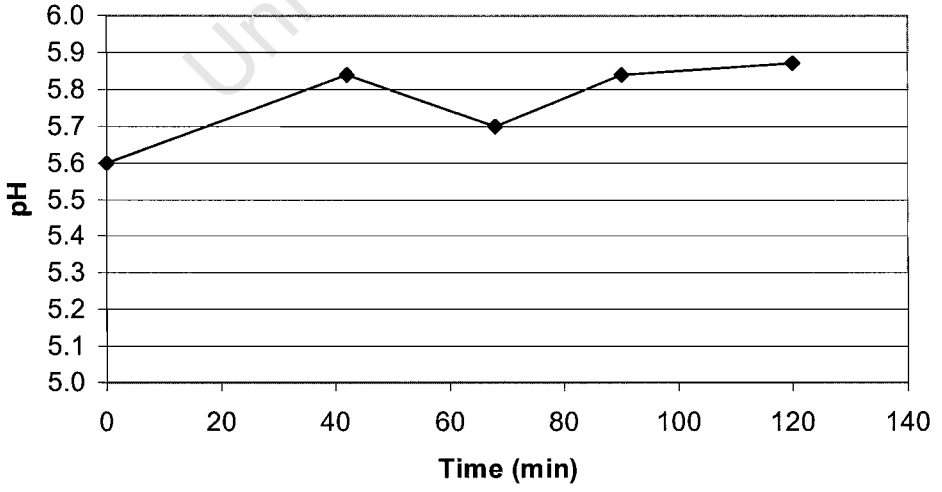

Figure 8.6 pH profile as a function of time (FO 1)

8.3.5 Quantitative analysis of sand pellets

Table 8.7. EDS analysis of sand pellets from the fluidised bed reactor

Position in Reactor (cm) ***Elements (Atomic %)***	***65***	***55***	***45***	***35***	***25***	***15***	***Reference***
O	48.94	49.22	52.11	52.87	54.35	51.95	53.44
Si	49.09	47.32	42.54	40.48	26.56	43.06	39.54
S	0.84	0.62	0.70	0.50	1.12	1.11	0.20
K	0.21	0.81	0.84	1.13	1.00	0.55	1.13
Ca	0.49	1.44	3.18	4.37	15.8	2.53	5.56
Cu	0.43	0.60	0.62	0.65	1.20	0.80	0.13

Pellets exposed for 90 minutes in the fluidised bed reactor were analysed using EDS analysis. Table 8.7 shows the analysis of sand pellets from sample points 1 through 5 along the reactor. The first of the five sample points is 15cm from the bottom of the reactor the rest are equally spaced at 10cm intervals. A control sand sample is used as a reference.

The sand particles only became fully coated with precipitate after at least 48 hours in the reactor, depending on the concentration of the inlet streams. After 90 minutes there was an observed increase in the amount of copper and sulphur on the sand particles when compared with the control. Ratios of copper to sulphide ranged from 1:1 to 1:2 but no conclusive results could be drawn from these ratios. It was only possible to conclude that there was some deposition of a copper sulphide species onto the sand as evidenced by an increase in atomic mass percentage of both compounds compared to the control.

8.3.6 SEM analysis

During preliminary testing in the pellet reactor, SEM (Scanning electron microscope) photographs of sand pellets were taken. Figure 8.7, may be used as a reference picture. Figure 8.8 shows a coating on the sand particles taken 10cm from the bottom of the reactor. These sand particles were in the reactor for 5 days. Figure 8.9 and

8.10 are sand particles taken 30cm from the bottom of the reactor. The particles are not entirely covered but a layer of precipitate is clearly visible.

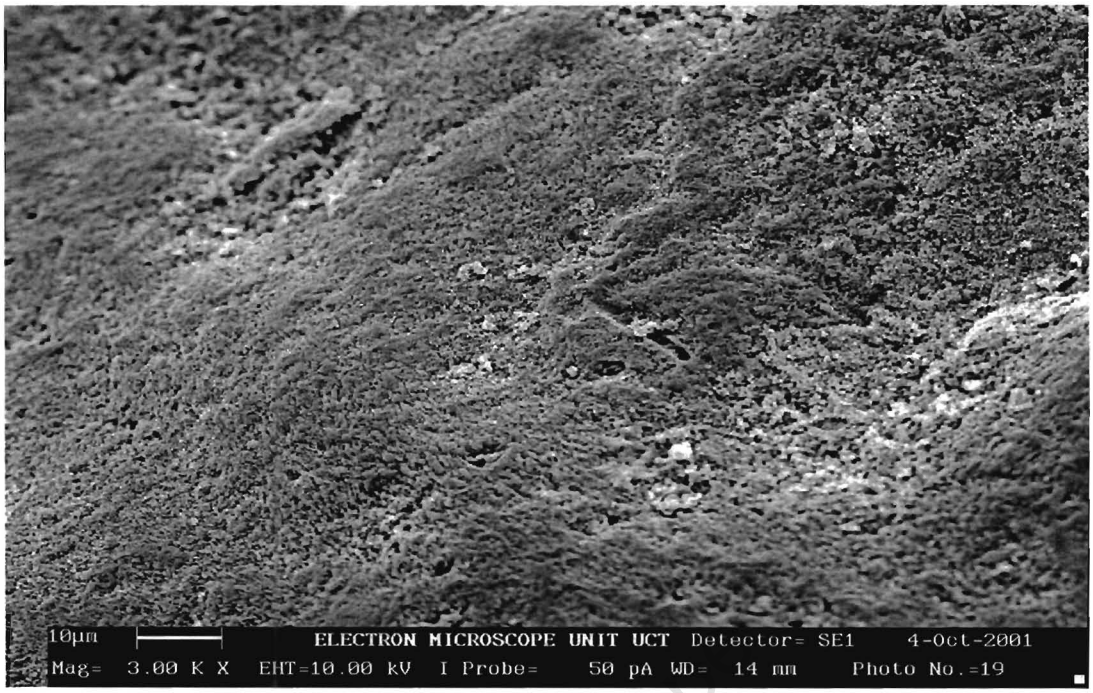

Figure 8.7 Blank sand particle. Magnitude 3K X

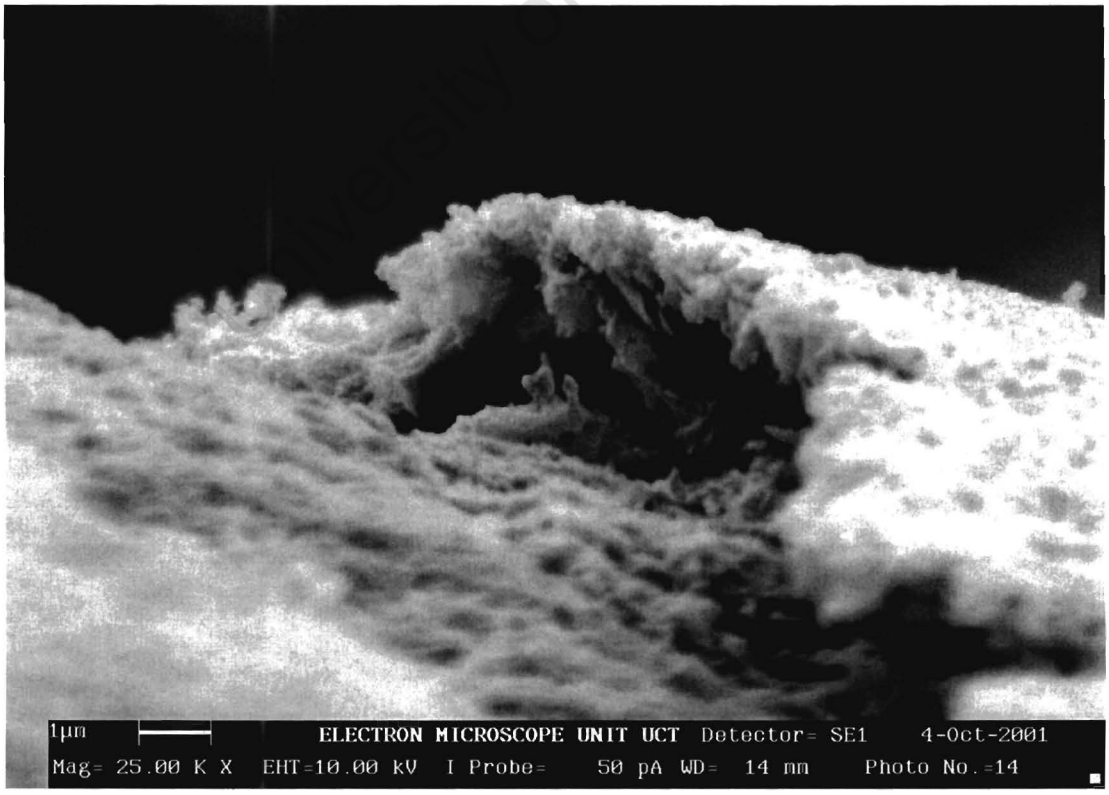

Figure8.8 Copper/Sulphide coating on sand particle 25K X

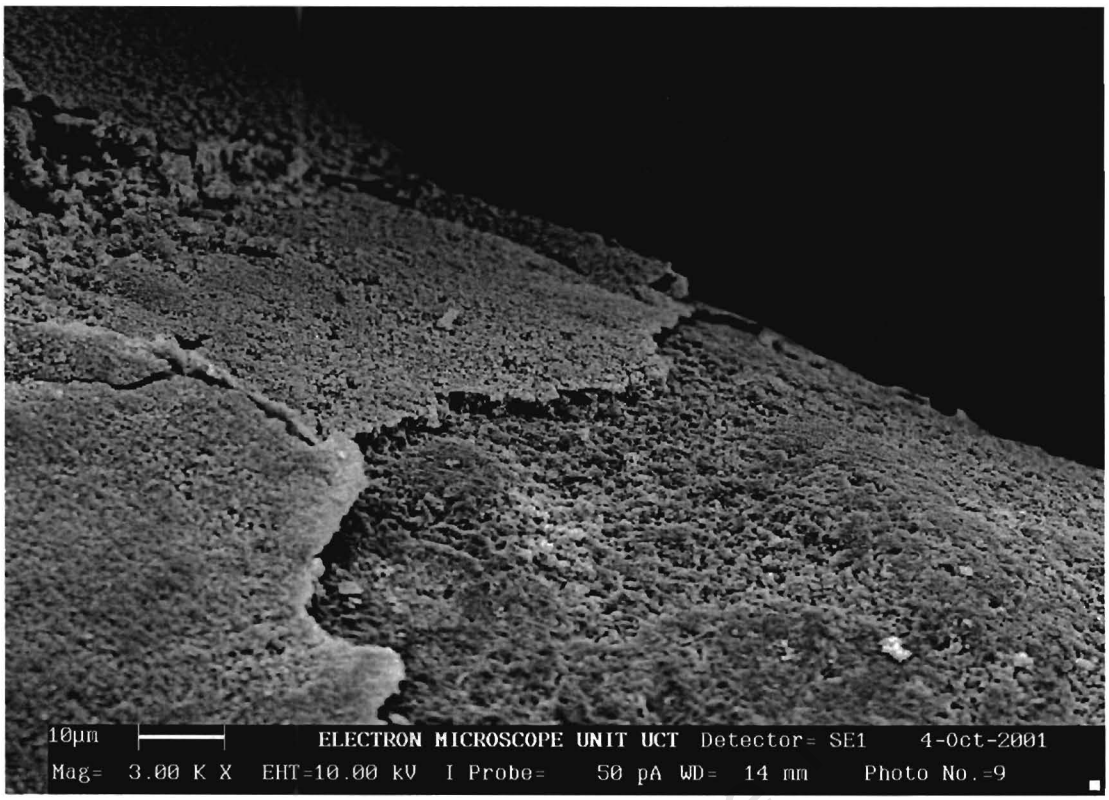

Figure 8.9 Copper/Sulphide coating on sand particle 3K X

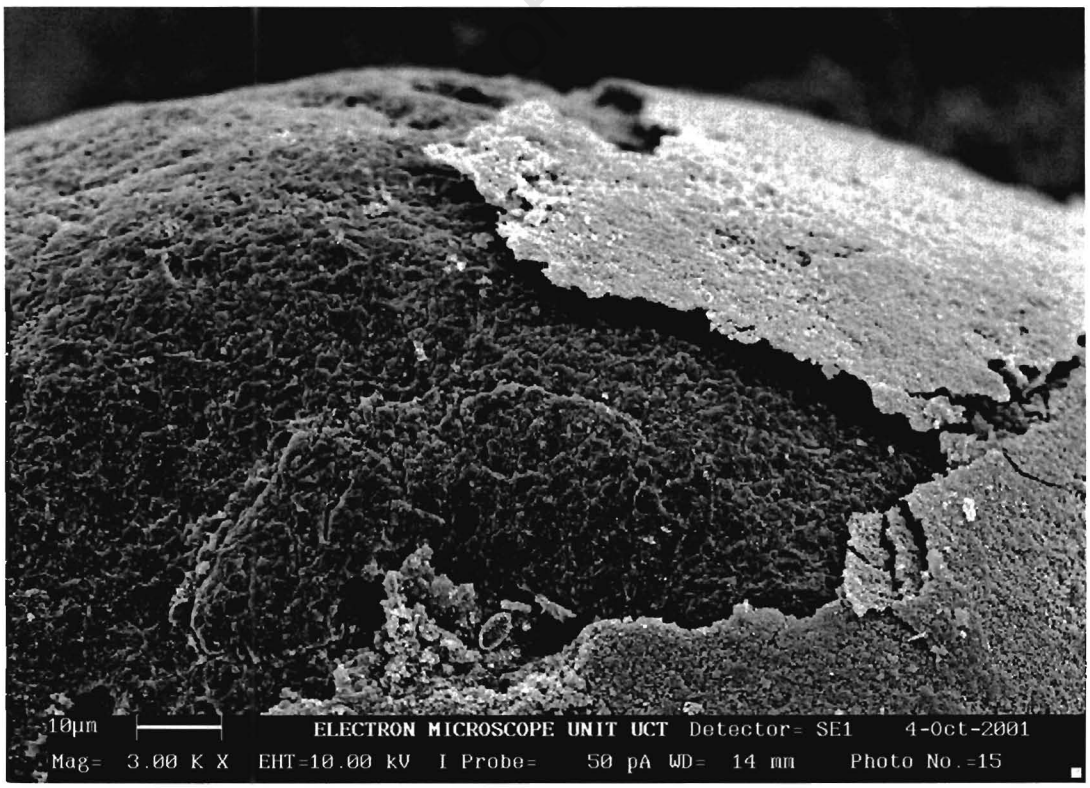

Figure 8.10 Copper/Sulphide coating on sand particle 3K X

8.3.7 Polishing

Treatment of the reactor effluent using *Azolla Filiculoides* gave promising results, and the copper concentration in the effluent stream was reduced to within legal limits. Figure 8.11 is the result of a preliminary testing performed with Azolla in a 20cm high, 2cm ID column. The results show rapid saturation of the Azolla with good initial recovery of copper. The accurate calculation of the loading of biomass is required. A much larger column would be required however. This has potential as a promising technique for post treatment.

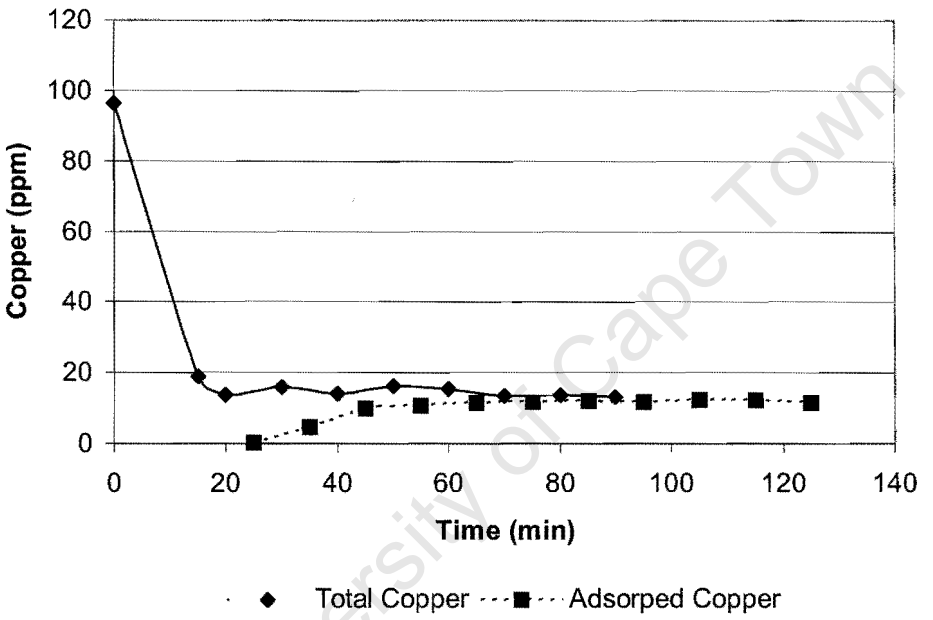

Figure 8.11 Copper concentration after post treatment as a function of time

8.3.8 Attrition Effects

Figure 8.12 shows the effect of shutting off the feed to the reactor, replacing it with water and keeping all other conditions constant. The conditions for the results shown in figure 8.12 are presented in table 8.8. A sudden decrease in copper concentration is observed after shutting off the flow. There does however seem to be some dissolution of the copper off the sand pellet as even after two hours of operating the column with water some copper is present in the effluent stream. There is still a slight difference between the dissolved concentration and fines possibly resulting from the attrition of particles.

Table 8.8 Attrition investigation conditions.

Variable	
S:Cu (mole:mole)	1.25
$[Cu^{2+}]$ (ppm)	100
Inlet flow (ml/min)	40
Recycle Ratio	1.76

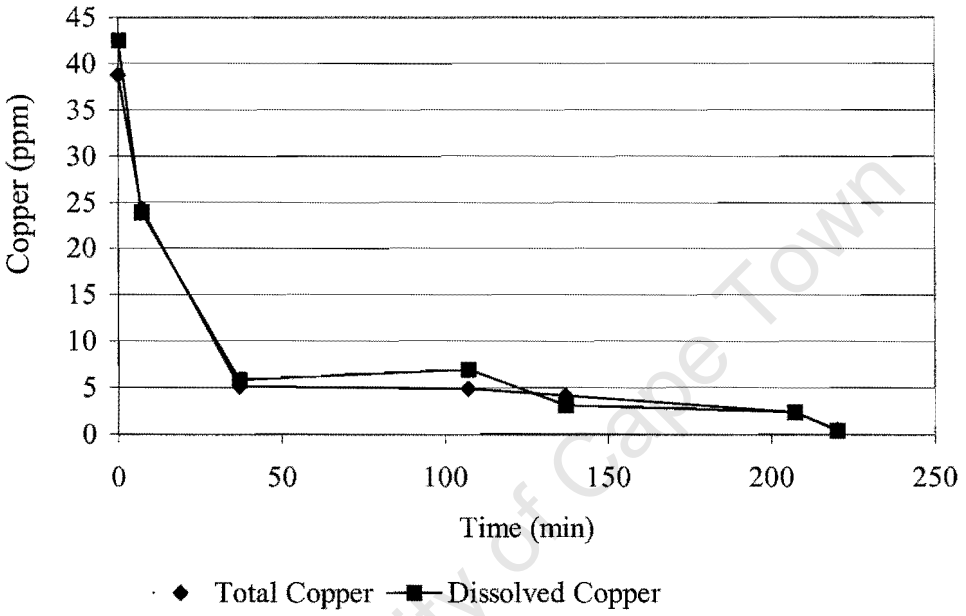

Figure 8.12 Copper concentration as a function of time after shutting off reactants

8.4 Surface Response Methodology

8.4 1 First-order model

In phase one a one-half 2^4 factorial design was used to screen factors (S:Cu (ppm:ppm) = A; [Cu] (ppm) = B; Flow rate (ml/min) = C; Recycle flow rate (ml/min) = D) and provide some information on the interaction of parameters. The half replicate consisting of thirteen experiments (Table 8-11), 8 for the half replicate and 5 centre points to calculate random error. Table 8-10 shows the encoded and natural variables for the factorial design. The 13 experiments were analysed using the SAS statistical package. The regression models for copper conversion and copper efficiency are given in equation (8-2) and (8-3) respectively. A t-test was used to

calculate the p-values (Table 8.9) for both sets of regression coefficients in equations (8-2) and (8-3). The t-test shows that the S:Cu ratio is the only significant term; $p_{copper\ conversion} = 0.0016$ and $p_{copper\ efficiency} = 0.0013$. This ratio is therefore the only variable that significantly impacts on the efficiency of the system.

The first order regression model

$$\text{Copper Conversion} = 44.56 + 29.53A - 0.03800B + 0.2711C + 0.02147D \quad (8\text{-}2)$$

$$\text{Copper Efficiency} = 43.58 + 30.10A - 0.02952B + 0.1724C + 0.02922D \quad (8\text{-}3)$$

Table 8.9 p-values for the first-order regression models

Variable	***p-value Copper Conversion***	***p-value Copper Efficiency***
Intercept	0.006	0.0064
S:Cu (mole:mole)	0.0016	0.0013
$[Cu^{2+}]$ (ppm)	0.2628	0.3726
Inlet Flow rate (ml/min)	0.1246	0.3022
Recycle (ml/min)	0.6017	0.4761

Table 8.10 Natural and encoded variables

Variable	***Natural Variable Value***	***Encoded Variable Level***
S:Cu (mole:mole)	1.5	-
	1	+
$[Cu^{2+}]$ (ppm)	150	+
	50	-
Inlet Flowrate	50	+
(ml/min)	30	-
Recycle	181	+
(ml/min)	141	-

Table 8.11 One-half 2^4 factorial design

Experiment No.	*A* *S:Ci*	*B* *[Cu^{2+}]*	*C* *Inlet flow*	*D* *Recycle*
FO1	1	1	1	1
FO2	0	0	0	0
FO3	1	-1	1	1
FO4	-1	-1	1	1
FO5	0	0	0	0
FO6	0	0	0	0
FO7	1	1	-1	-1
FO8	1	-1	-1	1
FO9	-1	1	1	-1
FO10	-1	-1	-1	-1
FO11	0	0	0	0
FO12	0	0	0	0
FO13	-1	1	-1	1

Table 8.12 Analysis of variance for copper conversion

Source of variation	*Degrees of freedom*	*SS*	*MS*	*F-value*	*Probability*
Model	4	529.56			
Quadratic Effects	1	63.43	63.43	11.87	$p<0.01$
Other Effects	3	75.06	25.02	4.680	$p>0.05$
Pure Error	4	21.83	5.34		
Total	12	689.43			

The analysis of variance (ANOVA) results are illustrated below in table 8.12. The F-values in Table 8.12 are greater than those in reference tables (Napier-Munn, 2001). This implies that quadratic terms need to be added to the regression equation in order to give a better estimate of the system and the interaction between variables. A linear regression model implies that there is no curvature in the surface and the calculated F-values prove that curvature exists. The model accounts for 77% of the variation in copper conversion (SS_{model}/SS_{total}). Table 8.13 shows similar results for the copper concentration. Once again there are significant quadratic effects and the model accounts for 76% of the variation in the copper efficiency. Since the quadratic terms

were significant, a second order model was required to more accurately describe the system.

Table 8.13Analysis of variance for copper efficiency

Source of variation	*Degrees of freedom*	*Sum of Squares (SS)*	*Mean Square (MS)*	*F-value*	*Probability*
Model	4	817.43			
Quadratic Effects	1	190.20	190.20	28.04	p<0.01
Other Effects	3	91.55	30.52	4.50	p>0.05
Pure Error	4	24.13	6.78		
Total	12	1126.32			

8.1.2 Second-order model

The first-order model reveals that the variables; copper concentration (B), inlet copper flow rate (C) and the recirculation flow (D) are insignificant in the first order model, although they do contribute to the interaction parameters. Initial second order model estimates using the SAS package, led to the omission of the flow rate variable. This omission of the flow rate was as a result of ridge analysis that showed an almost constant flow rate (40 ml/min) at the different coded radii for the copper removal and copper efficiency. The other factors showed a reasonable change over the various radii that were investigated (see appendix A8.4 for the full set of SAS analysis).

The second-order response surface for the real values are estimated by SAS is given for copper conversion in equation (8-3) and copper efficiency in equation (8-4).

$$\text{Copper Conversion} = -85.91 + 128.40\ A + 0.2437\ B + 0.9638\ D - 21.87\ A^2 - 0.001324\ B^2 - 0.002290\ D^2 - 0.01140\ AB - 0.3005\ AD + 0.000290\ BD \quad (8\text{-}3)$$

$$\text{Copper Efficiency} = -115.72 + 133.67\ A + 0.5806\ B + 1.062\ D - 19.92\ A^2 - 0.001841\ B^2 - 0.002435\ D^2 - 0.1275\ AB - 0.2926\ AD + 0.000290\ BD \quad (8\text{-}4)$$

The factors accounted for 60% of the variation in copper conversion and 58.6% of the variation in copper efficiency. Canonical analysis predicted the presence of a stationary point for both systems. Canonical analysis is best described by comparing it to a multiple regression. In multiple regressions two sets of variables are fitted to one response, however in canonical analysis a set of responses is matched to a set of variables. The three eigenvalues of the variables for the copper conversion as well as copper efficiency were all negative indicating that the stationary points were in fact maxima. The co-ordinates and responses of the predicted maxima are shown in Table 8.14.

Table 8.14 Second order predicted stationary points

Variable	***Natural value Copper Conversion***	***Natural value Copper Efficiency***
Predicted Response	113	114
S:Cu	2.6	2.8
$[Cu^{2+}]$ (ppm)	86	55
Recycle (ml/min)	45	42

It was possible to operate the system at these predicted maxima but these values were outside the experimental region and inconsistent with the model. A ridge analysis was therefore carried out.

Ridge analysis in Figure 8.13 and 8.14 predicted 100 percent removal would be achieved at a coded radius of 1 for copper removal and copper efficiency respectively (see Appendix A8.4 for the SAS analysis).

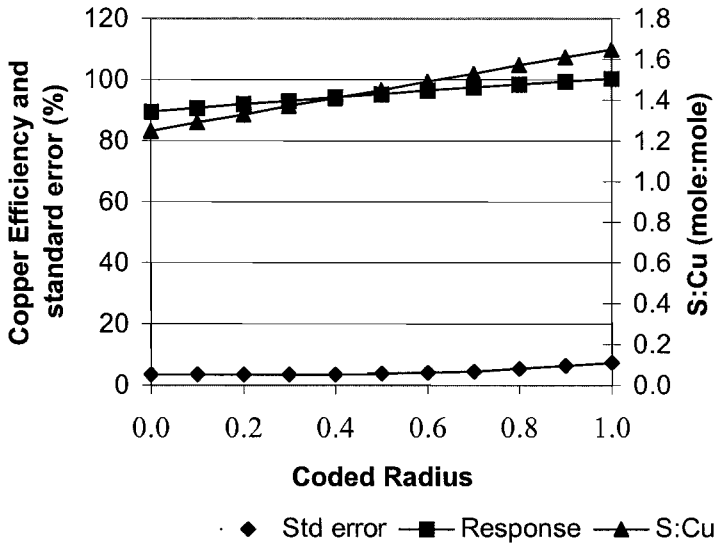

Figure 8.13 The Ridge of maximum response for copper Efficiency

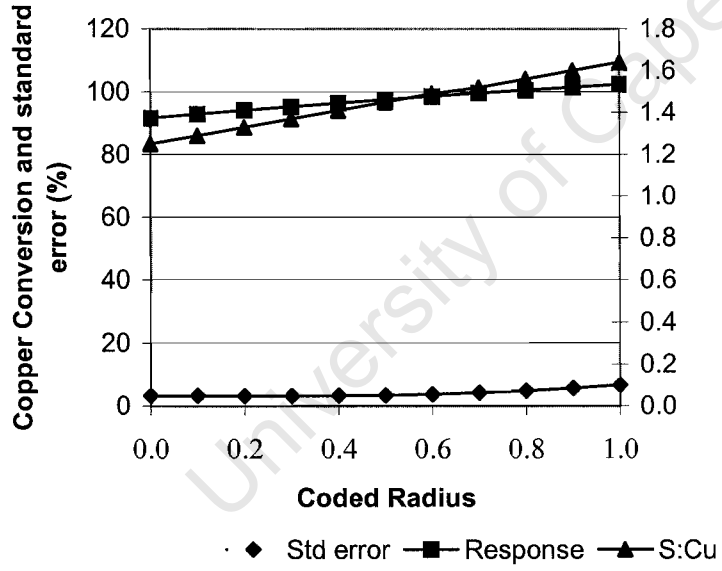

Figure 8.14 The Ridge of maximum response for copper conversion

As expected, an increased the S:Cu ratio leads to an increase in copper conversion and copper efficiency. A comparison is made between ridge analysis and experimental analysis for copper efficiency in Table 8.15. At a S:Cu ratio of 1.5:1 and a coded radius of 0.6, conditions strongly resemble those that gave similar results during the RSM experiments. The decrease in efficiency could be attributed to the high inlet

copper concentrations used in the experiments. Table 8.15 shows that the ridge analysis predicts that the optimum copper loading in the column would be a maximum value of 97ppm of copper.

Table 8.15 Ridge Analysis vs. experimental results

Variables	***Coded Radius 1***	***Coded Radius 0.6***	***FO 9***	***FO 13***
Estimated Response	100	96		
Copper Efficiency (%)			95	92
S:Cu (mole:mole)	1.6	1.5	1.5	1.5
$[Cu^{2+}]$ (ppm)	93	97	150	150
Recycle (ml/min)	121	130	100	181

Chapter Nine

Conclusions

9.1 Comparison between theoretical and experimental solubility values

Theoretical predictions showed that copper sulphide (CuS) rather than copper hydroxide ($Cu(OH)_2$) precipitated, due to the lower solubility of the copper sulphide over the entire pH range. The complexity of the CuS system led to various predicted solubility curves. The graph that was most representative for the CuS system predicted residual copper values within the range between 1×10^{-5} and 1×10^{-7}mol/l. The minimum measured value of 5×10^{-7}mol/l taken was found within this range. The simulation packages ASPEN PLUS™ and OLI Systems predicted that the CuS precipitate was the thermodynamically stable compound and that complete removal of copper was achieved under the given conditions.

9.2 The effect of local and global supersaturation on the formation of fines

Experimental work showed the significance of the influence of the supersaturation on the formation of fines. Homogeneous nucleation was found to be the cause of fines at high supersaturation values. Decreasing both the local and global supersaturation significantly reduced fines. A decrease in local supersaturation was achieved by decreasing the inlet concentrations at the inlet points and increasing the flow rate. Decreased global supersaturation was achieved by increasing the recirculation flow rate.

It was found that, once fines were formed, they persisted throughout the experiment. There was no agglomeration of fines onto the pellets and the only way to eliminate fines was to prevent their formation. This is in contrast with previous work on nickel carbonate in a fluidised bed reactor (Guillard and Lewis, 2001). Minimal fines were formed due to attrition of particles because of movement of particles in the reactor.

9.3 Copper removal efficiency

Copper was found to have a weak affinity for sand particles in the absence of sulphide. However, after the addition of sulphide, copper reacted with the sulphide and rapidly formed a CuS precipitate.

The pH value of the discharge stream was maintained to within reasonable discharge limits of between 6 and 6.5. An initial sharp decrease in the pH at the region around the acid inlet was moderated by the production of HS^- ions during the precipitation reaction. An increase in pH up the column corresponded to an increase in copper removal.

Steady state was reached in the reactor after 20 minutes of operation. Kinetics were found to be rapid with a significant decrease in copper concentration within the first 5 minutes. A maximum dissolved copper removal of 99.62% was achieved within the reactor and a total removal efficiency of 95.8%. A pH of 5 was found to promote faster kinetics and eliminated the need for post reactor pH adjustment.

9.4 Identification of important factors using Response Surface Methodology (RSM)

Factors found to influence supersaturation (S:Cu ratio, inlet copper concentration, inlet copper flow rate and recirculation) were investigated using a Response Surface Methodology (RSM) statistical design. The RSM identified the S:Cu ratio as the most influential variable in the fluidised bed system. A one-half 2^4 design identified that quadratic terms in the first order design were significant and that it was necessary to design a second-order experiment to map the curved surface that was found to exist.

9.5 Identification of a maximum on the curved surface

A second-order statistically designed experiment identified a maximum response of 114% on the curved surface at conditions: S:Cu ratio = 2.6, inlet copper concentration = 85.70 ppm and a recirculation of 44.97 ml/min. The inlet flow rate of the copper was subsequently omitted as an initial ridge analysis showed that it did not contribute

significantly to the surface and it remained approximately constant at 40ml/min. These conditions however, did not fall within system boundaries and a second ridge analysis was performed. Table 9.1 shows the predicted operating conditions as compared to the experimental limits.

Table 9.1 Second order predicted stationary points

Variable	***Natural value Copper Conversion***	***Natural value Copper Efficiency***	***Experimental Limits***
Predicted Response (%)	113	114	
S:Cu (mole:mole)	2.6	2.8	1-1.5
$[Cu^{2+}]$ (ppm)	86	55	100-150
Recycle (ml/min)	45	42	101-181

9.6 Conditions for maximum copper removal from ridge analysis

Operating conditions calculated from ridge analysis identified optimal conditions within the experimental boundaries. These conditions were validated by experiments performed at almost identical conditions and the predicted responses were attained. A comparison of the experimental and operating conditions are shown in Table 9.2.

Table 9.2 Ridge analysis vs. experimental results

Variables	***Coded Radius 1***	***Coded Radius 0.6***	***FO 9***	***FO 13***
Estimated Response	100	96		
Copper Efficiency (%)			95	92
S:Cu (mole:mole)	1.6	1.5	1.5	1.5
$[Cu^{2+}]$ (ppm)	93	97	150	150
Recycle (ml/min)	121	130	100	181
Copper Flow rate (ml/min)	40	40	50	30

It was concluded that maximum copper removal from a $CuSO_4$ stream could be achieved by controlling the factors affecting the local and global supersaturation in a fluidised bed reactor.

9.7 Recommendations

Future work should include an investigation into the effects of the sand size and different seeding materials. A possible material might include silicon balls, similar in texture to a flexible rubber hose. During preliminary test work in a beaker containing copper sulphate, it was observed that the CuS precipitate that formed after sparging H_2S in the batch reactor, clung to a silicon tube delivering the gas to the beaker. Successful work has been carried out by Feng *et al* (2000) using magnetite seeds in a batch system to remove metals from acid mine drainage.

References:

Baltpurvins, K.A., Burns, R.C., Lawrance, G.A. and Stuart, A.D., 1996. Use of the solubility domain approach for the modelling of the hydroxide precipitation of heavy metals from wastewater, *Environmental Science and Technology*, Vol 30, pp 1493-1499.

Baltpurvins, K.A., Burns, R.C., Lawrance, G.A., 1996. Heavy metals in wastewater: Modelling the hydroxide precipitation of copper (II) from wastewater using lime as the precipitant, *Waste Management*, Vol. 16, No. 8, pp717-725.

Barnes, L.J., Janssen, F.J., Scheeren, P.J.H., Versteegh, J.H. and Koch, R.O., 1991. Simultaneous microbial removal of sulphate and heavy metals from waste water, In *Proceedings of EMC'91:Non-Ferrous Metallurgy-Present and Future*, Elsevier Applied Science, London, UK pp. 391-402.

Becker, R. and Döring, W, 1935. *Ann. Physik,* 24, 719. In: Elving, P.J. and Kolthoff, I.M., 1979. *The formation and properties of precipitates*, Vol. 23, New York: Robert E. Krieger Publishing.

Bell, J., Dama, P., Buckley, C. and Stuckey D., 2002. Pre scale-up laboratory investigation of the anaerobic baffled reactor, *Chemical Technology*, June, pp 5-9.

Berthoud, A., 1912. Theorie de la formation des faces d'un crystal. *Journal de Chimique Physique,* **10**, 624-635. In: Mullin, J.W., 2001. *Crystallization*, 4th Edition, London: Butterworth-Heinemann.

Bhattacharyya, D., Jumawan, A.B. and Sun, G., 1980. Precipitation of heavy metals with sodium sulfide: Bench-scale and full-scale experimental results, *AIChe Symposium Series, Water*, 77(209), pp. 31-38.

Bollinger, J., Bourg, B., Gal, J. and Rouyer, P., 1992. Thermodynamic study in aqueous solutions of weakly soluble ionic compounds, *Talanta,* Vol. 39, No. 8, pp. 959-965.

Coulson, J.M. and Richardson, J.F., 1991. *Chemical Engineering*, 4th Edition, Vol. 2, Oxford: Butterworth-Heinemann.

Clontz, N.A. and McCabe, W.L., 1971. Contact nucleation of $MgSO_4$ $7H_2O$. *Chemical Engineering Progress Symposium Series No. 110,* **67**, 6-17. In: Mullin, J.W., 2001. *Crystallization*, 4th Edition, London: Butterworth-Heinemann.

Department of Water Affairs and Forestry (DWAF). 1998. Waste Management Series: Minimum requirements for the handling, classification and disposal of hazardous waste. 2nd Edition, CTP Book Printers, Cape Town, pp. 171.

Dryssen, D., 1988. Sulfide complexation in surface seawater, *Marine Chemistry*, Vol. 24, pp. 143-153.

Ebbing, D., 1990. *General Chemistry* 5th Edition, Boston: Houghton Mifflin Company.

Eckenfelder, W., 1966. *Industrial water pollution control*, New York: McGraw Hill.

Elving, P.J. and Kolthoff, I.M., 1979. *The formation and properties of precipitates*, Vol. 23, New York: Robert E. Krieger Publishing.

Feng, D., Aldrich, C. and Tan, H., 2000. Treatment of acid mine water by use of heavy metal precipitation and ion exchange, *Minerals Engineering*, Vol. 13, No. 6, pp. 623-624.

Franke, J. and Mersmann, A., 1995. The influence of the operational conditions on the precipitation process, *Chemical Engineering Science*, Vol. 50, No.11, pp. 1737-1753.

Gibbs, J.W., 1928. *Collected Works*, Longmans, London, p. 325. In: Elving, P.J. and Kolthoff, I.M., 1979. *The formation and properties of precipitates*, Vol. 23, New York: Robert E. Krieger Publishing.

Gösele, W. and Kind, M., 1991. *Versuche zum Einfluß der Vermischung auf die Qualität eines kontinuierlich gefällten Produktes,* Chem. Ing. Tech., **63**, n1, 59-62.

Guillard, D., 2001. *Nickel hydroxy-carbonate precipitation in a pellet reactor*, Masters thesis, University of Cape Town, Cape Town.

Hansford, G.S., Harrison, S.T.L. and Lewis, A.E., 2000. An investigation of the mechanisms and kinetics of bacterial sulphate reduction, *Progress Report,* Water Research Commission.

Henning, G., 1990. *Industrial Crystallization* 90, p113, ed. A Mersmann, Garmisch, FRG. In Söhnel, O. and Garside, J., 1992. *Precipitation basic principles and industrial application*, Oxford: Butterworth-Heinemann.

Hess, B. and Kok, D.J., 1996. *Kidney Stones Medical and Surgical Management*, Philadelphia: G. M. Preminger, Lippincott-Raven Publishers.

Kim, B.M., 1980. Treatment of metal containing wastewater with calcium sulfide, *AIChe Symposium Series, Water.*

Kind, M., 1999. Precipitation phenomena and their relevance to precipitation technology, *Proceedings of 14th International Symposium on Industrial Crystalization.*

Knobel, A.K. and Lewis, A.E., 2001. A mathematical model of a high sulphate wastewater anaerobic treatment system, *Water Research,* **36**, 257-265.

Kossel, W., 1934. Zur Energetik von Oberflächenvorgängen. *Annalen der Physik,* **21**, 457-480. In: Mullin, J.W., 2001. *Crystallization*, 4th Edition, London: Butterworth-Heinemann.

Kratochvil, D., Fourest, E. and Volesky, B. 1997. Biosorption of Cu from ferruginous wastewater by algal biomass, *Water Research*, **32**, 2760-2768.

Lewis, A., Peterson, K. and Lacour, S., 2002. Copper removal from acid mine drainage using a fluidised bed reactor, *Proceedings in 15th International Symposium on Industrial Crystallization, Sorrento, Italy.*

Licht, S., 1988. Aqueous solubilities, solubility products and standard oxidation-reduction potentials of the metal sulphides, *Journal of the Electrochemical Society*, Vol. 135, No. 12, pp. 2971-2975.

McAnally, S., Benefield, L. and Reed, R.B., 1981. Nickel removal from synthetic nickel-plating wastewater using sulphide and carbonate for precipitation and coprecipitation, *Proc. Ind. Waste Conference 39th, pp. 81-89.*

McAnally, S., Benefield, L. and Reed, R.B., 1984. Nickel removal from synthetic nickel-plating wastewater using sulphide and carbonate for precipitation and co precipitation, *Separation Science and Technology*, Vol. 19, pp 191-217,

Miers, H.A. and Isaac, F., 1904. Refractive indices of crystallizing solutions. *Journal of the Chemical Society,* **89**, 413-454. In: Mullin, J.W., 2001. *Crystallization*, 4th Edition, London: Butterworth-Heinemann.

Miller I. and Freund J.E., 1985. *Probability and Statistics for Engineers*, Prentice/Hall International, Inc., New Jersey.

Moosa, S., 2000. *A kinetic study on anaerobic sulphate reduction*, Doctoral thesis, University of Cape Town.

Mosselmans, J.F.W., Charnock, J.M., Garner, C.D., Pattrick R.A.D. and Vaughan, D.J., 1995. A XAS study of the structural changes undergone by amorphous copper sulphides when precipitated from solution, *Physica B: Condensed Matter,* Volumes 208-209, Issues 1-4, pp. 609-610.

Mullin, J.W., 2001. *Crystallization*, 4th Edition, London: Butterworth-Heinemann.

Myers, H. and Montgomery, D.C., 1995. *Response surface methodology. Process and product optimisation using designed experiments*, New York: Wiley.

Napier-Munn, T.J., 1996. An introduction to comparative statistics and experimental design for minerals engineers, Course notes, University of Queensland, 2nd Edition, version 2.2.

Nernst, W., 1904. Theorie der Reacktionsgeschwindingkeit in heterogenen Systemen. *Zeitschrift für Physikalische Chemie,* **27**, 1434-1444. In: Mullin, J.W., 2001. *Crystallization*, 4th Edition, London: Butterworth-Heinemann.

Nielsen, P.B., Christensen, T.C. and Vendrup, M., 1997. Continuous removal of heavy metals from FGD wastewater in a fluidised bed without sludge generation, *Elsevier Science Ltd.*, Vol. 36, pp391-397.

Noyes, A.A. and Whitney, W.R., 1897. Rate of solution of solid substances in their own solution. *Journal of the American Chemical Society,* **19**, 930-934. In: Mullin, J.W., 2001. *Crystallization*, 4th Edition, London: Butterworth-Heinemann.

Nyvlt, J., 1992. *Design of Crystallizers*, Institute of Inorganic Chemistry Czechoslovak Academy of Science Prague, Czechoslovakia.

Pattrick, R.A.D., Mosselmans, J.F.W., Charnock, J.M., England, K.E.R., Helz, G.R., Garner, C.D., and Vaughan, D.J., 1997. The structure of amorphous copper precipitates: An X-ray absorption study, *Geo. Et Cosmochimica Acta*, Vol. 61, No. 10, pp. 2023-2036.

Peters, R.W., Ku, Y. and Chang, T., 1983. Heavy metal crystallization kinetics in an MSMPR crystallizer employing sulfide precipitation, *AIChe Symposium Series, Advances in Crystallization from Solutions*.

Peters, R.W., Ku, Y., 1998. Batch precipitation studies for heavy metal removal by sulphide precipitation, *AIChe Symposium Series, Separation of Heavy Metals*.

Petersen, F.W., 2002. Stabilization of solid waste through the precipitation of a mineral phase, *Chemical Technology*, August, pp. 11-13.

Pohorcki, R. and Baldyga, J., 1988. Chem. Eng. Sci., 43, 1949. In: Söhnel, O. and Garside, J., 1992. *Precipitation basic principles and industrial application*, Oxford: Butterworth-Heinemann.

Randolph, A.D. and Larson, M.A., 1988. *Theory of particulate processes: Analysis and techniques of continuous crystallisation*, 2nd Edition, and San Diego: Academic Press.

Rhodes, M., 1998. *Introduction to Particulate Technology*, University of Monash, Australia ISBN 0-471-98482-5.

Rao, S.R. and Hepler, L.G., *Hydrometallurgy,* 2, 293, 1977. In Licht, S., Aqueous solubilities, solubility products and standard oxidation-reduction potentials of the metal sulfides, 1988. *Journal of the Electrochemical Society*, Vol. 135, No. 12, pp. 2971-2975.

SABS 2001 *"South African Standard Specification for Drinking Water"* SABS 241 publication.

Schöller, M., van Dijk, J.C. and Wilms, D., 1987. Recovery of heavy metals by crystallization in the pellet reactor, Environmental Technology.

Seckler, M.M., 1994. *Calcium phosphate precipitation in a fluidised bed*, Doctoral thesis, Delft University of Technology.

Smith, R.M., and Martell, A.E., 1976. *Critical Stability Constants*, Vol. 4, New York: Plenum Press.

Söhnel, O. and Garside, J., 1992. *Precipitation basic principles and industrial application*, Oxford: Butterworth-Heinemann.

Stickland-Constable, R.F., 1968. *Kinetics and Mechanism of Crystallization,* Academic Press, London. In: Mullin, J.W., 2001. *Crystallization*, 4th Edition, London: Butterworth-Heinemann.

Stickland-Constable, R.F., 1968. *Kinetics and Mechanism of Crystallization,* Academic Press, London. In: Randolph, A.D. and Larson, M.A., 1988. *Theory of particulate processes: Analysis and techniques of continuous crystallisation*, 2nd Edition, and San Diego: Academic Press.

Stumm, W. and Morgan, J.J., 1996. *Aquatic chemistry, chemical equilibria and rates in natural waters*, New York: Wiley.

Silvester, E.J., Grieser, F., Sexton, B.A., and Healy, T.W., 1991. *Spectroscopic studies on copper sulfide sols,* Langmuir 7, pp. 2917-2922. In Pattrick, R.A.D., Mosselmans, J.F.W., Charnock, J.M., England, K.E.R., Helz, G.R., Garner, C.D., and Vaughan, D.J., 1997. The structure of amorphous copper precipitates: An X-ray absorption study, *Geo. Et Cosmochimica Acta*, Vol. 61, No. 10, pp. 2023-2036.

Thoenen, T., 1999. Pitfalls in the use of solubility limits for radioactive waste disposal: The case of nickel in sulfidic groundwaters, *Nuclear Technology*, Vol. 126, pp. 75-87.

Tunay, O. and Kabdasli, N.I., 1994. Hydroxide precipitation of complexed metals, *Water Research*, Vol. 28, No. 10, pp. 2117-2123.

Valeton, J.J.P., 1924. Wachstum und Auflösung der Kristalle. *Zeitschrift für Kristallographi,* **59**, 483. In: Mullin, J.W., 2001. *Crystallization*, 4th Edition, London: Butterworth-Heinemann.

Van Hille, R., Lewis, A.E. and Duncan, J., 2002. Removal and recovery of copper from aqueous solution by non-viable biomass of *Azolla filiculoides*, *Water Research,* (in press.)

Volmer, M., 1939. *Kinetic der Phasenbildung,* Steinkopf, Dresden. In: Elving, P.J. and Kolthoff, I.M., 1979. *The formation and properties of precipitates*, Vol. 23, New York: Robert E. Krieger Publishing.

Weiss, N.J., 1985. SME Mineral Processing Handbook, New York: Society of Mining Engineers of the American Institute of Mining, Metallurgical and Petroleum Engineers Inc, Vol. 2.

Wilms, D., Buildeo Rai, P., van Dijk, J. and Schöller, M., 1988. Recovery of nickel by crystallization of nickel carbonate in a fluidised bed reactor, *VVT Symposium on Non-Waste Technology, Espoo, Finland.*

Zhou, M and Duncan, J.R., 1997. Removal and recovery of nickel from aqueous solution and electroplating rinse effluent using *Azolla filiculoides*, *Process Biochemistry*, **33**, pp. 249-255.

Zhou, P., Huang, J.C., Li, A. and Wei, S., 1999. Heavy metal removal from wastewater in fluidised bed reactor, *Water Research*, Vol. 33, No. 8, pp 1918-1924.

Appendix

Appendix A5

A5.1 Pump Calibration

Table A5-1. Masterflex pump calibration curve
Tubing 14

Graduation	time (s)	volume (ml)	Flow rate (l/min)	Flow rate (L/h)
1	120	11.2	0.006	0.34
1.5	120	26.4	0.013	0.79
2	120	41.9	0.021	1.26
2.5	120	58	0.029	1.74
3	120	73	0.037	2.19
3.5	180	134.9	0.045	2.70
4	60	53.1	0.053	3.19
4.5	60	61.7	0.062	3.70
5	60	69.9	0.070	4.19
5.5	60	78.1	0.078	4.69
6	60	85.9	0.086	5.15
6.5	60	93.2	0.093	5.59
7	60	101.6	0.102	6.10
7.5	60	110.3	0.110	6.62
8	30	59.7	0.119	7.16
9	30	67.43	0.135	8.09

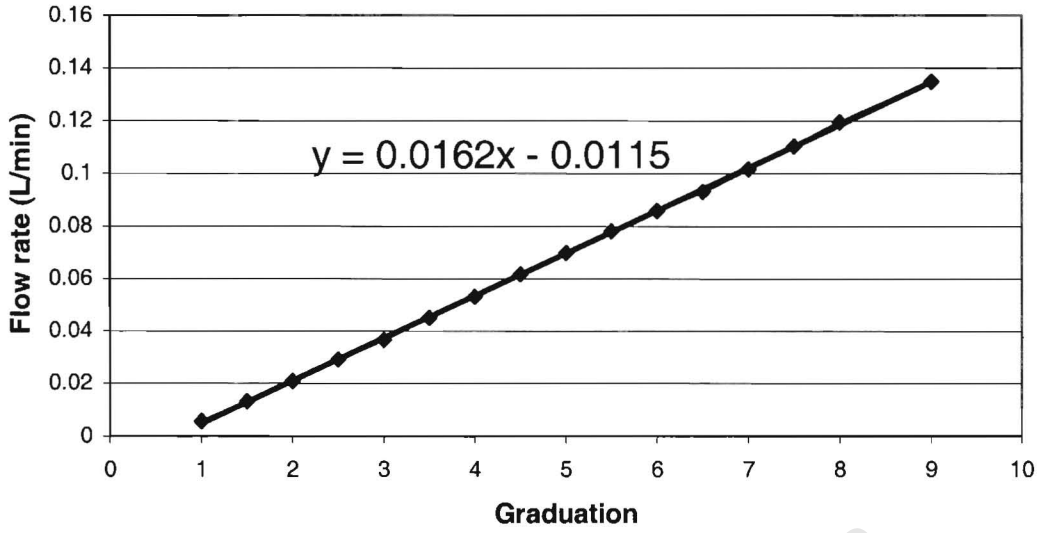

Figure A5.1 Masterflex pump calibration curve (tubing 14")

Table A5-1b Calibration for Masterflex pump (16" tubing)

Graduation	time (s)	volume (ml)	Flow rate (l/min)	Flow rate (l/h)	ml/min
1.00	60	21.7	0.022	1.30	21.7
0.78			0.003	0.18	3
1.45			0.040	2.40	40
1.50	60	47	0.047	2.82	47
1.63			0.050	3.00	50
2.00	60	71.4	0.071	4.28	71.4
2.50	60	97.8	0.098	5.87	97.8
2.72			0.110	6.62	110.4
3.00	60	126.4	0.126	7.58	126.4
3.50	30	76.3	0.153	9.16	152.6
4.00	30	89.9	0.180	10.79	179.8
4.15			0.190	11.40	190
4.50	30	101.9	0.204	12.23	203.8
5.00	30	115	0.230	13.80	230
5.12			0.244	14.62	243.59
5.50	20	87.3	0.262	15.71	261.9
6.00	20	95.7	0.287	17.23	287.1
6.50	20	105	0.315	18.90	315
7.00	20	116.5	0.350	20.97	349.5
7.50	15	96.8	0.387	23.23	387.2
8.00	15	101.2	0.405	24.29	404.8
9.00	15	115.8	0.463	27.79	463.2

Table A5-1c. Calibration for the Watson-Marlow

505S 16" tubing

RPM	Ave Flow rate ml/min
20	37.2
30	54.9
40	72.7
50	91.1
60	110.4
70	128.8
80	147.2
100	186.7
120	223.3
140	261.2
160	302.7
180	340.6
200	375.3
97	181.0
76	141.2
55	101.4

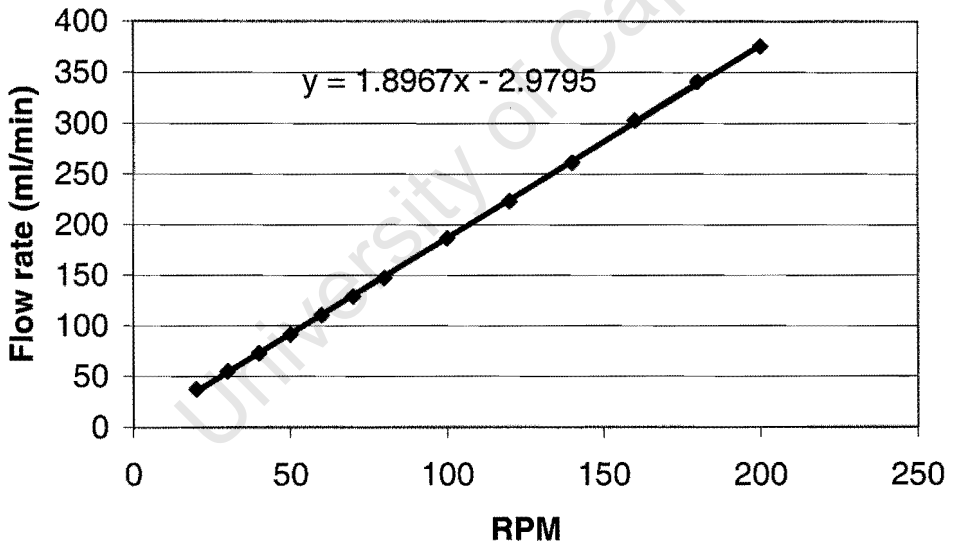

Figure A5.2 Wastson-Marlow 505S pump calibration (16" tubing)

Table A5-1d Calibration of the Watson-Marlow 505U pump (16" tubing)

pump speed RPM	g/min	ml/min
0.5	103.70	0.32
1	103.96	0.58
1.5	104.15	0.77
2	104.57	1.19
3	104.96	1.58
4	105.55	2.17
5	106.09	2.72
6	106.62	3.25
7	107.15	3.78
8	107.74	4.37
9	108.43	5.06
10	109.12	5.75
15	111.54	8.18
20	114.35	10.99
25	117.05	13.70
30	119.84	16.49
35	124.51	21.17
40	125.41	22.07
45	128.11	24.78
50	131.07	27.75

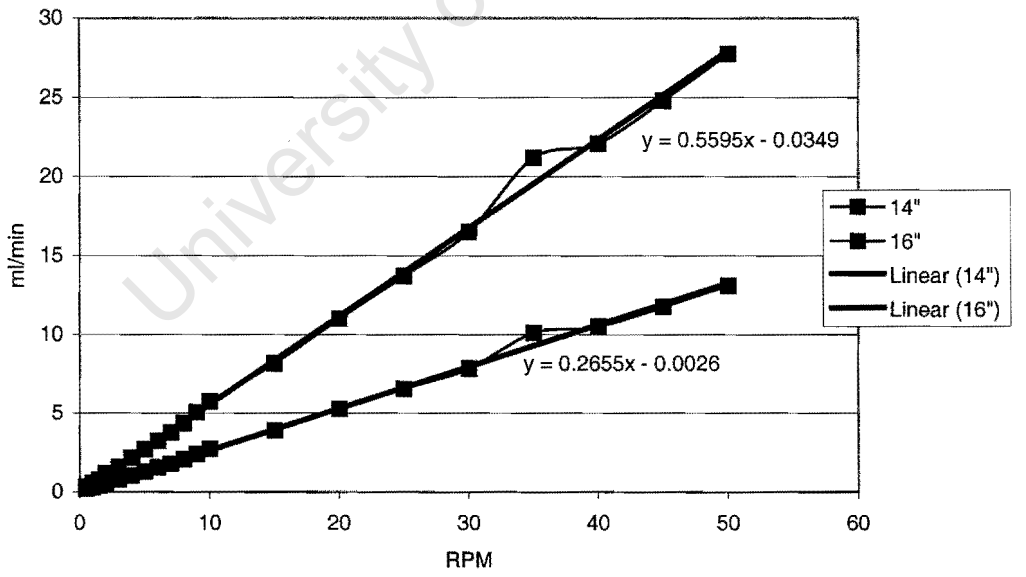

Figure A5.3 Watson-Marlow 505U pump calibration (14 and 16" tubing)

A5.2 Fluidisation velocities

Table A5-2 First Order Experimental Fluidisation Velocities

Experiment No	Fluidisation Velocity (ml/min)
FO1	231
FO2	181
FO3	151
FO4	231
FO5	181
FO6	181
FO7	131
FO8	211
FO9	151
FO10	131
FO11	181
FO12	181
FO13	211

A5.3 Reynold number calculation

$$Ga = \frac{\rho(\rho_s - \rho)gd^3}{\mu} \qquad \text{(A5-1)}$$

d = diameter of particles (m)

ρ_s = density of solid (kg/m^3)

ρ = Density of fluid (kg/m^3)

μ = viscosity of the fluid (Ns/m^2)

Diameter of sand	5.E-04	m
Density of liquid	998	kg/m^3
Density of sand	2550	kg/m^3
Viscosity of liquid	1.E-03	Ns/m^2
Ga	1897	

$$Ga = 150\frac{1-e_{mf}}{e_{mf}^3}\mathrm{Re}'_{mf} + \frac{1.75}{e_{mf}^3}\mathrm{Re}'^2_{mf} \quad \text{(A5-2)}$$

$\mathrm{Re}'_{mf} = 25.7\{\sqrt{1+5.53\times10^{-5}Ga}-1\}$ (Coulson and Richardson, 1980) (A5-3)

Ga	1897
Re'_{mf}	1.31

Appendix A6

A6.1 Explanation of solubility table

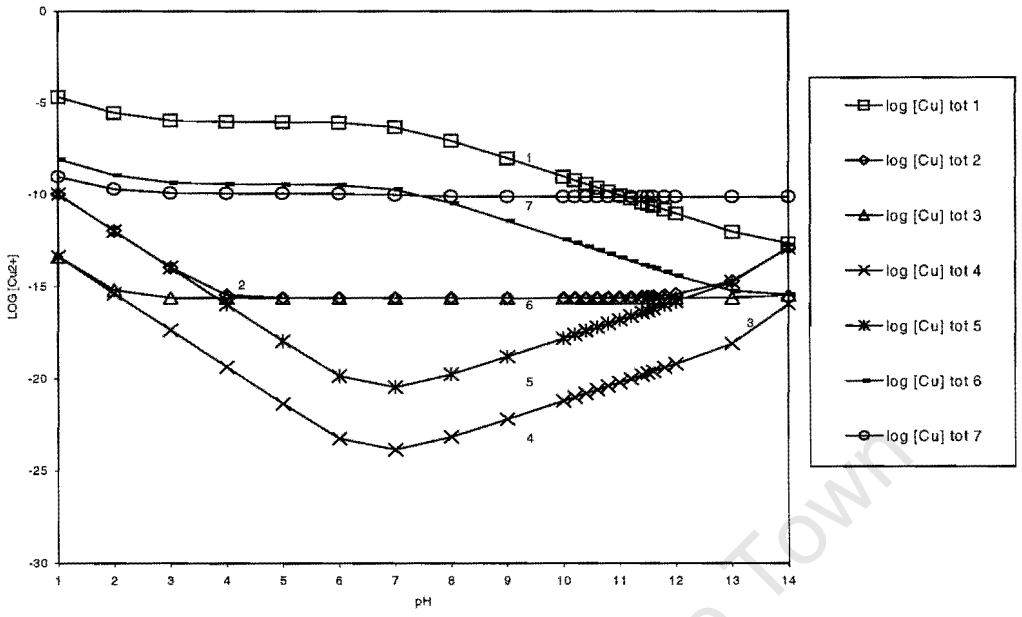

The following lists the species and references used for figure 5.2 repeated above:

log[Cu] tot 1:Dryssen for bi-sulphides, Bollinger for CuS and Licht for pKa values, system, all of the above equation taken into account.

log[Cu] tot 2:Licht for all constants except CuS system from Bollinger.
Species not used: CuHS and $Cu(HS)_2$.

log[Cu] tot 3 :Smith and Martell for all constants except CuS system from Bollinger
Without species $Cu(HS)_2$ and CuHS

log[Cu] tot 4 : Smith and Martell for all constants except CuS system from Bollinger
Without species $Cu(HS)_2$ and CuHS and CuS^o

log[Cu] tot 5 : Licht for all constants except CuS system from Bollinger.
Without species $Cu(HS)_2$ and CuHS and CuS^o

log[Cu] tot 6 : Dryssen for bi-sulphides, Smith and Martell for other constants except CuS from Bollinger.
All species taken into account.

log[Cu] tot 7 : Dryssen for CuS and Bi-sulphides, Smith and Martell for other constants.
All species taken into account.

Appendix A7

A7.1 Estimation of variance σ^2

For a linear system (Myers and Montgomery, 1995)

$$\mathbf{y} = \mathbf{X}\beta + \varepsilon \tag{A7-1}$$

$$\mathbf{y} = \begin{bmatrix} y_1 \\ y_2 \\ \cdot \\ \cdot \\ y_n \end{bmatrix}, \quad \mathbf{X} = \begin{bmatrix} 1 & x_{11} & x_{12} & \ldots & x_{1k} \\ 1 & x_{21} & x_{22} & \ldots & x_{2k} \\ \cdot & \cdot & \cdot & & \cdot \\ \cdot & \cdot & \cdot & & \cdot \\ 1 & x_{n1} & x_{n2} & \ldots & x_{nk} \end{bmatrix}, \quad \beta = \begin{bmatrix} \beta_1 \\ \beta_2 \\ \cdot \\ \cdot \\ \beta_n \end{bmatrix} \quad \varepsilon = \begin{bmatrix} \varepsilon_1 \\ \varepsilon_2 \\ \cdot \\ \cdot \\ \varepsilon_n \end{bmatrix}$$

In general; $\mathbf{y}$ is an $(n\times1)$ vector
$\mathbf{X}$ is a $(n\times p)$ matrix of the levels of the independent variables
β is a $(p\times1)$ vector of the regression coefficients
ε is an $(n\times1)$ vector of random errors

The aim is to find the least squares estimator $\mathbf{b}$, that minimizes

$$L = \varepsilon'\varepsilon = (y - \mathbf{X}\beta)'(y - \mathbf{X}\beta) \tag{A7-2}$$

$$\mathbf{X'Xb} = \mathbf{X'y} \tag{A7-3}$$

$$\mathbf{b} = (\mathbf{X'X})^{-1}\mathbf{X'y} \tag{A7-4}$$

The covariance matrix expresses the variance property of b:

$$\text{Cov}(\mathbf{b}) = E\{[\mathbf{b} - E(\mathbf{b})][\mathbf{b} - E(\mathbf{b})]'\} \tag{A7-5}$$

$$\text{Cov}(\mathbf{b}) = \sigma^2(\mathbf{X'X})^{-1} \tag{A7-6}$$

The estimation of σ^2 is therefore:

$$SS_E = \sum_{i=1}^{n}(y_i - \hat{y}_i)^2 = \mathbf{e'e} \tag{A7-7}$$

SS_E - Sum of squares

$$\mathbf{e} = y - \hat{y} = y - \mathbf{Xb} \tag{A7-8}$$

Therefore:

$$SS_E = (y - \mathbf{Xb})'(y - \mathbf{Xb}) \tag{A7-9}$$

$$SS_E = y'y - \mathbf{b}'\mathbf{X}'y \quad \text{(A7-10)}$$

Equation (A7-10) is called the error or residual sum of squares and has n-p degrees of freedom.

$$E(SS_E) = \sigma^2 (n - p) \quad \text{(A7-11)}$$

Estimate of σ^2 is

$$\sigma^2 = \frac{SS_E}{n-p} \quad \text{(A7-12)}$$

A7.2 Test for Significance of Regression

Hypothesis states

$H_o = \beta_1 = \beta_2 = \ldots = \beta_k = 0$

$H_1 = \beta_j \neq 0$ for at least one j

Rejection of H_0: Implies that at least one of the regressor variables $x_1, x_2, \ldots, x_k$ contributes significantly to the model.

$$S_{yy} = SS_R + SS_E \quad \text{(A7-13)}$$

Test: $$F_0 = \frac{SS_R / k}{SS_E /(n-k-1)} = \frac{MS_R}{MS_E} \quad \text{(A7-14)}$$

MS- mean square

F values may be found in tables in many statistical texts. The values are significant if the F value is more than the value found in the table. In order to use the degrees of freedom are needed for the MS_R numerator and the MS_E denominator.

Appendix A8

A8.1 Supersaturation tables

Table A8.1 Supersaturation calculations

Experiment		FO01	FO02	FO03	FO04	FO05	FO06	FO07
pH		5.7-5.8	6.66-6.92	6.27-6.57	6.35-6.55	6.61-6.92	6.16-6.35	6.61-6.92
Copper concentration	ppm	151.500	100.000	50.000	50.000	100.000	100.000	150.000
	mmol/l	2.405	1.587	0.794	0.794	1.587	1.587	2.381
Sulphide concentration	ppm	75.000	75.000	25.000	38.000	63.000	63.000	75.000
	mmol/l	2.329	2.329	0.776	1.180	1.957	1.957	2.329
S:Cu ratio		1.000	1.250	1.000	1.500	1.250	1.250	1.000
Recirculation Rate	ml/min	224.000	141.000	101.000	181.000	141.000	141.000	101.000
Flow rate of copper and sulphide solution	ml/min	50.000	40.000	50.000	50.000	40.000	40.000	30.000
Copper in RR	ppm	26.150	5.640	8.035	2.000	8.770	15.005	36.820
Copper in RR	mmol/min	0.093	0.013	0.013	0.006	0.020	0.034	0.059
Sulphide in RR	mmol/min	0.093	0.013	0.013	0.006	0.020	0.034	0.059
Sulphide in RR	ppm	13.283	1.803	1.840	0.821	2.804	4.798	8.433
RC+FF=MF		0.01	0.00	0.00	0.00	0.00	0.00	0.01
supersaturation ratio: C / Ceq (1e-37))		5.60E+34	3.70E+34	6.16E+33	9.37E+33	3.11E+34	3.11E+34	5.55E+34
Inlet SS		5.60E+31	3.70E+31	6.16E+30	9.37E+30	3.11E+31	3.11E+31	5.55E+31

Table A8.1 Supersaturation calculations (Cont.)

Experiment		FO08	FO09	FO10	FO11	FO12	FO13	Prelim.
pH			6.03-6.97	5.53-6.35	5.12-6.59	6.27-6.71	5.37-6.05	
Copper concentration	ppm	50.000	150.000	50.000	100.000	100.000	150.000	150.000
	mmol/l	0.794	2.381	0.794	1.587	1.587	2.381	2.381
Sulphide concentration	ppm	25.000	113.530	37.000	63.000	63.000	113.000	416.000
	mmol/l	0.776	3.526	1.149	1.957	1.957	3.509	12.919
S:Cu ratio		1.000	1.500	1.500	1.250	1.250	1.500	1.000
Recirculation Rate	ml/min	181.000	101.000	101.000	141.000	141.000	181.000	181.000
Flow rate of copper and sulphide solution	ml/min	30.000	50.000	30.000	40.000	40.000	30.000	110.000
Copper in RR	ppm	13.160	6.300	2.300	6.510	6.440	11.540	0.001
Copper in RR	mmol/min	0.038	0.010	0.004	0.015	0.014	0.033	0.000
Sulphide in RR	mmol/min	5.483	0.010	0.004	0.015	0.014	0.033	0.000
Sulphide in RR	ppm	0.004	1.443	0.527	2.081	2.059	4.736	0.000
RC+FF=MF		0.00	0.01	0.00	0.00	0.00	0.01	0.03
supersaturation ratio: C / Ceq (1e-37))		6.16E+33	8.75E+34	9.55E+33	3.11E+34	3.11E+34	8.36E+34	3.08E+35
Inlet SS		6.16E+30	8.39E+31	9.12E+30	3.11E+31	3.11E+31	8.36E+31	3.08E+32

(Copper concentration in feed (mmol/l) + Copper mass concentration in recycle (ppm) * recycle flow rate (ml/min)/ 1000 (l/ml))*(Inlet Sulphide concentration (mmol/l))

Formula for C/Ceq (Equation 8-1)

A8.2 List of experiments

Table A8.2 2^4 first-order half replicate design.

	S/Cu mol:mol	[Cu] ppm	Cu flow rate ml/min	Recyle ml/min
FO1	1	150	50	181
FO2	1.25	100	40	141
FO3	1	50	50	101
FO4	1.5	50	50	181
FO5	1.25	100	40	141
FO6	1.25	100	40	141
FO7	1	150	30	101
FO8	1	50	30	181
FO9	1.5	150	50	101
FO10	1.5	50	30	101
FO11	1.25	100	40	141
FO12	1.25	100	40	141
FO13	1.5	150	30	181

Table A8.3 Second Order Design

	S/Cu	[Cu] ppm	Flow rate ml/min	Recyle ml/min
SO1	1.25	100	23.18	141
SO2	1.25	15.9	40	141
SO3	1.25	100	40	73.72
SO4	1.6705	100	40	141
SO5	1.25	100	40	208.28
SO6	0.8295	100	40	141
SO7	1.25	100	56.82	141
SO8	1.25	184.1	40	141

Figure A8.1. FO1: Concentration as a function of postion in the bed

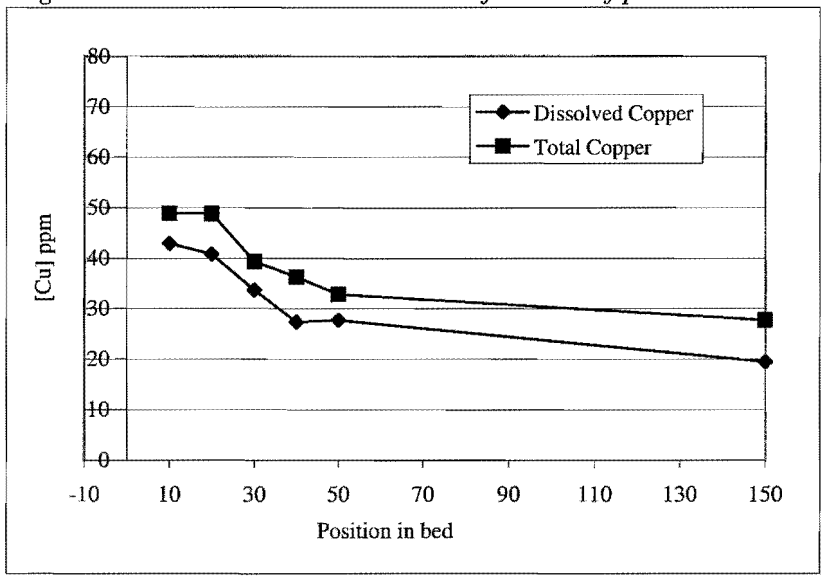

Figure A8.2. FO2: Concentration as a function of postion in the bed

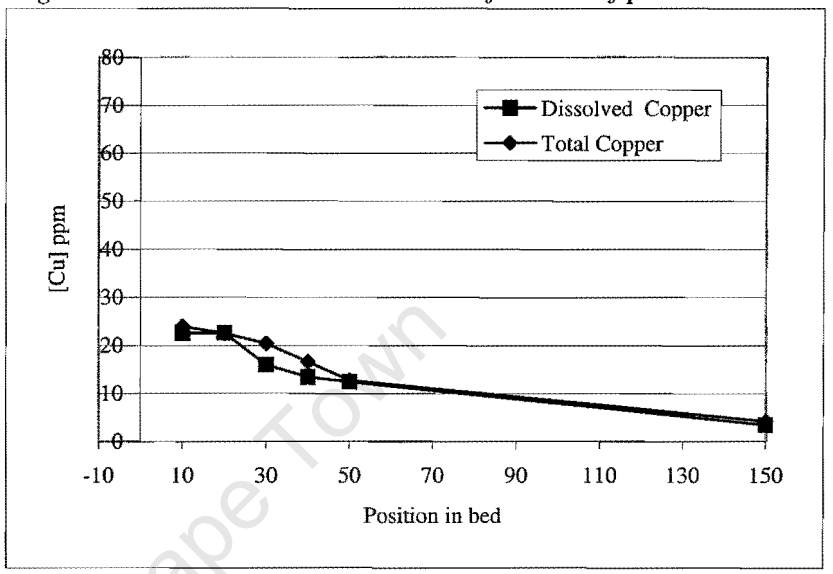

Figure A8.3. FO3: Concentration as a function of postion in the bed

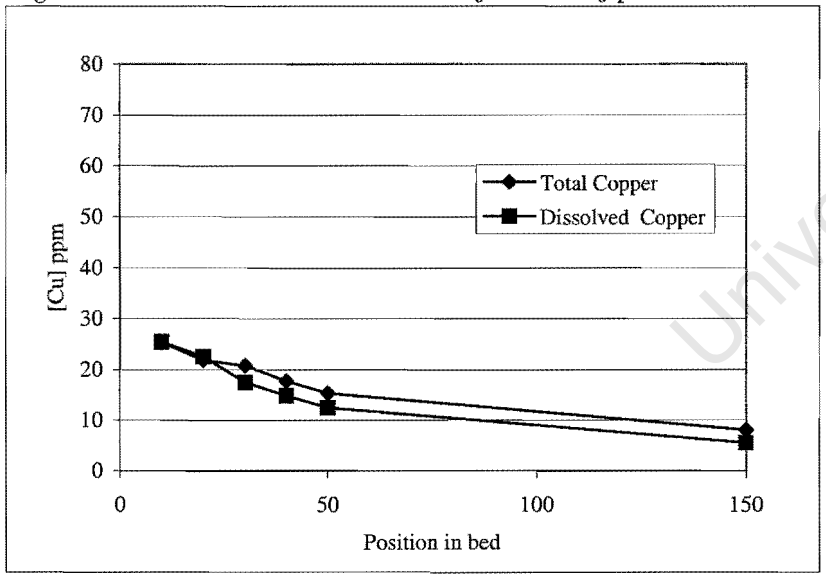

Figure A8.4. FO4: Concentration as a function of postion in the bed

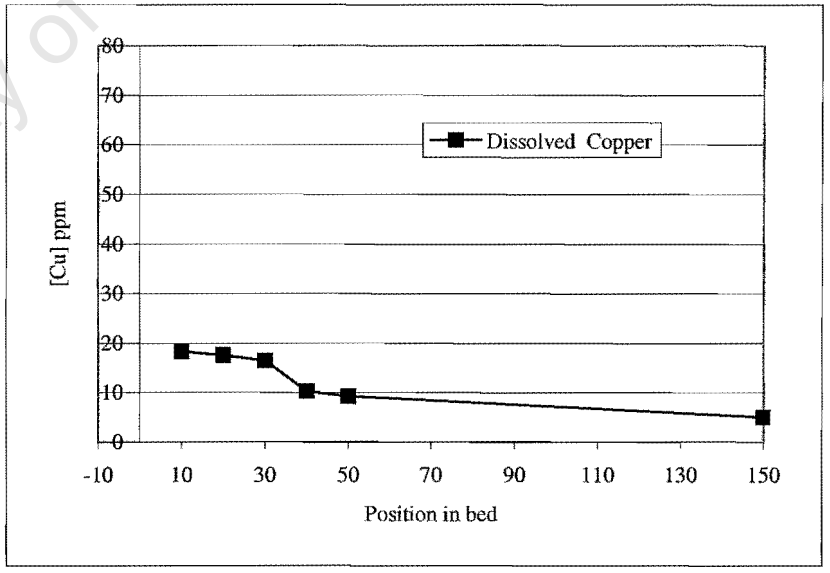

Figure A8.5. FO5: Concentration as a function of postion in the bed

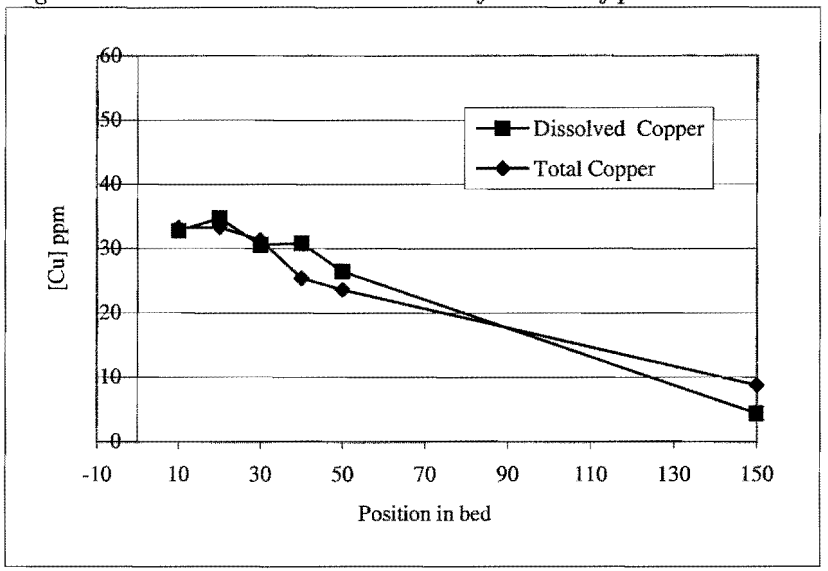

Figure A8.6. FO6: Concentration as a function of postion in the bed

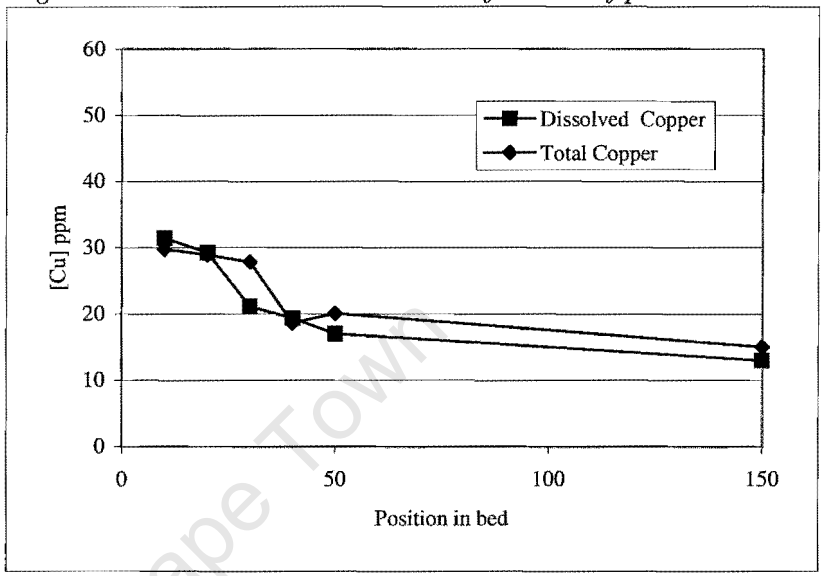

Figure A8.7. FO7: Concentration as a function of postion in the bed

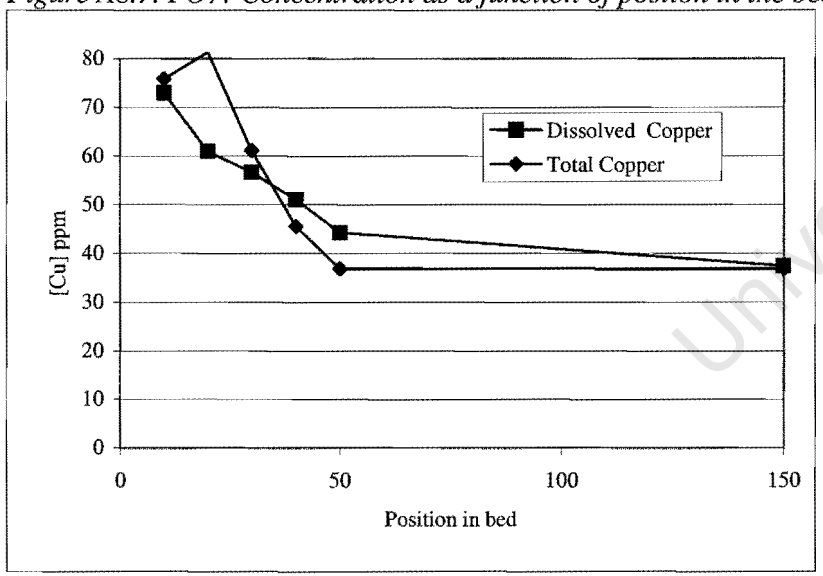

Figure A8.8. FO8: Concentration as a function of postion in the bed

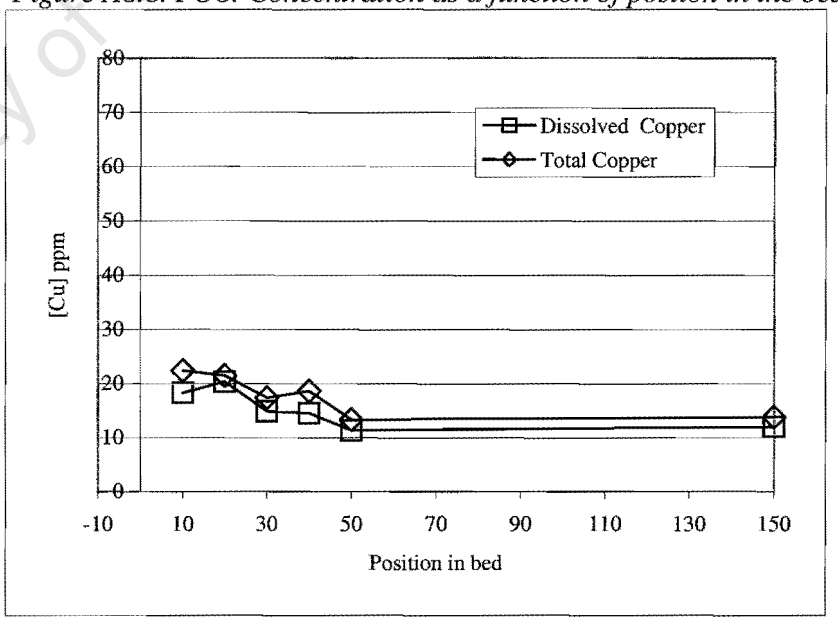

Figure A8.9. FO9: Concentration as a function of postion in the bed

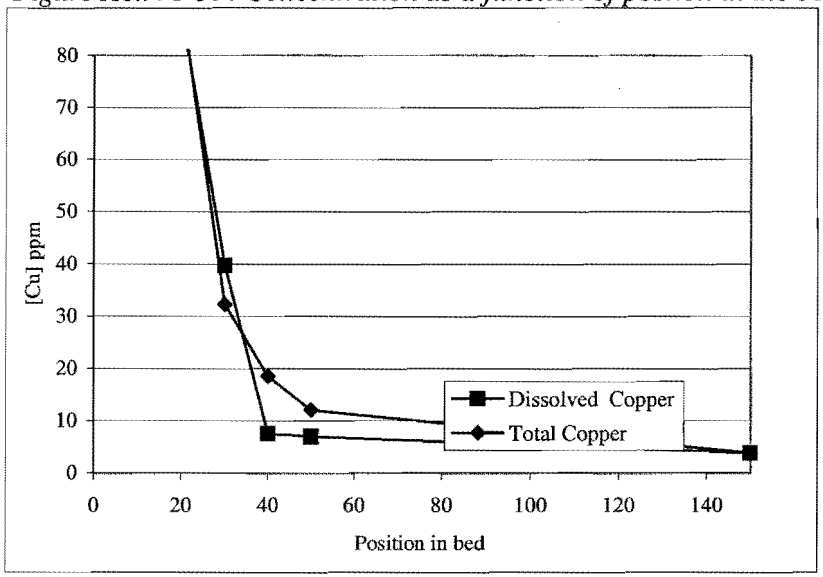

Figure A8.10. FO10: Concentration as a function of postion in the bed

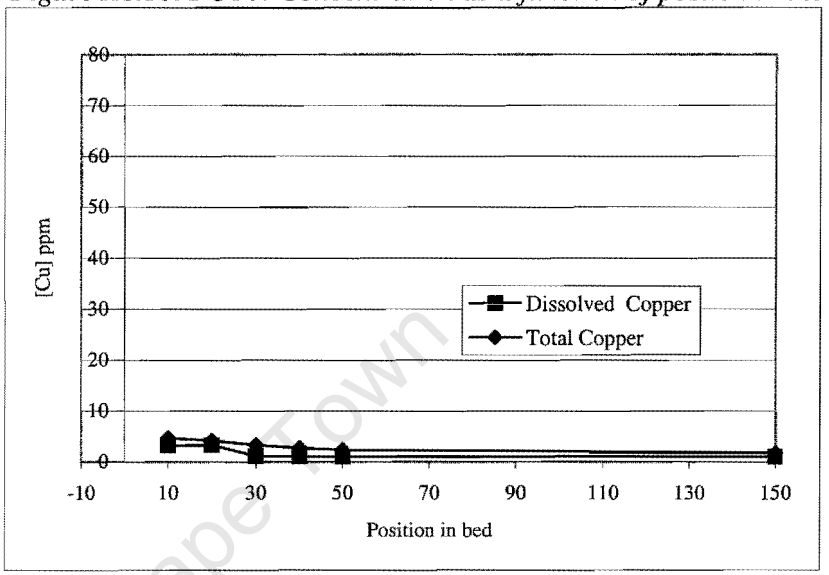

Figure A8.11. FO11: Concentration as a function of postion in the bed

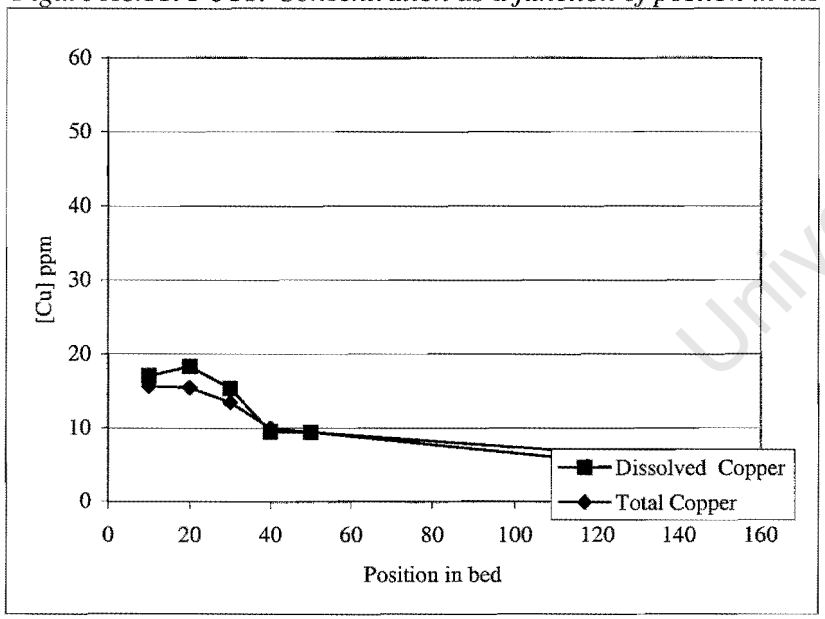

Figure A8.12. FO12: Concentration as a function of postion in the bed

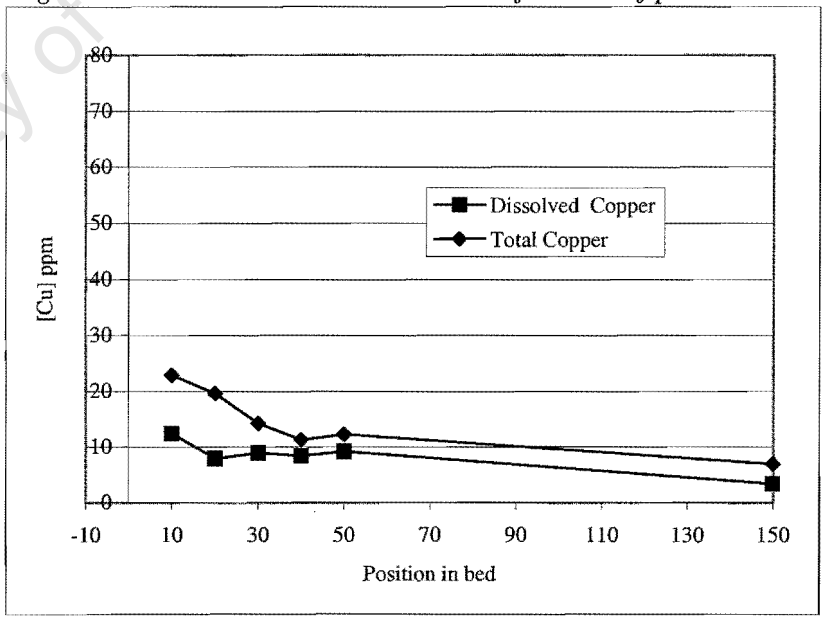

Figure A8.13. FO13: Concentration as a function of postion in the bed

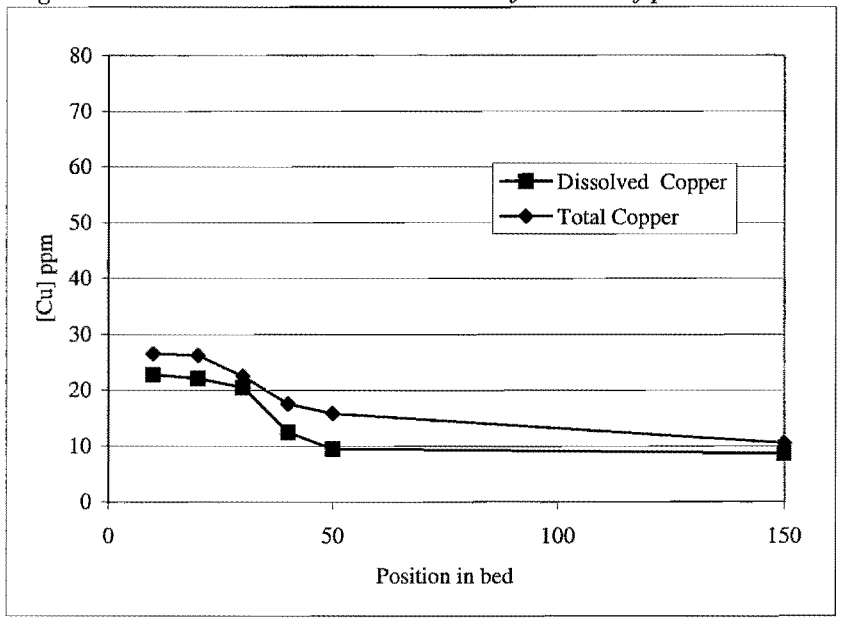

Figure A8.14. FO1: Concentration as a function of time

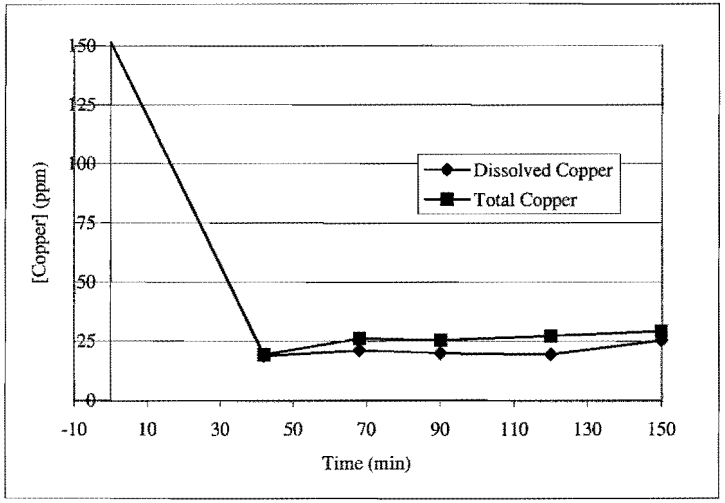

Figure A8.15. FO2: Concentration as a function of time

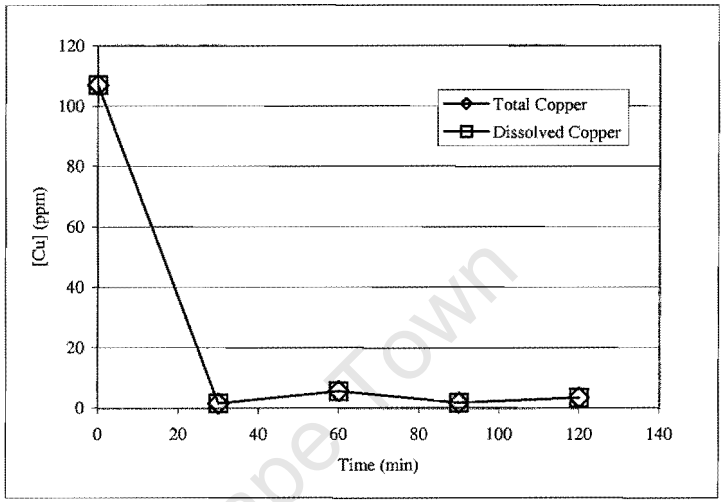

Figure A8.15. FO3: Concentration as a function of time

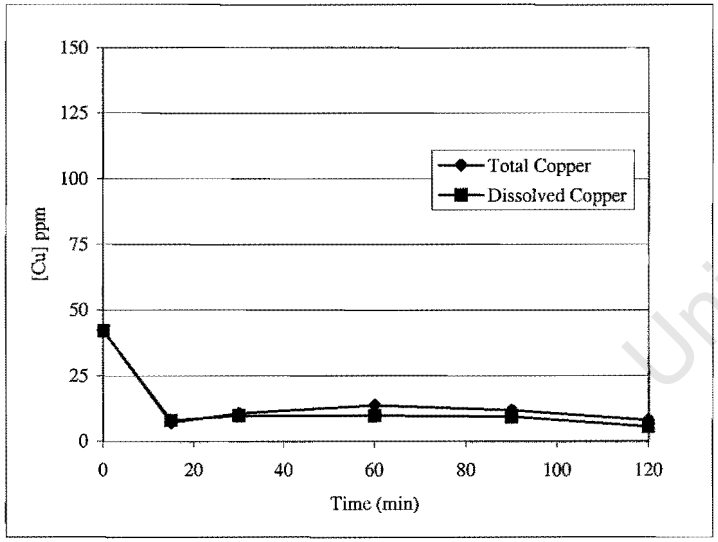

Figure A8.17. FO4: Concentration as a function of time

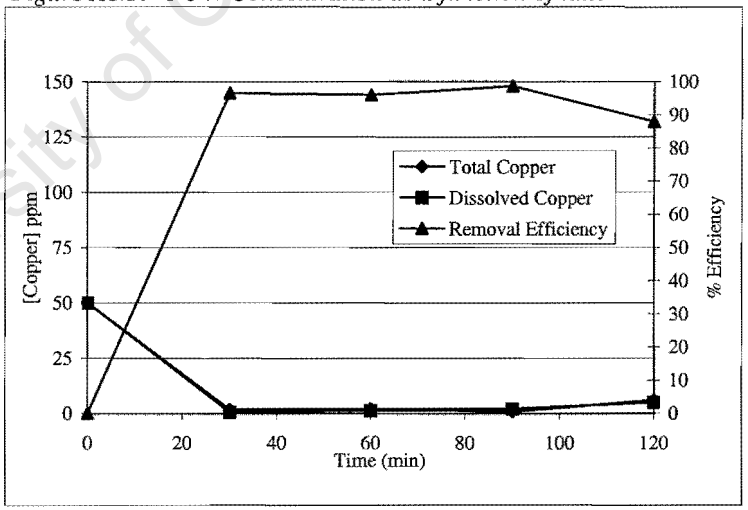

Figure A8.18. FO5: Concentration as a function of time

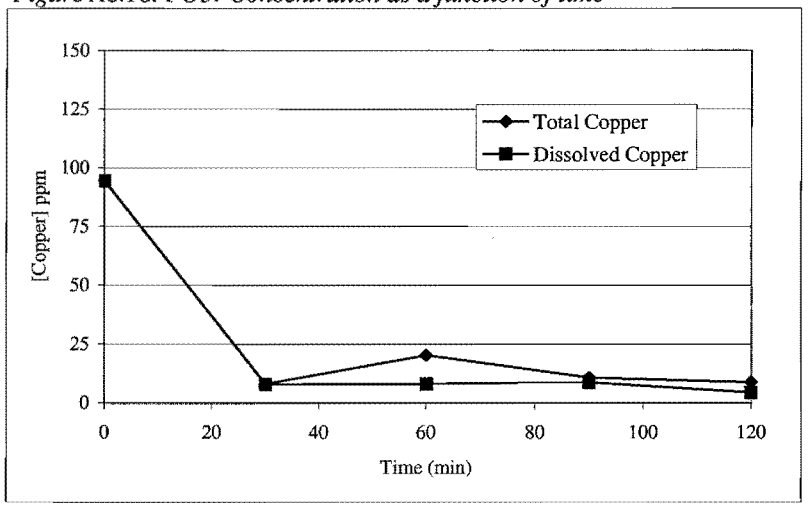

Figure A8.19. FO6: Concentration as a function of time

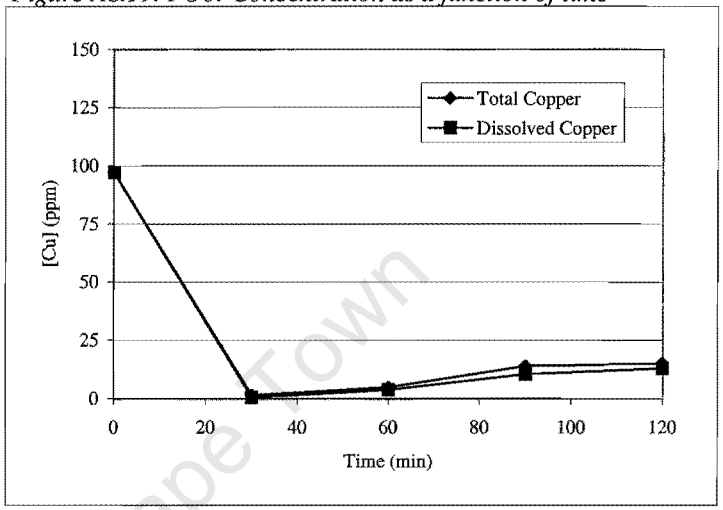

Figure A8.20. FO7: Concentration as a function of time

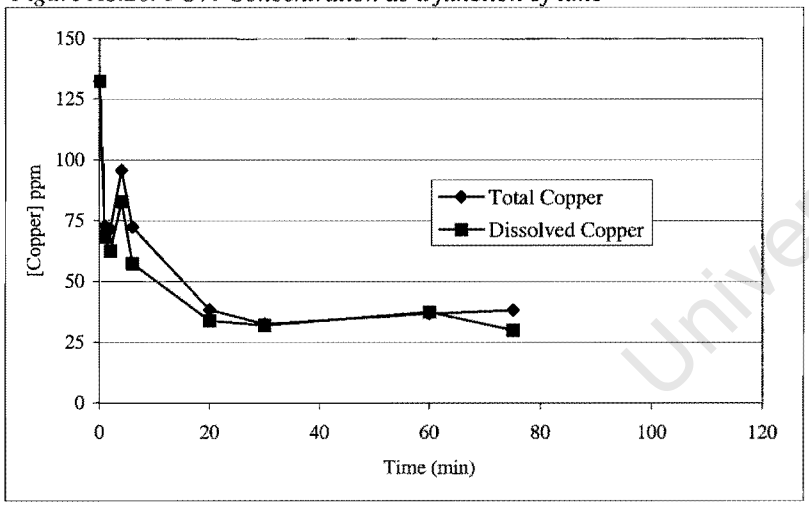

Figure A8.21. FO8: Concentration as a function of time

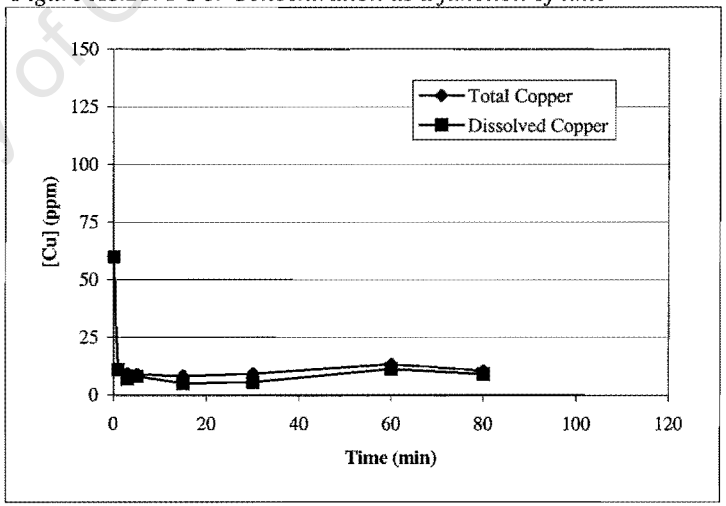

Figure A8.22. FO9 Concentration as a function of time

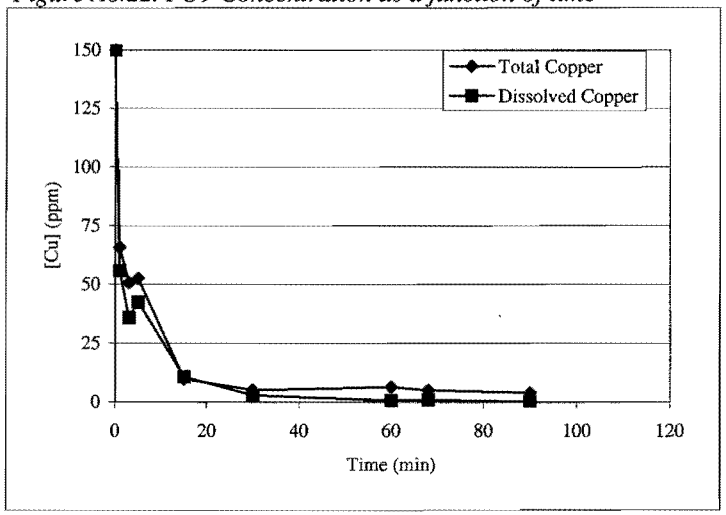

Figure A8.23. FO10: Concentration as a function of time

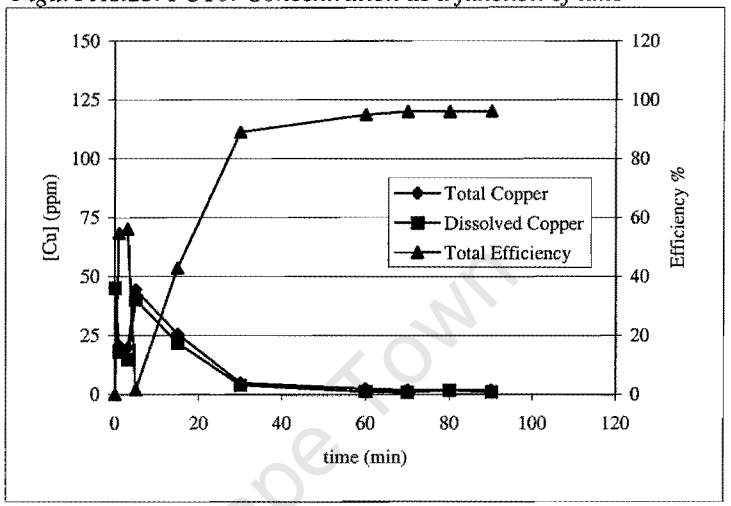

Figure A8.24. FO11: Concentration as a function of time

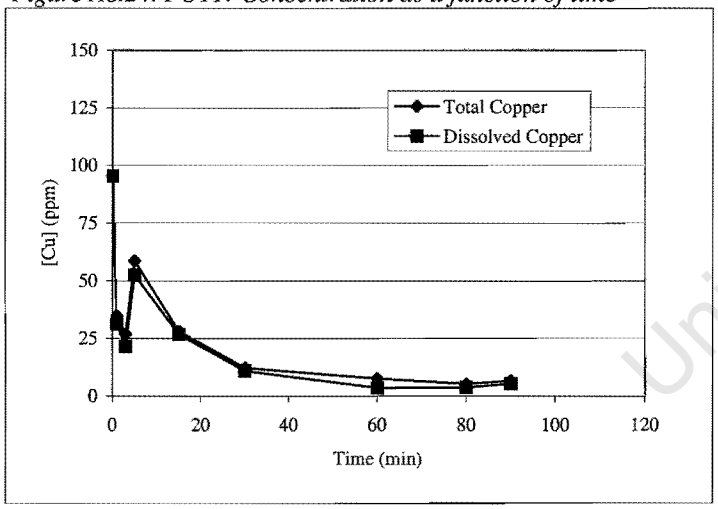

Figure A8.25. FO12: Concentration as a function of time

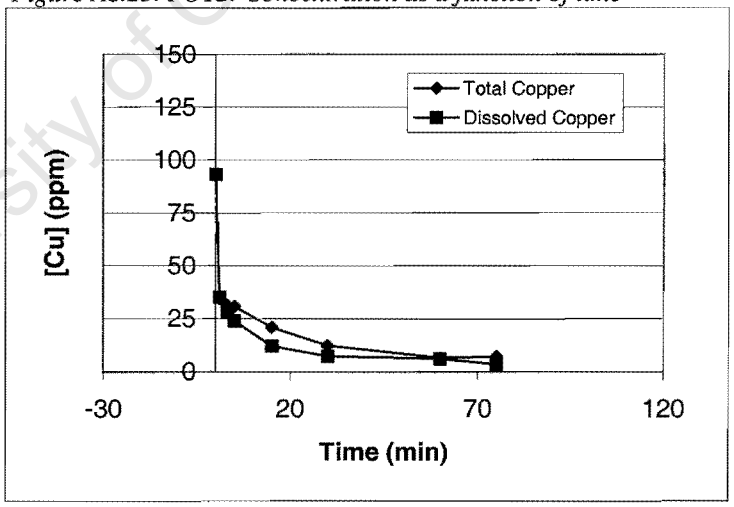

Figure A8.26. FO13: Concentration as a function of time

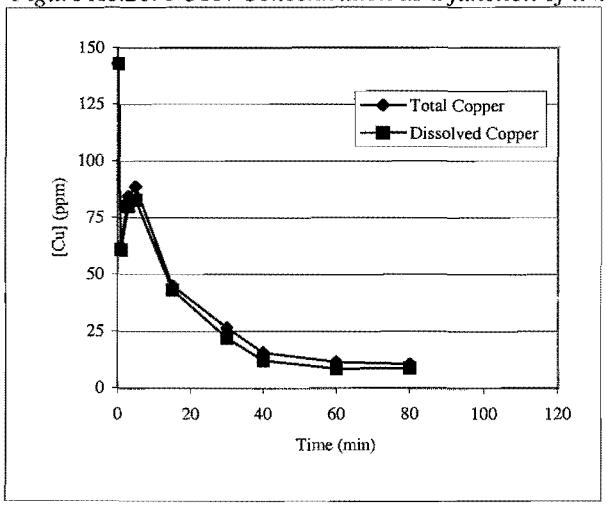

Appendix A8.4

SAS Results

2nd Analysis

ANALYSIS OF KAREN'S DATA WITH CORRECTED DATA

FIRST ORDER MODELS

COPPER CONVERSION (COCO)

Fitted first order model:

COCO = 44.5592 + 29.5250A - 0.03808B + 0.2711C + 0.02147D
(12.0410) (6.3220) (0.03161) (0.1580) (0.03951)

t-test	p=0.0060	p=0.0016	p=0.2628	p=0.1246	p=0.6017

Significant

The factor labels are
A : S/Cu B : [Cu] C : Flow rate D : Recycle

The analysis of variance is as follows:

Source of variation	DF	SS	Mean Square	F value	Prob>F	
Model	4	529.56355				
Quadratic effects	1	63.42729	63.42729	11.865	p<0.01	0.05
Other effects	3	75.05984	25.01995	4.680	p>0.05	Not sig
Pure error	4	21.38312	5.34578			
Total	12	689.43380				

529.56/689.43.

The model accounts for 76.8% of the variation in Copper Conversion.

COPPER EFFICIENCY (COEF)

Fitted first order model:

COEF = 43.5856 + 30.1050A - 0.02952B + 0.1724C + 0.02922D
(11.9099) (6.2532) (0.03127) (0.1563) (0.03908)

t-test	p=0.0064	p=0.0013	p=0.3726	p=0.3022	p=0.4761

The analysis of variance is as follows:

Source of variation	DF	SS	Mean Square	F value	Prob>F	
Model	4	505.28835				
Quadratic effects	1	95.96748	95.96748	14.147	p<0.02	
Other effects	3	33.30694	11.10230	1.637	p>0.05	Not sig
Pure error	4	27.13412	6.78353			
Total	12	661.69689				

The model accounts for 76.4% of the variation in Copper Efficiency.

COPPER CONVERSION – COPPER EFFICIENCY (DIFF)

Fitted first order model:

DIFF =	0.9735	- 0.5800A	- 0.00855B	+ 0.09875C	- 0.00775D
	(5.0768)	(2.6655)	(0.01333)	(0.06664)	(0.01666)
t-test	p=0.8527	p=0.8332	p=0.5391	p=0.1767	p=0.6542

The analysis of variance is as follows:

Source of variation	DF	SS	Mean Square	F value	Prob>F
Model	4	10.20030			
Quadratic effects	1	3.35686	3.35686	1.179	p>0.05
Other effects	3	13.67425	4.55808	1.160	p>0.05
Pure error	4	11.38908	2.84727		
Total	12	38.62049			

The model accounts for 26.4% of the variation in the Difference.

SUPERSATURATION (SUPER)

Fitted first order model:

SUPER =	32.1963	- 15.0450A	+ 0.8951B	+ 0.4401C	- 0.2164D
	(36.5059)	(19.1670)	(0.09584)	(0.4792)	(0.1198)
t-test	p=0.4035	p=0.4551	p=0.0001	p=0.3852	p=0.1085

The analysis of variance is as follows:

Source of variation	DF	SS	Mean Square	F value	Prob>F
Model	4	16890.7745			
Quadratic effects	1	272.8757	272.8757	4.390	p>0.05
Other effects	3	947.9842	315.9947	5.084	p>0.05
Pure error	4	248.6427	62.1607		
Total	12	18360.2771			

The model accounts for 92.0% of the variation in Supersaturation.

Derek Chalton

21 May 2002

KAREN'S DATA : FITTED SECOND ORDER RESPONSE SURFACE MODELS

COPPER CONVERSION

The fitted second order model is

COPPER CONVERSION = -95.5268 + 136.5599*S/CU + 0.282284*CU

SE (127.9371) (125.4447) (0.394034)

PROB>T 0.4743 0.3046 0.4919

- 0.012421*FLOWRATE + 0.987791*RECYCLE - 21.4165*S/CU^2

(2.607937) (0.608874) (39.4615)

0.9963 0.1392 0.6005

- 0.001313*CU^2 + 0.004288*FLOWRATE^2 – 0.002273*RECYCLE^2

(0.000987) (0.024663) (0.001541)

0.2159 0.8658 0.1745

- 0.011400*S/CU*CU - 0.2320*S/CU*FLOWRATE - 0.30050*S/CU*RECYCLE

(0.269719) (1.3486) (0.337149)

0.9672 0.8672 0.3960

The factors accounted for 60.2% of the variation in COPPER CONVERSION. The following is the Canonical analysis:

Canonical Analysis of Response Surface
(based on coded data)

		Eigenvectors		
Eigenvalues	S_CU	CU	FLOWRATE	RECYCLE
1.398309	-0.219461	0.004140	0.972341	0.079834
-1.857157	0.868279	-0.023557	0.232023	-0.437838
-9.288595	0.008558	0.999299	0.000669	-0.036440
-12.400032	0.444809	0.028801	0.026808	0.894761

Stationary point is a saddle point.

Estimated Ridge of Maximum Response for Variable COPPERCO

Coded Radius	Estimated Response	Standard Error
0.0	91.282002	4.082189
0.1	92.543999	4.072989
0.2	93.757854	4.052478
0.3	94.928405	4.042221
0.4	96.058959	4.078277
0.5	97.152007	4.208309
0.6	98.209644	4.483003
0.7	99.233838	4.943169
0.8	100.226620	5.610302
0.9	101.190239	6.486912
1.0	102.127295	7.563779

Coded	Uncoded Factor Values			
Radius	S_CU	CU	FLOWRATE	RECYCLE
0.0	1.250000	100.000000	40.000000	141.000000
0.1	1.291213	100.246432	40.072459	139.711242
0.2	1.331900	100.406631	40.107021	137.989826
0.3	1.372129	100.501409	40.096795	135.975524
0.4	1.411971	100.546224	40.033945	133.758671
0.5	1.451475	100.552416	39.909196	131.399740
0.6	1.490658	100.528391	39.711480	128.941519
0.7	1.529506	100.480530	39.427702	126.416635
0.8	1.567965	100.413845	39.042701	123.852409
0.9	1.605934	100.332446	38.539584	121.274151
1.0	1.643258	100.239889	37.900706	118.707412

COPPER EFFICIENCY

The fitted second order model is

COPPER EFFICIENCY = -94.2847 + 123.8507*S/CU + 0.538489*CU

SE (139.6830) (136.9617) (0.430210)

PROB>T 0.5166 0.3894 0.2422

- 0.496602*FLOWRATE + 1.030685*RECYCLE - 19.7260*S/CU^2

(2.847372) (0.664775) (43.0847)

0.8654 0.1555 0.6579

- 0.001836*CU^2 + 0.001810*FLOWRATE^2 – 0.002427*RECYCLE^2

(0.001077) (0.026928) (0.001683)

0.1224 0.9479 0.1831

- 0.12750*S/CU*CU + 0.23350*S/CU*FLOWRATE – 0.292625*S/CU*RECYCLE

(0.294482) (1.47241) (0.368102)

0.6752 0.8775 0.4471

The factors accounted for 58.8% of the variation in COPPER EFFICIENCY.

Canonical Analysis of Response Surface
(based on coded data)

		Eigenvectors		
Eigenvalues	S_CU	CU	FLOWRATE	RECYCLE
0.789885	0.316493	-0.051788	0.940626	-0.111233
-1.556325	-0.847917	0.167220	0.338512	0.372134
-12.153409	0.218652	-0.590671	-0.014256	0.776592
-14.031974	0.364774	0.787695	-0.020710	0.496032

Stationary point is a saddle point.

Estimated Ridge of Maximum Response for Variable COPPEREF

Coded Radius	Estimated Response	Standard Error
0.0	89.453626	4.456975
0.1	90.694786	4.446931
0.2	91.885400	4.424535
0.3	93.034239	4.413331
0.4	94.146711	4.452667
0.5	95.226411	4.594554
0.6	96.275947	4.894320
0.7	97.297391	5.396610
0.8	98.292539	6.125166
0.9	99.263063	7.083270
1.0	100.210609	8.261726

Coded	Uncoded Factor Values			
Radius	S_CU	CU	FLOWRATE	RECYCLE
0.0	1.250000	100.000000	40.000000	141.000000
0.1	1.291446	100.315055	39.881887	139.997399
0.2	1.332524	100.111237	39.799593	138.535479
0.3	1.373189	99.571310	39.759329	136.774211
0.4	1.413483	98.807876	39.766494	134.813472
0.5	1.453457	97.891133	39.826470	132.716463
0.6	1.493149	96.866429	39.944928	130.524844
0.7	1.532578	95.764397	40.127910	128.267576
0.8	1.571742	94.606767	40.381782	125.966072
0.9	1.610617	93.409796	40.713090	123.637247
1.0	1.649163	92.186325	41.128325	121.295372

For the above analysis, it might be useful to consider omitting one or more negligible factors from the model, e.g. Flowrate. I took the liberty of dropping Flowrate and the resulting analysis produced a maximum point for both response variables!

leave out PROB but include SE!

- Trying fit surface + all terms contribute to surface.
- Drop term other te change . . don't drop terms, cause do m contribution
- is optimum place t work?

OMITTING FLOWRATE

COPPER CONVERSION

The fitted second order model is

COPPER CONVERSION = -85.9140 + 128.4140*S/CU + 0.243663*CU

SE	(92.1588)	(102.5840)	(0.417344)
PROB>T	0.3712	0.2366	0.5711

+ 0.963788*RECYCLE - 21.8701*S/CU^2 - 0.001324*CU^2

(0.572616)	(35.7248)	(0.000893)
0.1205	0.5529	0.1662

- 0.002290*RECYCLE^2 - 0.01140*S/CU*CU – 0.300500*S/CU*RECYCLE

(0.001396)	(0.244714)	(0.305893)
0.1290	0.9637	0.3470

\- + 0.000290*CU*RECYCLE

(0.001529)
0.8531

The factors accounted for 60.0% of the variation in COPPER CONVERSION.

Canonical Analysis of Response Surface
(based on coded data)

Factor	Critical Value Coded	Uncoded
S_CU	3.221337	2.604572
CU	-0.169981	85.704560
RECYCLE	-1.427375	44.966243

Predicted value at stationary point 113.428132

Eigenvalues	Eigenvectors S_CU	CU	RECYCLE
-1.727277	0.892287	-0.071416	-0.445784
-9.275706	0.151206	0.977656	0.146031
-12.598255	0.425395	-0.197707	0.883148

Stationary point is a maximum.

Estimated Ridge of Maximum Response for Variable COPPERCO

Coded Radius	Estimated Response	Standard Error	Uncoded Factor Values S_CU	CU	RECYCLE
0.0	91.616210	3.267410	1.250000	100.000000	141.000000
0.1	92.876192	3.260183	1.291257	100.227951	139.712301
0.2	94.087378	3.245788	1.331959	100.327668	137.994349
0.3	95.254202	3.246334	1.372180	100.320429	135.982635
0.4	96.379472	3.298310	1.412003	100.226025	133.764491
0.5	97.465030	3.448313	1.451501	100.060875	131.396987
0.6	98.512133	3.742420	1.490734	99.838069	128.918472
0.7	99.521661	4.213096	1.529750	99.567921	126.355449
0.8	100.494251	4.873070	1.568585	99.258562	123.726733
0.9	101.430371	5.719613	1.607270	98.916434	121.046003
1.0	102.330377	6.742830	1.645829	98.546685	118.323421

COPPER EFFICIENCY

The fitted second order model is

COPPER EFFICIENCY = -115.7230 + 133.6694*S/CU + 0.58060*CU

SE (100.5908) (111.9699) (0.455529)

PROB>T 0.2744 0.2577 0.2287

+ 1.061981*RECYCLE - 19.9175*S/CU^2 - 0.001841*CU^2

(0.625007) (38.9935) (0.000975)

0.1174 0.6196 0.0856

- 0.002435*RECYCLE^2 - 0.12750*S/CU*CU – 0.292625*S/CU*RECYCLE

(0.001523) (0.267104) (0.333881)

0.1382 0.6425 0.3995

- - 0.000292*CU*RECYCLE

(0.001669)

0.8644

The factors accounted for 58.6% of the variation in COPPER EFFICIENCY.

Canonical Analysis of Response Surface
(based on coded data)

Factor	Critical Value Coded	Uncoded
S_CU	3.846591	2.867491
CU	-0.534828	55.020964
RECYCLE	-1.464471	42.470394

Predicted value at stationary point 114.448923

Eigenvalues	Eigenvectors S_CU	CU	RECYCLE
-1.423956	0.912451	-0.150270	-0.380593
-11.407537	0.198197	-0.651425	0.732368
-14.733942	0.357981	0.743683	0.564611

Stationary point is a maximum.

Estimated Ridge of Maximum Response for Variable COPPEREF

Coded Radius	Estimated Response	Standard Error	Uncoded Factor Values S_CU	CU	RECYCLE
0.0	89.594690	3.566360	1.250000	100.000000	141.000000
0.1	90.832638	3.558472	1.291543	100.328989	139.992169
0.2	92.021139	3.542760	1.332666	100.170185	138.529564
0.3	93.168064	3.543355	1.373349	99.706011	136.776933
0.4	94.277885	3.600085	1.413654	99.043288	134.832557
0.5	95.353278	3.763808	1.453650	98.246006	132.756277
0.6	96.395929	4.084820	1.493400	97.353997	130.585893
0.7	97.406947	4.598552	1.532952	96.393066	128.346219
0.8	98.387087	5.318901	1.572344	95.380551	126.054131
0.9	99.336884	6.242887	1.611605	94.328488	123.721469
1.0	100.256724	7.359711	1.650758	93.245468	121.356772

Derek Chalton

15 June 2002